“Analysis of microscope images”

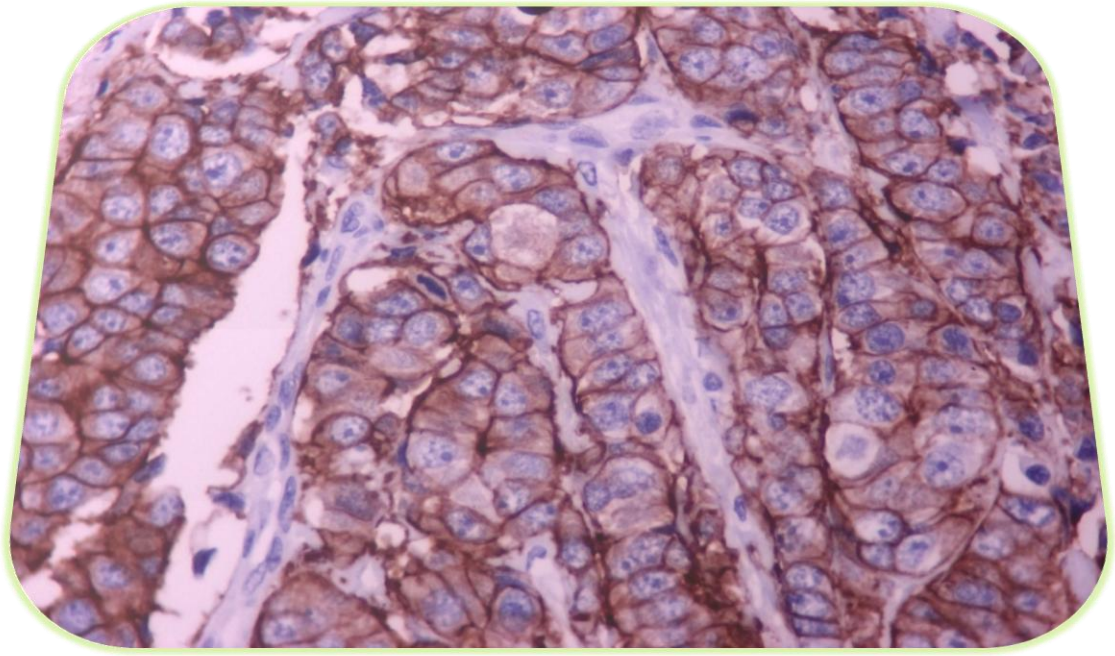

A thesis presented

by

Livanos George

to

The Department of Electronics and Computer Engineering

in partial fulfillment of the requirements

for the degree of the Master Diploma

Technical University of Crete

Supervisory Committee: **Professor Zervakis Michalis (Supervisor)**
Professor Liavas Athanasios
Professor Petrakis Euripides

October 2013

Contents

A c k n o w l e d g e m e n t s

I would like to express my appreciation to Professor Michalis Zervakis for the great amount of time, effort, support and mainly his patient guidance throughout the time that I have been working on this thesis. I also thank Professor Athanasios Liavas and Euripides Petrakis for reading and correcting my thesis.

Special thanks to medical specialists Maria Kafousi, Sofia Bolioti and biology expert Dr Ekaterini Bei for their kind support and contribution during the evaluation and validation procedure of the implemented immunohistochemical image segmentation algorithm proposed in this thesis.

Preface

Breast cancer constitutes one of the most frequent types of cancer among women, yet it can be efficiently treated and cured when it is diagnosed in the first stages. Over the last years, medical advances have led to the identification of numerous tumor biomarkers facilitating the understanding of the molecular basis of tumor progression and treatment response. Prognostic markers aim to objectively estimate the patient's overall outcome, while predictive markers focus on the objective evaluation of the possible benefits from a specific clinical intervention.

The HER2/neu oncogene is notable both for its role in the pathogenesis of breast cancer and for its selection as a target of treatment. It is considered to be overexpressed in tumors with much higher level than the relatively low degree in normal tissue. Overexpression of this receptor in breast cancer is associated with increased disease recurrence, poorer relapse-free survival and worse prognosis. Because of its prognostic role as well as its ability to predict response to trastuzumamb , breast tumors are routinely checked for overexpression of HER2/neu.

In this thesis we study the process of tissue characterization from both a macro and micro point of view. In particular, we study polarimetric imaging of tissue at macroscopic level and microscope imaging of stained cells at molecular level. An emerging area of tissue discrimination at macroscopic level employs multispectral polarization imaging technology. Diffused polarimetric reflection and backscattering provides unique, discriminatory material signatures based on the depolarization of the impinging waves from different materials, which maximize the sensitivity and discrimination power of object imaging and identification techniques. Fusing statistical analysis with polarimetric principles can be proved a powerful tool for analyzing the different properties of operational modalities and/or materials depicted in digital images. The efficiency of imaging techniques in discriminating material structures can be further improved via contrast measurement and enhancement in digital images.

Qualitative and quantitative Her2 protein evaluation has been achieved using immunohistochemistry (IHC) on frozen and archival tissues, a widely adopted technique due to the standardization of the internal procedural steps and its easy and low-cost applicability to any laboratory. Immunohistochemistry is a method for detecting specific antigens in tissues or cells based on an antigen-antibody reaction

and facilitates the identification of a large number of proteins, enzymes and tissue structures, thus it has become a powerful and widely used tool in many medical research laboratories as well as clinical diagnostics. We focus on, and try to exploit, the fact that IHC "stains" the membranes of HER2 overexpressed cells, monitoring them with a characteristic color in the extracted microscope images. When reporting results, the degree of HER2 protein overexpression measured is scored according to the intensity of membrane staining and the percentage of tumor cells stained. The evaluation procedure is usually performed qualitatively by a pathologist, who carefully observes the IHC samples via microscopy and manually calculates the presence of cancer cells in the breast tissue, assigning scores according to appropriate criteria. Yet, the interpretation of such results is subjective and causes certain inconsistencies upon the diagnosis, as the result is highly dependent on the experience of the specialist and the quality of the tissue preparation stage.

Both of these areas are treated via analytic tools in this thesis, as follows. Aiming at a concrete procedure of quantifying the contrast effects of the Stokes parameter polarimetric imaging technique, we considered a statistical modeling of the digitally recorded images. The experimental setup was guided by the idea of using simple objects with optical properties similar to more complex compounds (such as biological tissues) in order to emulate a biological scenario that would be optically homogeneous and absorbing medium. Typically, micro calcifications depending upon their shape, geometry and composition can be classified as precursors of malignancies in breast mammography. The simulation performed through the experiments could act as a simulating, pre-clinical procedure in order to expand the proposed methodology to biomedical applications.

More precisely, we apply robust fitting of the intensity distributions of the various materials depicted in the acquired images using mixture models and associate the image contrast with the separability of model distributions. The proposed approach based on histogram modeling as the sum of Gaussian-like distributions provides a simple, yet effective means of pixel labeling and object segmentation, based on the statistical structure of the intensity distribution within the region of interest. In order to determine how well the estimated model approximates the initial distribution, the mean squared error (MSE) is used for revealing the "goodness of fit". Finally, as an attempt to measure and verify the detection rates of our experimental

result we adopt the accuracy, as well as specificity and sensitivity of the object discrimination procedure. The values of the quantitative evaluation metrics confirm the accuracy of the presented technique, giving rise to its direct application to biomedicine.

On a similar goal to make immunohistochemical studies for molecular analysis more objective, quantitative techniques based on computer-assisted microscopy and image analysis must be developed. Our research in this area is focused on the automated detection of Her-2 neu protein in tissues, an indication of probable cancer existence, in order to diagnose breast cancer at its earlier stages and help the patience cure the disease with higher probability. The goal of this thesis is an attempt to process the extracted IHC microscope images of breast tissues and automatically determine/define the impact of cancer on the specific female organism. Advanced image analysis techniques are adopted in order to accurately segment the cells within the sample images and precisely extract their membrane contour and degree of staining. We exploit a variety of algorithms in a modular way, in order to achieve specific tasks. Color deconvolution through model conversion and thresholding enhances the pixel intensity differences between the regions of interest in the test images, while mean-shift clustering reveals the key segments for the evaluation procedure. Edge following and linking via the watershed and active contours algorithms is performed in order to extract the complete border of the cell membranes. Finally the percentage and intensity of their staining is calculated, yielding the tissue characterization according to the IHC scoring system. The comparison of results generated by the proposed algorithm with the classification performed by the specialist who evaluated the same tissue samples confirms the efficiency and prospect of the presented work.

The chapters in this Thesis present the theoretical study and experimental tests in the previous two areas of tissue characterization at different levels, along with the results obtained and the conclusions generated.

1. Introduction

1.1. Breast cancer

Cancer is considered the abnormal growth of cells that results in the formation of tumors in different section of the body. This abnormality should not be confused with two basic and natural functions of the human organism:

- Tissue regeneration, taking place when tissue sections are rebuilt due to injury, malfunctions or surgery
- Hyperplasia, taking place when the organism intends to build up normal tissue in order to balance its functionality (e.g. a nephron grows up when the other has been removed)

Cancer is a disease that arises in molecular level. The irregular and excessive cell proliferation and growth mutates physiological cells into cancerous, leading to tissue destruction and system organ malfunction. In order to comprehend the cancer generation mechanism, a deep study of the endocellular functions and extracellular interactions is necessary.

During the cell division stage (mitosis), the basic procedure for the survival and conservation of an organism, unnecessary daughterly cells, due to gene disorder, may be generated, while the old cells do not complete their life circle. Thus, the balance between normal cell division rate and normal cell death has been unsettled. This redundant amount of cells form abnormal lumps (tumors), utilize the physical and chemical environment needed for normal cells to remain functional, eliminating their "resources" and decelerating the function their role implies. The human organism is not able to recognize the cancerous cells due to their similarity to the physiological ones and does not activate the immune system, facilitating their growth and invasion. Over the time, these tumors may metastasize to other parts of the body, affecting other organs as well. The cancer generation is mainly controlled by two classes of genes: a) **oncogenes**, which deregulate the control point of cell replication, leading to irregular and unbounded cell proliferation and b) **tumor-suppressive**, which intercept the uncontrolled action of oncogenes. Carcinogenesis includes the following stages:

- **Provocation phase**, normally lasting 15-30 years or less in case of long-lasting exposure to cancerous environmental factors, when abnormal cells are generated
- **In situ phase**, when progressive dysplasia turns to carcinoma in local tissue sections
- **Percolation phase**, when cells with malignant characteristics are proliferated with rapid rate and are capable of penetrating the cell membrane and invade to neighboring tissue or reach until the blood or node vessels
- **Dispersion phase**, when cancer cells overcome the initial growth area and are transferred, alone or in groups, to other regions via blood or lymphatic system affecting other organs or systems too [1].

Cancer is not infectious and "selective", it can affect every person, at every period of his/her life. Sometimes cells are genetically predisposed to mutate to cancerous and the exposure to different aggravating factors, such us radiation, chemical substances, venomous infections, environment, age, poor diet and day

life style might activate this mutation. In addition, this genetic cancerous predisposition might be inherited from generation to generation.

There exist over 200 types of cancer, each one needing its own treatment and cure scheme, having different response and tolerance to therapy [2]. All tumors are not cancerous, yet potentially dangerous for human health. Cancerous disease is mainly described with the terms carcinoma, neoplasm or malignant tumor and constitutes the second most frequent cause of death in developed countries after the cardiovascular diseases. Yet, the majority of cancers can be treated, especially if diagnosed in early stage.

Cancer diagnosis aims at identifying its type and position within the human body in order to predict the tumor evolution rate and schedule the appropriate treatment procedures. This is not easy, especially in the primary steps of the disease, as the asymptomatic period endures months or even years. As a result, the diagnosis might take place when the tumor has been widely grown, locally or peripherally. Symptoms such as palpable tumors, insistent cough and hematuria must activate the patient. The specialist is offered numerous means in his/her way to cancer diagnosis; these include hematological analysis, cytological and histological examination or imaging modalities. Thanks to the progress of medicine, the enrichment and development of the laboratory equipment, almost half of the diagnosed cancer types are cured, even with total absence of recrudescence. In the case of practically incurable cancer types/stages, the appropriate treatment offers months or even years of a generally qualitative life for the patient, eliminating symptoms such as a cough, pain or catatonia. Yet, as always claimed, prevention is the best prognosis and treatment.

A typical cancer identification tool is biopsy, a process where a tissue sample from the candidate pathogenic section is received in order to be examined under the microscope. Tissue samples are prepared surgically or via the fine needle procedure. Microscopic examination will reveal the extent of tumor malignancy and determine the follow-up of the patient. The most standard of tumor classification is the TNM system, where the expert assigns a score on each of the three system parameters:

- T (Tumor) – tumor size and growth extent
- N (Nodes) – extent to which the tumor has spread in the neighboring nodes
- M (Metastasis)– extent of metastasis to remote regions of the body

Thus, the disease stage is characterized as **in situ** (locally generated), **aggressive** (invasion to neighboring tissue sections) or **metastatic** (metastasis to other organs). As regards cancer treatment, this includes the classical approaches of surgery, radiation, chemotherapy, immunotherapy and the newly developed biological therapy and hormone therapy, reinforced by research studies and programs targeting at the understanding of the genetic mechanism of cancer cells.

Breast cancer constitutes one of the most frequent types of cancer among women. It is estimated that almost half a million new incidences of breast cancer are diagnosed in Europe, while in America, based on incidence rates, a woman has a one in nine chance to develop breast cancer a time period within her life [3]. Over the last years, the survival percentage has been raised significantly, although it differs not only among countries but also among health centers, emphasizing

that breast cancer can be efficiently treated and cured when it is diagnosed in the first stages.

The majority of breast tumors are not malignant. They are usually vesicas (sacs containing liquids) or fiber-nodes (solid masses of fibers and nodes) and are easily and effectively treated via surgical removal. Although the mechanisms that activate breast cancer are not known, factors such as inheritance, age, menopause (late menopause or early beginning of catamenia decrease the breast cancer risk), childbearing, contraception treatment (women under treatment have limited risk), hormone therapy and fat consumption determine the appearance risk of the disease [4].

Symptoms such as touchable nubbins, changes in the size, shape, color and texture of breast or nipple or armpit swelling should alarm the person for examination. Annual mammography examination for women over fifty years old and monthly mirror self-examination of breast are routine examinations that can facilitate the early diagnosis of the disease, which is essential for the effective treatment of cancer. Clinical diagnostic methods include:

- **Mammography**, where X-ray radiation efficiently reveals abnormalities in tissue physiology, even in very preliminary stages, which overcomes the instantaneous pain felt due to the pressure exercised on the breast
- **Sonography**, where echo sounds emitted by the breast are received by a microphone, leading to further determination of any possible abnormality (e.g. if the tumor is in solid or liquid phase)
- **Color Doppler**, where color imaging of the tumor area takes place and its malignancy or not is determined
- **Magnetic Tomography**, where the magnetic radiation absorbed by the breast tissue is measured and depicted in a slide revealing any suspicious finding within the examined body section
- **Needle aspiration/biopsy**, where cells are received from the tumor via the needle and are sent to a cytological/histopathological laboratory for further examination, having the drawback of limited efficiency due to the possibility of not precisely targeting the tumor
- **Surgical removal**, where the tumor is invasively removed from the body section after total anesthesia and is then sent for biopsy evaluation.

Current therapy approaches have significantly increased the survival period of the patient; the selection of the treatment methods depends on the type of cancer (ductal carcinoma, lobular carcinoma, angiosarcoma), the stage of the disease, the patient's age and medical history, the size of the tumor and its classification under the microscope. For the early stages surgical removal of the tumor or even the whole breast is recommended, supplemented by radiotherapy in the affected tissue in order to exscind the remaining malignant cells and/or possible hormone or drug therapy for more efficient prolepsis and control of the spawning of cancer. For the latter stages, hormone therapy or chemotherapy are adopted among a wide variety of drugs that can meet the needs and specificity of each individual organism along with radiotherapy which targets on possible metastasis to other organs or systems. The lymph nodes in the axillary area are also carefully examined as they are considered the most important and probable "carrier mean" to transfer cancerous cells to other sections of the organism.

1.2. The HER2/neu oncogene

The mutation of cells to cancerous is considered as a destabilization of the factors that control their natural growth or the augmentation of their receptors, which leads to auto-stimulation of their growth. Early clinical cancer diagnosis is almost impossible, as the common procedures are incapable of detecting cell masses/tumors of size over 1-2 cm. When cancer is evolved in the human organism, tumor cells or body tissues may produce substances that can be detected in blood, tissues or urea via monoclonal antibodies and are characterized as tumor markers. Sometimes tumor biomarkers, also known as oncoproteins, are present during the physiological growth of tissue. The need for detecting such markers arises in the period prior to diagnosis, when the specialist suspects the presence of cancer and during the treatment period, after diagnosing the disease, in order to attend and control its evolution. Recent medical advances have led to the identification of numerous tumor biomarkers facilitating the understanding of the molecular basis of tumor progression and treatment response. Prognostic markers aim to objectively estimate the patient's overall outcome, while predictive markers focus on the objective evaluation of the possible benefits from a specific clinical intervention. Although a wide variety of biomarkers have been tested and achieved promising outcomes, a limited number of these have been adopted in standard clinical practice over the past decades [1, 5].

The HER-2 gene (also called HER2/neu, c-erB2, ERBB2 or neu) is notable for its role in the pathogenesis of breast cancer and as a target of treatment. It derived its name from a neuroglioblastoma cell line in rat (called "neu"), where it was discovered more than 25 years ago and encodes a cell membrane surface-bound receptor tyrosine kinase, forming a proto-oncogene located at the long arm of human chromosome 17 [6]. It is named HER2 because it has similar structure to human epidermal growth factor receptor, or HER1. In human cancers, c-erB2 is activated via gene amplification, which is a genomic mutation where a small fragment at chromosome band 17q12-q21 is multiplied in a cell up to 100 folds. HER2 is co-localized, and thus most of the time co-amplified with the gene GRB7, which is, as well, a proto-oncogene (active in e.g. breast cancer, testicular germ cell tumor, gastric cancer, and esophageal cancer). This gene amplification leads to overexpression of its protein product, which disturbs the HER-receptor family signaling networks and forms heterodimers with EGFR, HER-3 and HER-4 upon binding of their ligands [7]. In addition, overexpressed HER-2 proteins form HER2-HER2 homodimers, the major oncogenic activation mechanism. Findings in the early 1990's revealed that antibodies to the extracellular domain of HER-2 inhibit growth of HER-2 positive cell lines, which gave rise to test the most promising growth inhibitory antibody as an anti-cancer drug.

One of DNA's major functions is to serve as the blueprint for the manufacturing of the proteins that are used to keep cells alive. Like all proteins, the HER2 protein is the result of certain patterns of DNA. The segment of DNA that codes for HER2/neu is called an "oncogene" and it is the HER2/neu oncogene that produces the HER2/neu protein. All normal epithelial cells contain 2 copies of the HER2 gene and express low levels of HER2 receptor on the cell surface. In some cases, during oncogenic transformation, this segment of DNA becomes damaged as the cells reproduce and the number of gene copies per cell is increased, leading to an increase in mRNA transcription and a 10- to 100-fold

increase in the number of HER2 receptors on the cell's surface, called overexpression. This process is illustrated in Figure 2.1.

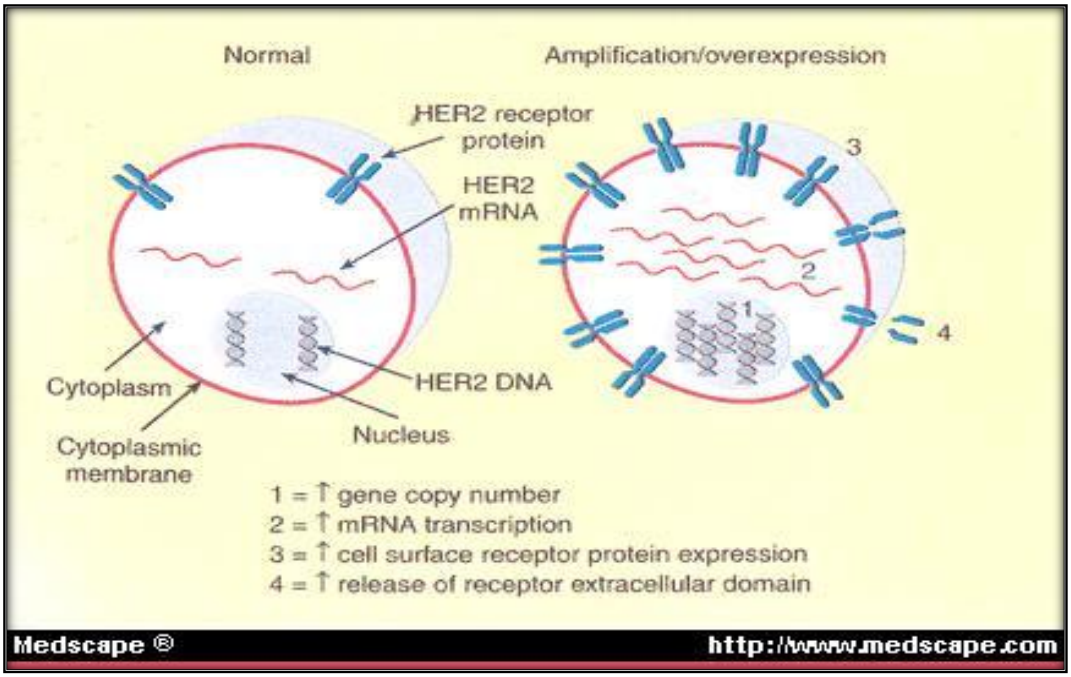

Figure 2.1: Indicators of HER2 status: gene or DNA amplification and mRNA or protein overexpression (Source: Medscape)

In vitro and animal studies indicate that HER2 gene amplification and protein overexpression play a key role in oncogenic transformation, tumorigenesis and metastasis [8]. It is pointed out that the growth of tumors and cancer cell lines that overexpress the HER2 receptor is inhibited by anti-HER2 monoclonal antibodies, further indicating the role of HER2 gene amplification/receptor overexpression in oncogenesis. Gene amplification/receptor overexpression has been demonstrated in breast, ovarian, bladder, gastric, and pancreatic tumors. Gene amplification is associated with aggressive cell behavior and poor prognosis, as depicted in Figure 2.2.

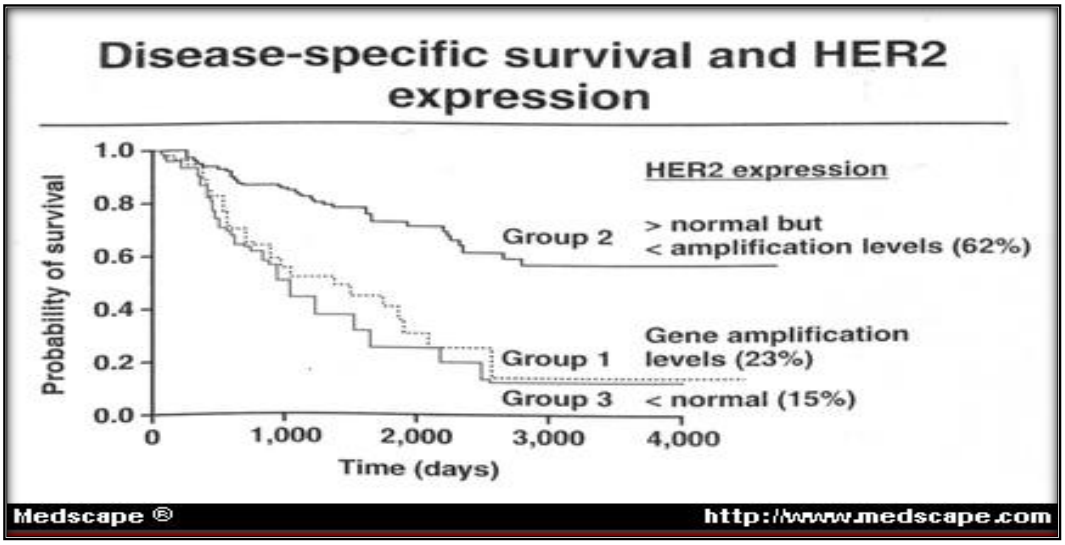

Figure 2.2: Disease-specific survival and HER2 expression (Source: Medscape)

Some tumors show receptor overexpression without gene amplification and have a more favorable prognosis, yet the biologic significance of this variant is less certain. In general, the presence of HER2 amplification/overexpression appears to be a key factor in malignant transformation and is predictive of a poor prognosis in breast cancer.

The prognostic role of HER-2/neu amplification or overexpression lies on the weak unfavorable prognosis in untreated breast cancer patients while its predictive implications include resistance to hormonal therapy [9], resistance to chemotherapy [10, 11], responsiveness to doxorubicin [12] and, mainly, responsiveness to Trastuzumamb (Herceptin) therapies [13,14]. Approximately 15-20 percent of breast cancers appear an amplification of the HER2/neu gene or overexpression of its protein product. Overexpression of this receptor in breast cancer (also met in other types of cancer too) is associated with increased disease recurrence and worse prognosis. Because of its prognostic role as well as its ability to predict response to trastuzumamb, breast tumors are routinely checked for overexpression of HER2/neu. Herceptin is a monoclonal antibody that was developed specifically to target the HER2/neu protein expressed only in the cancer cells while leaving normal cells (which don't overexpress the protein) unaffected. This makes Herceptin different from chemotherapy, which kills all rapidly dividing cells, both healthy and cancerous, but sort of like tamoxifen, which only work in hormone-responsive tumors.

Breast cancer was the first tumor type in which abnormalities of HER2 gene copy number and/or expression were associated with reduced disease-free and overall survival. Scientists have focused on HER2 over the past 25 years and have succeeded in confirming overexpression. Patricia Rovelon, a nurse from the Institut Gustav Roussy in Villejuif, France, pointed out that HER2 is universally accepted as a new prognostic marker and predictor of therapeutic response. But she and other speakers cautioned that the prognostic value of HER2 varies, depending on the assay method used. Leaders in the field of HER2 have stressed the importance of developing a simple and accurate method of determining HER2, one that is both inexpensive and reproducible. If breast cancer is tested for HER2 status, the results will be graded as positive or negative. If the results are graded as **HER2 positive,** that means that the HER2 genes are over-producing the HER2 protein and that those cells are growing rapidly and creating the cancer. Tumors are faster growing, more aggressive and less sensitive to chemotherapy and hormone therapy. If the results are graded as **HER2 negative,** then the HER2 protein is not causing the cancer. There is also a middle situation, generally considered as healthy but needing attention every few months, where there is a controlled augmentation of the HER2 protein. The main methods for testing HER2 breast cancer are [15]:

- **IHC: ImmunoHistoChemistry** - this test measures the production of the HER2 protein by the tumor. The test results are ranked as 0, 1+, 2+, or 3+. If the results are 3+, the cancer is HER2-positive.
- **FISH: Fluorescence In Situ Hybridization** - this test uses fluorescent probes to look at the number of HER2 gene copies in a tumor cell. If there are more than 2 copies of the HER2 gene, then the cancer is HER2 positive.

The 2 techniques currently used to measure HER2 gene copies are quantitative polymerase chain reaction (PCR) and fluorescence *in situ* hybridization (FISH). The process for PCR is fully automated and requires only minimal amounts of tumor tissue. This method will allow retrospective studies to be performed with archival tissue. FISH also only requires small tissue samples and has extreme sensitivity to detect amplification from a histologic section. However, FISH is not widely available in hospital laboratories. The result of this method can vary considerably if the assay is not standardized and is thereby dependent on the skill of the pathologist. A more widely used test is immunohistochemistry (IHC), which measures HER2 protein expression. IHC has been specifically adapted for detection of HER2 protein using specific antibodies. The advantages of this method are that it can be used on fresh and archival tissue and that it utilizes technical and human resources readily available in pathology laboratories. Unfortunately, there are some disadvantages of this method. IHC uses different antibodies with different binding affinities and different epitope specificities, thereby creating differences in HER2 overexpression rates. In addition, HER2 overexpression scoring systems differ and often rely on subjective measures of staining intensity and pattern. When IHC staining techniques that are too sensitive are employed, it becomes problematic to differentiate between normal versus the high HER2 protein levels that are associated with gene amplification. The enzyme-linked immunosorbent assay (ELISA) is another method of testing HER2 protein in serum samples. While the technology is simple and well suited to automation, it may produce significantly different results to those obtained with IHC and FISH. While IHC and FISH measure HER2 receptor protein (mostly intracellular) and gene amplification respectively, ELISA specifically measures levels of the extracellular HER2 receptor proteins released into the plasma from HER2 overexpressing tumors.

It is widely acknowledged that the ideal test for HER2 status is one that is simple to perform, specific, sensitive, standardized, stable over time, and allows archival tissue to be assayed. At present, the test that best meets these criteria is IHC. A detailed analysis of Immunohistochemistry will be given in section 2.2.2. With standardization of laboratory testing and appropriate quality control in place, the reliability of IHC will be improved further. It is expected that FISH will become more widely used in the future as well. Figure 2.3 illustrates the standardized diagnosis – treatment scheme followed by pathologists for Her2/neu evaluation. It is noted that in ambiguous Her2/neu status estimation a combination of the two methodologies is adopted for assessing a valid and robustly interpreted result.

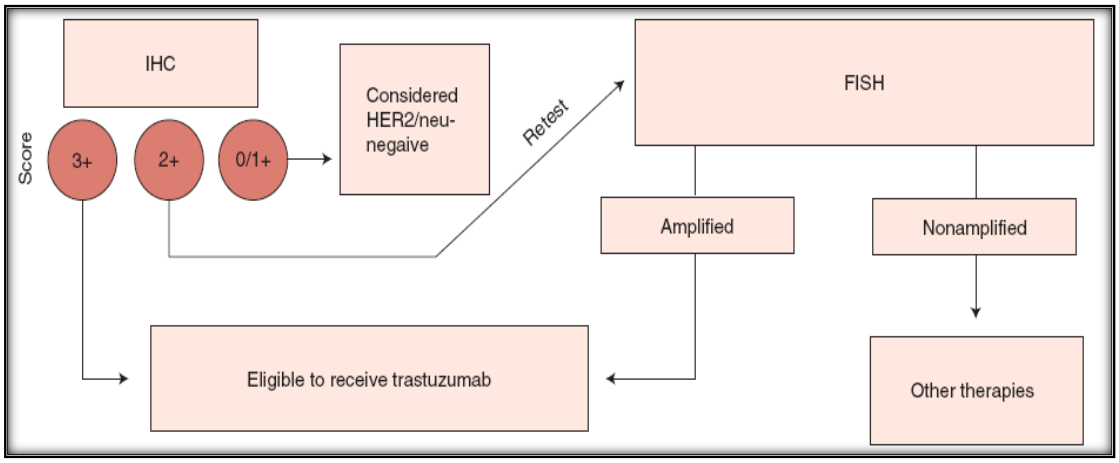

Figure 2.3: Standardized Her2/neu cancer diagnosis-treatment scheme

Standard management in the treatment of many solid tumors has improved in recent years, yet many metastatic solid tumors remain incurable. Factors that limit the success of treatment include drug resistance and lack of tumor selectivity. Although progress has occurred in cytotoxic therapy for breast cancer, interest in new interventions continues. Because of the ability of the immune system to target specific responses, the area of immunotherapy has great potential in future management of cancer.

Many patients who are currently being tested for HER2 status are women with metastatic breast cancer who have been heavily pretreated. Therefore, it is important to gather information about the patient's health history, performance status, all prior treatments, emotional well being, as well as the understanding of the disease status, the meaning of HER2 testing and its possible implications. Nurses may collaborate with other practitioners in obtaining any or all of this information. It is also critically important to involve family members in the process of gathering accurate and thorough information.

It is also useful for oncology nurses who counsel patients to be fully aware of the advantages and disadvantages of the various testing methods and the impact that these test methods and results may have in terms of prognosis and treatment for the patient. This may require detailed communication with the pathologist about how the test sample was obtained, clarification with the laboratory about the test method employed (and its potential variability) and discussion with the oncologist to interpret the results. Knowledge of testing methods and a determination of the accuracy of results is critical to appropriately identify patients that may benefit from anti-HER2 therapies.

Problem Setup and Thesis Overview

The main contribution of the present master thesis covers fields of tissue evaluation. The objective is to thoroughly analyze tissue-imaging modalities that enable tissue characterization. We explore two main modalities, one in exploratory phase based on polarimetry and the other based on IHC and microscopy. The former concept enables a rough but fast exploration of tissue matter at macroscopic level, while the second enables the more detailed analysis of microscope images of tissue obtained through the procedure of immunohistochemistry (IHC). IHC is the localization of antigens in tissue sections by the use of labeled antibody as specific reagents through antigen-antibody interactions that are visualized by a marker such as fluorescent dye, enzyme, radioactive element or colloidal gold [16].

Our contribution in polarimetric image analysis is based on the modelling of intensity distributions for different materials. Alternatively, our research on IHC microscopy is focused on the automated detection of Her-2 neu (also known as Cerb-2) protein overexpression in tissues in order to diagnose breast cancer at its earlier stages and help the patient cure the disease with higher probability. The preparation and the processing of tissues is a purely medical, so complicated, issue and is not the main chapter of our thesis, however it is of substantial importance. A well prepared tissue will secure a clear and informative image. We are interested in automatically extracting the degree of protein overexpression on the cell membranes through image processing based on the characteristic identities the diseased tissues reveal after the application of immunochemistry.

There is limited literature and very few techniques developed for this research area. The usual procedure is the visualization of these IHC samples by a specialist (a pathological anatomy specialist), who carefully observes the extracted images under the microscope and manually calculates the number of affected cells within the breast tissue. Unfortunately, characterizing a tissue as diseased, healthy, semi-healthy or little-diseased cannot always be done subjectively. Two doctors may extract different results and conclusions for the same patient. Thus, the automation of this procedure becomes very critical, though very intriguing.

In order to formulate our analysis we need to explore the technical concepts of polarimetry and IHC microscopy. This is done in Section 2, where we present the fundamentals of these modalities, analyze the technological state of the art and present the novelties of our thesis in relation to these technical concepts. The image processing background that will form the analysis basis for the detailed form of IHC images is presented in Section 3. We discuss the state of art techniques used in histological images and discuss their advantages and limitations. The proposed methodology analysis is introduced in Section 4. We present the state of the art in segmentation methods related to IHC also addressing Her2 overexpression. Overall we deal with cell segmentation, membrane staining evaluation and tissue classification. Related work has been performed in cell segmentation; we discuss and compare our methodology with other techniques. The other two issues are rather new and have been developed partially and rather sporadically. Our study forms a systematic evaluation methodology and explores the potential of tissue classification based on a “ground truth” evaluation from an experienced doctor. Finally, the conclusions of our study are presented in Section 5 along with issues of further research.

2. Imaging Modalities

The contribution of this thesis relates to the effective identification of biological characteristics depicted in biomedical images derived using two fundamental imaging modalities: a) polarimetric imaging and b) optical microscopy. Image processing for feature extraction and statistical analysis for evaluation are utilized, aiming at diagnostic metrics for evaluating human tissue, which is crucial for cancer status diagnosis, characterization and treatment. In the following sections we present a detailed analysis of the fundamental aspects of each imaging approach along with the evaluation algorithms implemented. These algorithms are tested and evaluated on a number of images. By utilizing polarimetric imaging we extract characteristics of the tissue in a macroscopic level of analysis based on the optical identities of the tissue elements, studying their interaction with polarized light. Information about the shape, size and physical state (solid or liquid) of such tissue elements can be extracted. By utilizing microscope imaging of tissue slides we are capable of studying tissue at a cellular level, obtaining information about its morphology, shape characteristics (shape, perimeter, area) of cells and the distinct composite segments of each cell (cell nuclei, cell membranes, connective tissue)

2.1. Polarimetric Imaging

Diffused polarimetric reflection and backscattering provides unique, discriminatory material signatures, based on the depolarization of the impinging waves from different materials, which maximize the sensitivity and discrimination power of object imaging and identification techniques. With the development of multispectral polarization imaging technology, it is becoming more and more important to integrate polarimetric, spatial and spectral information so as to improve target discrimination based on optical contrast, which is essentially based on the physical properties of the materials involved.

Polarimetry is a technique that measures the extent to which a substance interacts with plane polarized light. It relies on the properties of polarization of backscattered light and results in distinct signatures related to surface smoothness, orientation and target composition [16, 17]. Further contrast enhancement of the target can be achieved by modulating the background of the target through doping with polar and high-index-of-refraction molecules [18, 19]. When linearly polarized light is passed through a substance containing optically active molecules (chiral molecules) or nonchiral molecules arranged asymmetrically, a rotation of the polarization vector take place. This phenomenon is called optical rotation or optical activity. Glucose molecules and most of the biological molecules such as proteins or enzymes are optically active molecules. Utilizing the rotation of the polarization vector enforced by optically active (chiral) molecules, together with efficient polarimetric interrogation techniques, yields both optical clearing and enhanced contrast capabilities, as initially reported in [20-22]. In fact, the use of active dopants aims at minimizing the refractive index differences between the target and the surrounding medium, resulting to an increase of both the degree of polarization (DOP) and the degree of linear polarization (DOLP). On the other hand, Stokes-parameter (polarimetric) imaging can capture such differences of the refractive index and leads to enhanced image contrast in the acquired images due to its potential to detect weakly backscattered linearly polarized radiation, in the presence of highly backscattered depolarized radiation. In fact, using optically active dopants in conjunction with polarimetric imaging yields an efficient recognition and

representation of specific molecular signatures for disease characterization and molecular imaging.

Recently [22], backscattered laser beam contributions from biological fluids doped with optically active molecules were reported utilizing single-detection auto-balanced polarimetric detection principles. The outcome of that study indicates that both Detective Quantum Efficiency (DQE) and DOLP of backscattered optical signals increase with increasing the concentrations of molecular optically active dopants. This translates to enhanced signal-to-noise ratio and contrast. The efficiency of imaging techniques in discriminating material structures can be further improved via contrast measurement and enhancement in digital images. In essence, the acquired images can be algorithmically enhanced so as to increase the perceived contrast of different materials, thus facilitating the discrimination and the study of material properties. One of the goals of this thesis was to supplement the above assumptions and support qualitatively and quantitatively the efficiency of detecting modalities in polarimetric data through statistical analysis and histogram modeling approaches.

2.1.1. Polarimetric imaging fundamentals

Image samples processed in this work were captured utilizing the Multifunctional Polarimeter System of the University of Akron, depicted in Figure 2.4. This is a highly reconfigurable and scalable in-house designed optical system, equipped with a combination of the objective and tube lenses, with enhanced multispectral, polarimetric, macroscopic, and microscopic imaging capabilities. Prior to any measurements, multiple calibration procedures of the optical system were undertaken to ensure optimal optical system alignment and control of the polarization systematic errors. The calibration procedures along with the intensity of the finally incident beam in the CCD camera is controlled by the relevant position and rotation of the polarizers and the retarders.

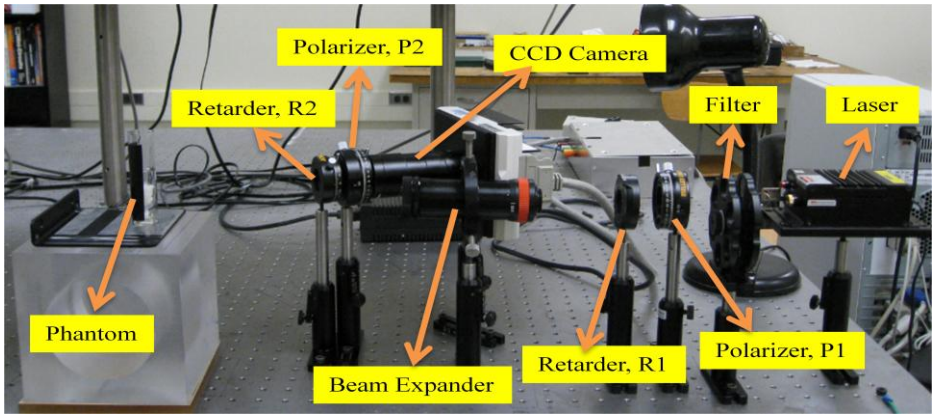

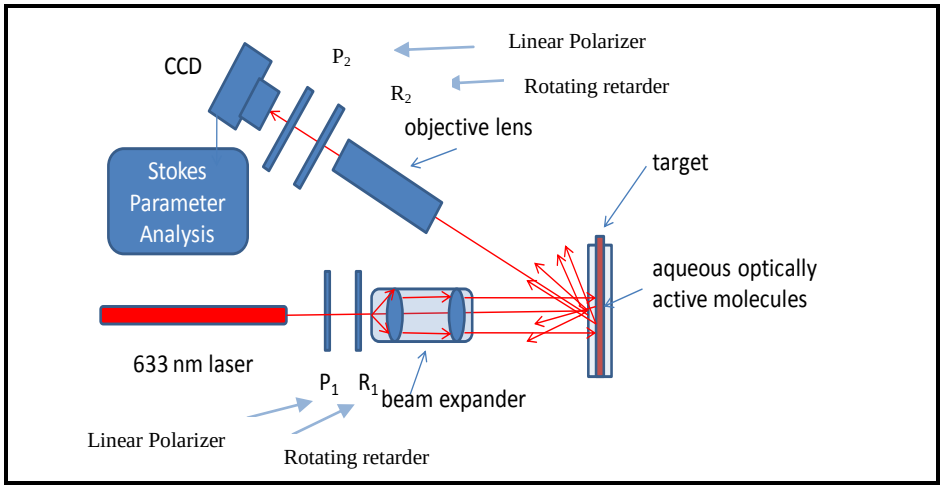

Figure 2.4 The Multifunctional Polarimeter Imaging System of the University of Akron

A target phantom is stimulated by a laser beam and the backscattered light is captured through a carefully designed and calibrated "detection line". The optical transceiver geometry consisted of a transmitter generator and a receiver analyzer. The imaging system contained two arms; a polarization generating branch and a polarization analyzing branch. Light from the laser source was sent through the polarization generating branch that consists of a neutral density filter (attenuator) determining the wavelength of the emitted light, a linear polarizer P1, a quarter-wave retarder R1 and a beam expander. The light from the laser was passed through a neutral density filter onto a linear polarizer P1. The linearly polarized light then passed through a quarter-wave retarder R1 which converted it to circularly polarized light. The circularly polarized light was then allowed to illuminate the phantom. The polarization analyzing branch contained a quarter-wave retarder R2 followed by a linear polarizer P2 (parallel to P1) which was placed in front of a CCD camera in backscattering geometry as shown in Figure 2.4. The retarder R2 was used to convert the circularly polarized light remitted by the phantom to linearly polarized light and this light was sent to the CCD camera through a linear polarizer P2 . The polarizer P2 was always kept fixed parallel to P1 to account for the polarization sensitivity of the detector. The retarder R2 was rotated from 0^o to 180^o in steps of 22.5^o such that the backscattered light intensity contributions by the phantom in the direction of the analyzing branch were acquired by the CCD camera. When both the polarizers P1 and P2 are oriented for maximum transmission, they are said to be co-polarized or parallel to each other and when P1 is oriented for maximum transmission and P2 is oriented for minimum transmission, they are said to be cross-polarized or perpendicular to each other. Therefore, eight intensity images were obtained. The Degree of Polarization (DOP) and Degree of Linear Polarization (DOLP) was estimated by measuring the Stokes parameters of backscattered signals, relating the detected backscattered signal intensities to the Stokes parameters, through the Mueller matrices of the analyzer optics, by means of the "Fourier Analysis using a Rotating Quarter-Wave Retarder Method" [23].

The transmitter generator system consisted of a laser beam of desired wavelength coupled to a Melles Griot FPG 001 linear polarizer and to a λ/4

retardation plate. Specifically, a New Focus Berek polarization compensator, operating between 200 nm and 1600nm was used as a variable quarter wave. On the other side, the receiver analyzer geometry consisted of a high performance Mitutoyo objective lens and a tube lens coupled both to a λ/4 phase retarder. The light output from the phase retarder was directed into the input of a charge coupled device (CCD) after passing through a Melles Griot FPG 001 linear polarizer. The polarimetric imaging system was utilized to image a specific ROI of the target, with a 50-60X total magnification, taking into account the magnification of the objective lens of the CCD camera, achieving optical performance of a microscope. An electrically cooled 1401E Photometrics Sensys/Roper Scientific digital (CCD) camera has been used throughout these experiments consisting of a Kodak KAF1401E, scientific grade 1317x 1035 electronic image array, with an active imaging area of 9.0mm x 7.0mm. This camera offers 6.8 x 6.8 μm pitch resolution, high-quantum efficiency, and 12 bit digitization. Experiments were performed under backscattered light geometry. The polarization interaction with the scattering medium, displayed as a transformation of the polarization state, is captured by a CCD camera, producing the polarimetric images.

The states of polarization of a target can be characterized through its four Stokes parameters (S_0, S_1, S_2, and S_3). These Stokes parameters can be written as a column matrix form, called Stokes vector, according to:

$$S=\begin{pmatrix} S_0 \\ S_1 \\ S_2 \\ S_3 \end{pmatrix} \quad (2.1)$$

For a partially polarized light, the total light intensity, S_0, is offered in terms of the three polarization states S_1, S_2, and S_3 as [24]

$$S_0^2 \geq S_1^2 + S_2^2 + S_3^2 \quad (2.2)$$

where S_0 is the total detected light intensity, of which S_1 expresses the difference between linear horizontal and vertical polarization states, S_2 expresses the difference between the linear +45◦ and −45◦ polarization states, and S_3 expresses the difference between the right and left circular polarization states. For the needs of this study, we mention that the polarimetric arrangement of the "Rotating Retarder Polarimeter Method" [25] was combined with the "Polarimetric Measurement Matrix Method" [26], in order to obtain enhanced DOLP and DOP images. The proposed methodology allows one to estimate the four Stokes parameters of the target based on the Mueller Matrix of the optical system. The Stokes vector $\boldsymbol{S}_{out}$, at the input of the detector, is related to the incident Stokes vector $\boldsymbol{S}_{inc}$ at the input of the analyzer through the Mueller matrix M, where M describes the elements of the analyzer polarization of the phase retarder and the polarizer in front of the

detector, including instrumental polarization and polarization sensitivity of the detector, defined as:

$$M=M_p \cdot M_r \qquad (2.3)$$

where M_r and M_p are the Mueller matrices of the analyzer retarder and polarizer elements, respectively. Yet, the Stokes vector at the input of the detector will be approximated following the next formula:

$$\boldsymbol{S_{out}} = \boldsymbol{M S_{inc}} \qquad (2.4)$$

where $\boldsymbol{S_{inc}} = (\boldsymbol{s_0} \quad \boldsymbol{s_1} \quad \boldsymbol{s_2} \quad \boldsymbol{s_3})^T$ is the Stokes vector incident on the polarization state analyzer. The Mueller matrix for an optical system is a 4x4 array that maps the transformation between the Stokes vector S_{inc} incident on an object and the vector S_{out} that is transmitted or deflected or scattered from the object. The Mueller matrix also captures information about all the optical components that are present in the system between the incident and the transformed vector. This means that each of the components can be individually characterized by its own Mueller matrix M_i and the resulting matrix M can be expressed as a product of all the individual Mueller matrices. There are numerous ways of measuring the Stokes parameters of a beam of light and the most common is the Fourier analysis method that uses a rotating quarter-wave retarder to obtain the Fourier coefficients having the advantage that the Stokes vector can be directly obtained from the Fourier coefficients. To obtain the coefficients, the total Mueller matrix must be derived from the various components of the system. The experimental setup of the system shows that the Stokes vector of the beam scattered from the sample is affected by the rotating retarder and the linear -45^o polarizer.

In order to get familiar with the concepts above, an example of Stokes parameter calculation is presented in the following lines. Let the Mueller matrix of a rotating quarter –wave retarder of angle θ be:

$$M_r = \begin{pmatrix} 1 & 0 & 0 & 0 \\ 0 & \cos^2 2\theta & sin2\theta \cos 2\theta & \sin 2\theta \\ 0 & sin2\theta \cos 2\theta & \sin^2 2\theta & -cos2\theta \\ 0 & \sin 2\theta & cos\, 2\theta & 0 \end{pmatrix} \qquad (2.5)$$

In addition, let the Mueller matrix of the linear horizontal linear polarizer be:

$$M_p = \begin{pmatrix} 1 & 1 & 0 & 0 \\ 1 & 1 & 0 & 0 \\ 0 & 0 & 0 & 0 \\ 0 & 0 & 0 & 0 \end{pmatrix} \qquad (2.6)$$

The polarimetric system acquires q-optical polarimetric images (q is determined by the different values of rotating angle θ), obtained through optical interrogation of the target. The Mueller calculus equation is:

$$S_{out} = M_p M_r(\theta_q) S_{inc}$$

$$\begin{pmatrix} s_{out0} \\ s_{out1} \\ s_{out2} \\ s_{out3} \end{pmatrix} = \frac{1}{2}\begin{pmatrix} 1 & 1 & 0 & 0 \\ 1 & 1 & 0 & 0 \\ 0 & 0 & 0 & 0 \\ 0 & 0 & 0 & 0 \end{pmatrix}\begin{pmatrix} 1 & 0 & 0 & 0 \\ 0 & \cos^2 2\theta_q & \sin 2\theta_q \cos 2\theta_q & \sin 2\theta_q \\ 0 & \sin 2\theta_q \cos 2\theta_q & \sin^2 2\theta_q & -\cos 2\theta_q \\ 0 & \sin 2\theta_q & \cos 2\theta_q & 0 \end{pmatrix}\begin{pmatrix} s_0 \\ s_1 \\ s_2 \\ s_3 \end{pmatrix}$$

$$= \frac{1}{2}\begin{pmatrix} 1 & \cos^2 2\theta_q & \sin 2\theta_q \cos 2\theta_q & \sin 2\theta \\ 1 & \cos^2 2\theta_q & \sin 2\theta_q \cos 2\theta_q & \sin 2\theta_q \\ 0 & 0 & 0 & 0 \\ 0 & 0 & 0 & 0 \end{pmatrix}\begin{pmatrix} s_0 \\ s_1 \\ s_2 \\ s_3 \end{pmatrix} \qquad (2.7)$$

The Stokes parameter in the front of the detector, after passing through the retarder-polarizer configuration, is:

$$S_{out} = \frac{1}{2}\left(S_0 + S_1 \cos^2 2\theta + S_2 \sin 2\theta \cos 2\theta + S_3 \sin 2\theta\right)\begin{pmatrix} 1 \\ 1 \\ 0 \\ 0 \end{pmatrix} \qquad (2.8)$$

But $S_{out0}=I(\theta_q)$= output I at the detector, proportional to the incident intensity is given as:

$$\begin{aligned} S_{out0} = I(\theta_q) &= \frac{1}{2}\left(S_0 + S_1 \cos^2 2\theta_q + S_2 \sin 2\theta_q \cos 2\theta_q + S_3 \sin 2\theta_q\right) = \\ &= \frac{1}{2}\left(S_0 + S_1 \frac{\cos 4\theta_q - 1}{2} + \frac{S_2}{2}\sin 4\theta_q + S_3 \sin 2\theta_q\right) = \\ &= \frac{1}{2}\left(S_0 - \frac{S_1}{2} + \frac{S_1}{2}\cos 4\theta + \frac{S_2}{2}\sin 4\theta_q + S_3 \sin 2\theta_q\right) \end{aligned} \qquad (2.9)$$

Rewriting the intensity expression $I(\theta_q)$ in terms of its trigonometric half-angle formula reduces it to the standard form of the truncated Fourier series given in Equation 2.10. It is seen from this expression that the output intensity is described by four Fourier coefficients namely A (the DC component), B, C and D (the frequency harmonics):

$$\begin{aligned} S_{out0} = I(\theta_q) &= \frac{1}{2}\left(a_0 + \sum_{n=1}^{\infty} a_n \cos n\omega t + \sum_{n=1}^{\infty} b_n \sin n\omega t\right) = \\ &= \frac{1}{2}\left(A + B\cos 4\theta_q + C \sin 2n\theta_q + D \sin 4n\theta_q\right) \end{aligned} \qquad (2.10)$$

where $\omega t=2\theta_q$ and θ_q is the step size of the rotation of the analyzer retarder. It is seen that the Stokes parameters can be obtained from coefficients A, B, C, D combing equations 2.9 and 2.10, resulting in :

$$S_0 = A-B, \quad S_1 = 2B, \quad S_2 = 2D \text{ and } S_3 = C \qquad (2.11)$$

where $A = S_0 - S_1/2$, $B = S_1/2$, $C = S_3$ and $D = S_2/2$

The degree of polarization (DOP) and linear polarization (DOLP), can be then estimated in terms of Stokes parameters, S_0, S_1, S_2, S_3 as:

$$DOLP = \frac{(S_1^2 + S_2^2)^{1/2}}{S_0} \quad (2.13)$$

$$DOP = \frac{(S_1^2 + S_2^2 + S_3^2)^{1/2}}{S_0} \quad (2.14)$$

2.1.2. Extraction of material properties

An attempt was made to further expand the detection principles of [22] by fusing active-dopant polarimetric modalities with digital imaging concepts, for effectively exploring and quantifying physical properties of materials. The contribution of this thesis to polarimetric imaging is to further explore the impact of optically active and high-index of refraction molecules on the image quality, by doping the surrounding background of the target. All the Stokes parameters images were quantified based on established image metrics and statistically analyzed. The dual hypothesis was that: a) the polarized (DOLP and DOP) images are superior to the total intensity (S_0) images; and b) polarimetric images acquired through doping of the background would be of superior image quality from both polarimetric only and non-polarimetric images. Specifically, three different experiments are analyzed, where the reference images include a structure ("target" or "phantom") immersed into aqueous solution surrounded by optically active substances ("dopants") in various concentrations. The experiments at the material level consider the impact of optically active molecules on the image quality, by doping the surrounding background of the target. The experimental setup is illustrated in Figure 2.5. In all experiments presented, the simple experimental dopants are used with the aim of imitating the behaviour of more complex materials (such as biological tissues), acting as a simulating, pre-clinical procedure in order to expand the proposed methodology to biomedical applications. The idea of the phantom design is to emulate a biological scenario that would be optically homogeneous and absorbing medium.

In the **first set of experiments**, DOP images with a 40 x magnification factor at different concentrations of the enzyme L-Phenylalanine in aqueous solution are extracted using a broadband light source at wavelength of 830 nm. A twisted plastic wire phantom with a refractive index of 1.46, similar to hydrated collagen (n=1.47) and diameter 1mm, attached to a glass test tube was used as the phantom for this set of experiments.

In the **second set of experiments**, the testing phantom consists of a plastic hollow cylindrical structure (index of refraction 1.55) immersed into 11 ml of water. The DOLP images for different concentrations of alcohol and salt aqueous solution using broadband light source at 633nm were obtained. The polarimetric imaging system was utilized to image a specific ROI of the target, with a 50-60X total magnification, taking into account the magnification of the objective lens of the CCD camera.

In the **third set of experiments** the biological phantom consisted of a cluster of polypropylene spheres (refractive index n=1.49) with diameter 2mm and high-density polyethylene spheres (refractive index n=1.54) with diameter 3.5mm bonded with epoxy adhesive (refractive index n=1.65) immersed in

water solution. Six DOLP images with a 40X magnification were obtained for different concentrations of glucose aqueous solution using broadband light source at 655nm. This set of experiments was performed following the above experimental properties so that to emulate biological compounds, namely, calcified structures (n=1.53), hydrated collagen (n=1.47) and highly calcified mineralized structures (n=1.65). Typically, micro calcifications depending upon their shape, geometry and composition can be classified as precursors of malignancies in breast mammography. Systematic differences between hydrated collagen in the intensities between the collagen of malignant, benign and normal tissue groups appear to be due to a significantly lower structural order within the malignant tissues [27].

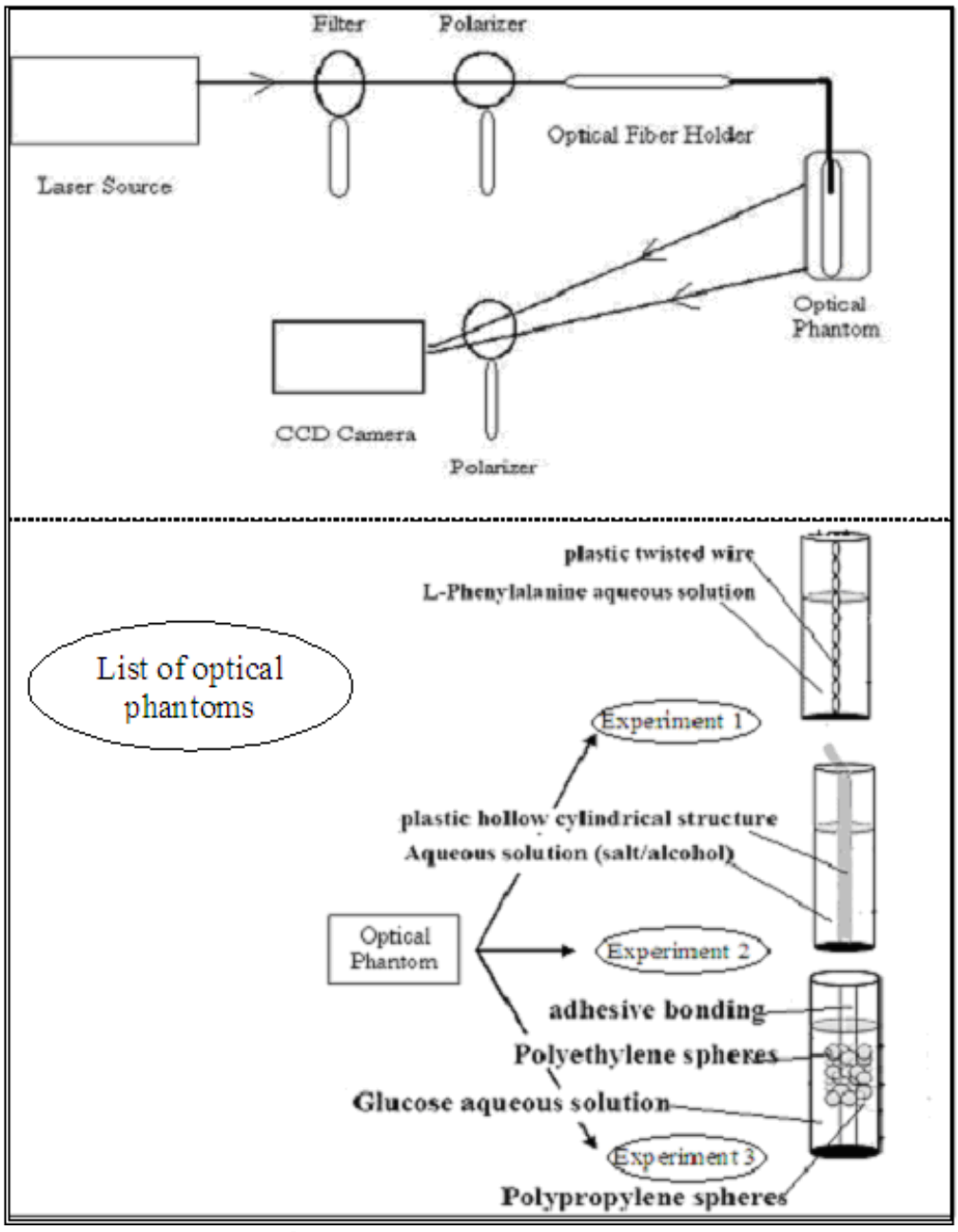

Figure 2.5 Experimental setup

Aiming at a concrete procedure of quantifying the contrast effects of the tested imaging technique, we consider a statistical modeling of the digitally recorded DOLP images. More precisely, we apply robust fitting of the intensity distributions of the various materials depicted in the acquired images using mixture models and associate the image contrast with the separability of model distributions. Of course, several methods could have been tested for the purpose of digital image segmentation and object discrimination. Clustering methods could have been used instead based on either discriminant functions or distance metrics [28]. Such methods mostly aim at data driven partitioning of the image space. Nevertheless, the modeling approach proposed can exploit and test multiple stochastic fitting models and provides further flexibility in setting up histogram thresholds between fitted histogram models, for effective object separation. In a different direction, the overall histogram distribution may be directly decomposed into object components through principal component analysis [28], but such approaches require an extensive database of images from multiple experiments, which is difficult to obtain. The proposed approach based on histogram modeling provides a simple, yet effective means of pixel labeling and object segmentation, based on the statistical structure of intensity distribution within the region of interest.

A thorough analysis of the digital image distribution is performed, based on fitting the intensity histogram of the acquired images using mixture models, revealing additional characteristics of the polarized object structures [29]. Overall, the novelty of the proposed methodology combining polarimetry with digital image enhancement is twofold; (1) it can quantify the efficiency of polarimetric imaging modalities in discriminating materials of interest and (2) enables improved segmentation and discrimination of materials through the enhancement of fitted-model differences. The proposed methodology is tested with different histogram forms of DOLP and DOP images on the three sets of experiments. The physical purpose of these experiments is examining the effect of different chiral or high index of refraction molecules (glucose, salt, alcohol and L-Phenylalanine) when used as molecular contrast agents, in the image quality of a detected target immersed in an aqueous solution. The tangible outcome of our study is that enhanced DOLP and DOP is achieved with increasing the concentration of the optically active molecules, providing both optical clearing and enhanced contrast capabilities.

The model description of a histogram from a particular object can be used to effectively assign local pixels to the region of that object through the corresponding probability implied by the fitted statistical distribution. Normally, there is a variety of possible distributions that may serve as basis functions for the fitted model, which can be evaluated through theoretical or computational means. For instance, the histogram of a compact intensity region may be well fitted by a Gaussian distribution. According to Zhuang et al. [30], a smoothed gray-level histogram, convolved with a low-pass filter, is identical to a mixture of Gaussian distributions. That is, each object of an image can be represented as a Gaussian-like distribution in the entire gray level histogram with different mean, variance and magnitude values. This assumption transforms the histogram decomposition problem to that of estimating the parameters of a mixture distribution. This estimation process is

based on statistical, heuristic and iterative approaches, as well as on decision based criteria. For the estimation of parameters the authors of [31] have adopted the trust-region reflective Newton method as an iterative optimization tool in order to find the optimal parameters of their model. The expectation maximization algorithm is another iterative technique used for parameter estimation, which converges toward the maximal solution of the likelihood function [32].

In order to determine how well the estimated model approximates the initial distribution, several criteria have been successfully used for revealing the “goodness of fit”. As such a metric for our model we use the mean squared error (MSE), quantifying the amount by which the estimated curve $\bar{X}$ differs from the original one X, as:

$$E = \frac{1}{n-1} \sum_{i=1}^{n} (X_i - \bar{X}_i)^2, \tag{2.15}$$

where n is the number of samples i. We also consider the dB gain in the Signal-to-Noise-Ratio (SNR), defined as:

$$SNR = 10 \log_{10} \frac{\sum_{i=1}^{n} X_i^2}{\sum_{i=1}^{n} (X_i - \bar{X}_i)^2} \tag{2.16}$$

Depending on the properties of the imaging modality, the regions of different materials in the recorded image can be modeled and discriminated by means of the intensity or the texture of the corresponding region. For instance, two materials that absorb different portions of the incident radiation would be recorded as image regions of quite different intensities. In this case, the use of mixture models applied directly on the intensity of a smoothed intensity histogram could enable the separation of two distinct models, one for each material region. Alternatively, if the imaging modality favors the dispersion and extensive diffuse of light at grain levels, then the texture of different material regions would be preferred as a discriminant factor. In such cases, the modeling of the distribution of variance as an expression of texture would be most appropriate for characterizing the structure of material regions [33]. Furthermore, in the case of imaging modalities operating at quite low wavelengths, the combination of intensity and texture attributes could be appropriate for characterizing the contrast among different regions.

In order to suppress possible noise contamination in the intensity distribution, we process the local mean images obtained from 5x5 moving average filtering. In a similar way, the local variance images are acquired through the application of a 5x5 moving variance window shifted along the pixels of the entire image. The discrimination of image regions based on mean-intensity differences suggests the use of Gaussian-like distributions, while the discrimination based on texture measures such as variance necessitates the use of the Chi-Square distribution according to the theoretical analysis of variance. In essence, the Gaussian model for mean-intensity distribution is justified by either the assumption of a compact region for each

material, as in [33], or the central-limit theorem guiding the distribution of the local mean operator. Furthermore, the Gaussian assumption by itself enforces the chi-square distribution on the local variance estimates [34].

Using the Gaussian and the Chi-Square distributions as basis functions we can define the mixture of Gaussian and the mixture of Chi-Squared distributions for the mean intensity and variance, respectively. The input images to be processed include a structure of interest (or "target") and a surrounding region (or "background"). Due to the camera lens, the recorded image involves a circular region of interest (ROI), as depicted in Figure 2.6 and a supplementary area at the corners of the rectangular image, which is an irrelevant area. Thus, the mixture of Gaussians can be represented as a sum of three distributions; one that represents the target, one that represents its surrounding medium and one that represents the remaining region of non-interest, according to the following form:

$$f(x;\, A_i, \mu_i, \sigma_i) = \underbrace{A_1 \cdot \exp\left(-\frac{(x-\mu_1)^2}{2\sigma_1^2}\right)}_{\text{Target}} + \underbrace{A_2 \cdot \exp\left(-\frac{(x-\mu_2)^2}{2\sigma_2^2}\right)}_{\text{Background}} + \underbrace{A_3 \cdot \exp\left(-\frac{(x-\mu_3)^2}{2\sigma_3^2}\right)}_{\text{Remaining area}}, \quad (2.17)$$

where A_1, A_2, A_3 are the amplitude factors, μ_1, μ_2, μ_3 are the means and $\sigma_1^2, \sigma_2^2, \sigma_3^2$ are the variances of the distributions of the target, surrounding medium and remaining area, respectively. If we model the circular ROI only, then the last function in the model can be eliminated. Similarly, the mixture of (two) Chi-Square functions of interest can be represented as

$$f(\chi^2; \mathbf{A}, \mathbf{n}) = \underbrace{A_1 \cdot \frac{1}{2^{n_1/2} \cdot \Gamma(n_1/2)} \cdot (\chi^2)^{n_1/2-1} \cdot e^{-\chi^2/2}}_{\text{Target}} + \underbrace{A_2 \cdot \frac{1}{2^{n_2/2} \cdot \Gamma(n_2/2)} \cdot (\chi^2)^{n_2/2-1} \cdot e^{-\chi^2/2}}_{\text{Background}} \quad (2.18)$$

where $\Gamma(.)$ is the Gamma function, A_1, A_2 are the amplitude factors, and n_1, n_2 are the degrees of freedom of the distributions of the target and the surrounding medium, respectively. The term "degrees of freedom" is defined as the number of terms in the final calculation of a statistic, herein the chi-squared distribution that vary freely. The distribution of the local variance image of the remaining area has no significant contribution, as this region appears homogenous, thus its variance equals to values near zero. The mean of the χ^2 distribution is n, its variance is $2n$ and its mode equals to $n-2$ [34]. As the degrees of freedom increase, the Chi-Square function approximates the Gaussian one.

Having accurately defined the model of our hypothesis, the estimation of its optimal parameters is then performed in the least square sense. Thus, we need to find parameters vector p that best fits the equation (minimize the least square error):

$$\min_p \frac{1}{2} \left\| f(x;p) - y(x) \right\|_2^2 = \min_p \frac{1}{2} \sum_{i=1}^{m} \left(f(x_i;p) - y(x_i) \right)^2 \quad (2.19)$$

where x is the input data vector of size m (in our case m=255, which is the number of the different gray intensity levels), y is the observed histogram of x,

f(.) is the hypothetical model function and *p* is the parameters vector to be optimized. When we perform comparisons of different material types or concentrations under the same experimental setup, then we might need to scale the mixture models under comparison, so that the background mean remains fixed. In such cases a scaling procedure is also implemented, which aligns the background means but otherwise preserves the shapes of model distributions.

Each imaging system is characterized by its own spatial, spectral and intensity resolution, expressing its ability to sense and detect even small differentiations within regions of the image. Overall, the better the contrast achieved the better the effectiveness in correctly segmenting the regions associated with different materials in the image. The acquired contrast is an attribute of the imaging modality used and can be quantified by metrics applied on the recorded image. Furthermore, histogram processing of the digital image can further contribute to contrast enhancement. Thus, the selection of appropriate models for the different areas of the histogram not only enables the quantification of contrast but can also facilitate the process of contrast enhancement.

In order to quantify robust contrast metrics, we employed the statistical modeling schemes of the polarimetric input images. We have already analyzed the modeling of the distribution of intensities of the various materials depicted in the acquired image. Here, we associate the image contrast with the separability of model distributions. The distance of the distribution centers reflects the structural differences of the two regions (target and surrounding medium). Thus, we propose to use the *Difference of Modes (DoM)* as a contrast measure of images [29]. The larger the difference the better the two regions are discriminated, which reveals contrast enhancement. For the mixture of Gaussians model, the contrast metrics is defined as the difference of the distribution means (equivalent to modes). Alternatively, for the mixture of Chi-Square functions, the contrast measure is computed as the difference of the modes of the foreground and the background distributions.

In order to compare the effects of the optically active molecules at different concentration levels, we model the distributions of the acquired images. In the first set of experiments, within the area of interest, marked by a circle, we find low-intensity water segments mixed with the optical dopant at higher intensity levels. Due to the high magnification of the detection system, however, these regions are heavily contaminated by noise, which masks the intensity distributions of individual materials. In order to partially alleviate this problem, we process the local mean images obtained from 5x5 moving average filtering. This filtering fulfils the required condition analyzed in [33] about the smoothing of the gray level histogram in order to perform distribution modeling via Gaussian-like distributions. The resulting image is depicted in the upper middle part of Figure 2.6. The corresponding histogram in the lower middle part of Figure 2.6, can be approximated as a mixture of three Gaussian distributions: one distribution representing the target/foreground (the plastic twisted wire), one distribution representing the surrounding medium/background (L-Phenylalanine molecules in the glass test tube containing water) and one distribution for the remaining area outside the circle, according to equation (2.17).This modeling scheme using the mixture of Gaussians is essential under the assumption of Gaussian noise

contamination in the original image. Indicative optimal parameters of the estimated mixture model are shown in Table 2.1. The distance of distribution means reflects the structural differences of the two regions. Thus, we use the difference of model means as a contrast measure of images at different concentrations.

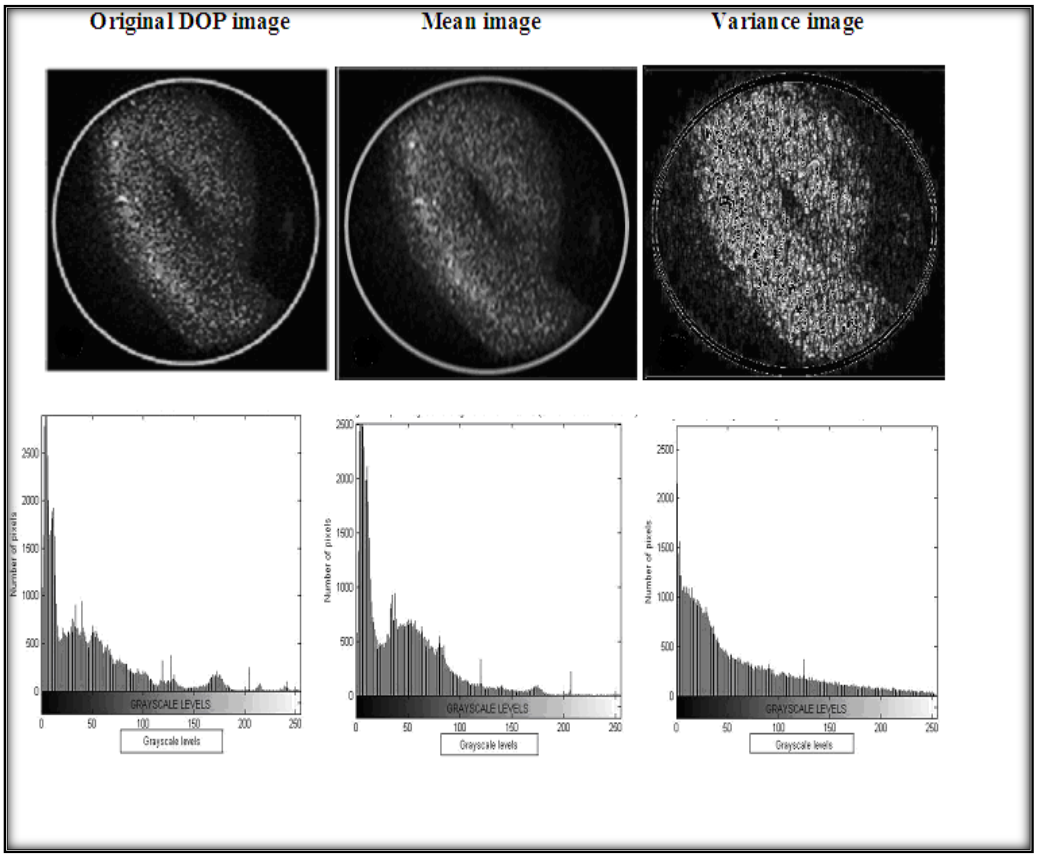

Figure 2.6. First experiment: Original, mean and variance images (first row) along with their corresponding histogram distributions (second row) for a certain concentration of phenylalanine in aqueous solution

Furthermore, we also consider the local variance image (upper right part of Figure 2.6) in an attempt to exploit the texture differences between the (smooth) aqueous solution and (more active) the twisted wire area. For the variance image, the appropriate distributions characterizing the two regions become chi-square (χ^2) distributions. From both the form of the image and its histogram in Figure 2.6 we can verify that the distribution of the background (surrounding medium) imposes fewer degrees of freedom (smaller variance values) than the distribution of the foreground (target), which is spread over the upper part of the dynamic range, at high values. This tendency is verified by the estimated model parameters n_1 and n_2 in Table 2.1. We model the entire image distribution through a mixture of two χ^2 functions estimated by best fit on the histogram through least squares optimization and use their modes in the proposed contrast measure. The difference of model modes in the variance image is used as an additional contrast measure at different concentrations.

The two contrast measures for the different concentrations of phenylalanine are depicted in Figure 2.7 indicating a clear contrast increase with concentration. The difference of modes for either the mean or the variance images has been considered with respect to the scaled range of [0, 255].

Table 2.1: Optimal parameters of the mixture model

Mean image parameters	μ_1	σ_1	μ_2	σ_2	μ_3	σ_3
Optimal parameters	**45**	**35**	**6**	**5**	**4**	**0,01**
Variance image parameters	**n_1**			**n_2**		
Optimal parameters	**3**			**11**		

The original and the model-estimated histograms are shown in the first row of Figure 2.8, for the local mean and variance images at the left and right parts, respectively. The proximity of the two curves, as well as the effectiveness of our approximation, is supported by the "goodness of fit metrics", reflecting a MSE value of order $5x10^{-3}$ and a SNR value at the order of 10dB. By decomposing the estimated mixture models, we can easily derive the image regions being modeled by each individual distribution. The corresponding target and background regions using the mean and variance signals are illustrated in the second and third rows of Figure 2.8, respectively. The mean image appears more robust in segmenting the target regions of interest, whereas the variance image segments better the surrounding medium regions. Thus, the two forms of images can be used complementary in order to best segment all regions of interest. At this point we should notice that by further modifying the fitted models we can obtain enhanced separation of materials and better discrimination of the regions of interest.

The adopted goodness of fit tests reflect a MSE value of order $5x10^{-3}$ and a SNR value at the order of 10dB for the second set of experiments and a MSE of $2x10^{-3}$ and a SNR db gain value of order 10dB for the third set of experments, demonstrating a capability of accurately detecting both the solution and the target area, confirming the encouraging results of the proposed methodology. Further results and analysis can be found in [29] . The experimental results of this study emphasize the potential of the DOLP-polarimetric modality in biomedical applications, since the experimental setup and calibration of the structures can simulate the function and behavior of human body molecules and substances.

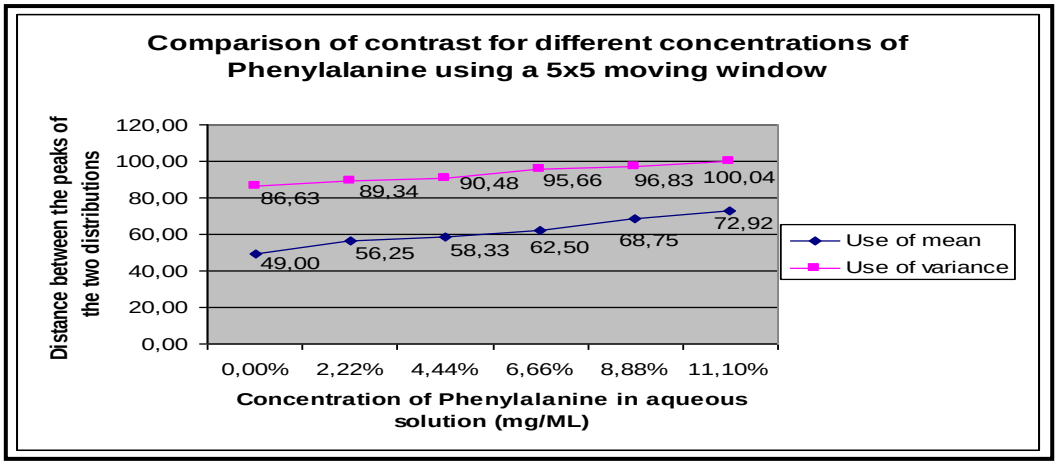

Figure 2.7 First experiment: Difference of modes (DoM) for the mean and variance images versus concentration of aqueous L-Phenylalanine

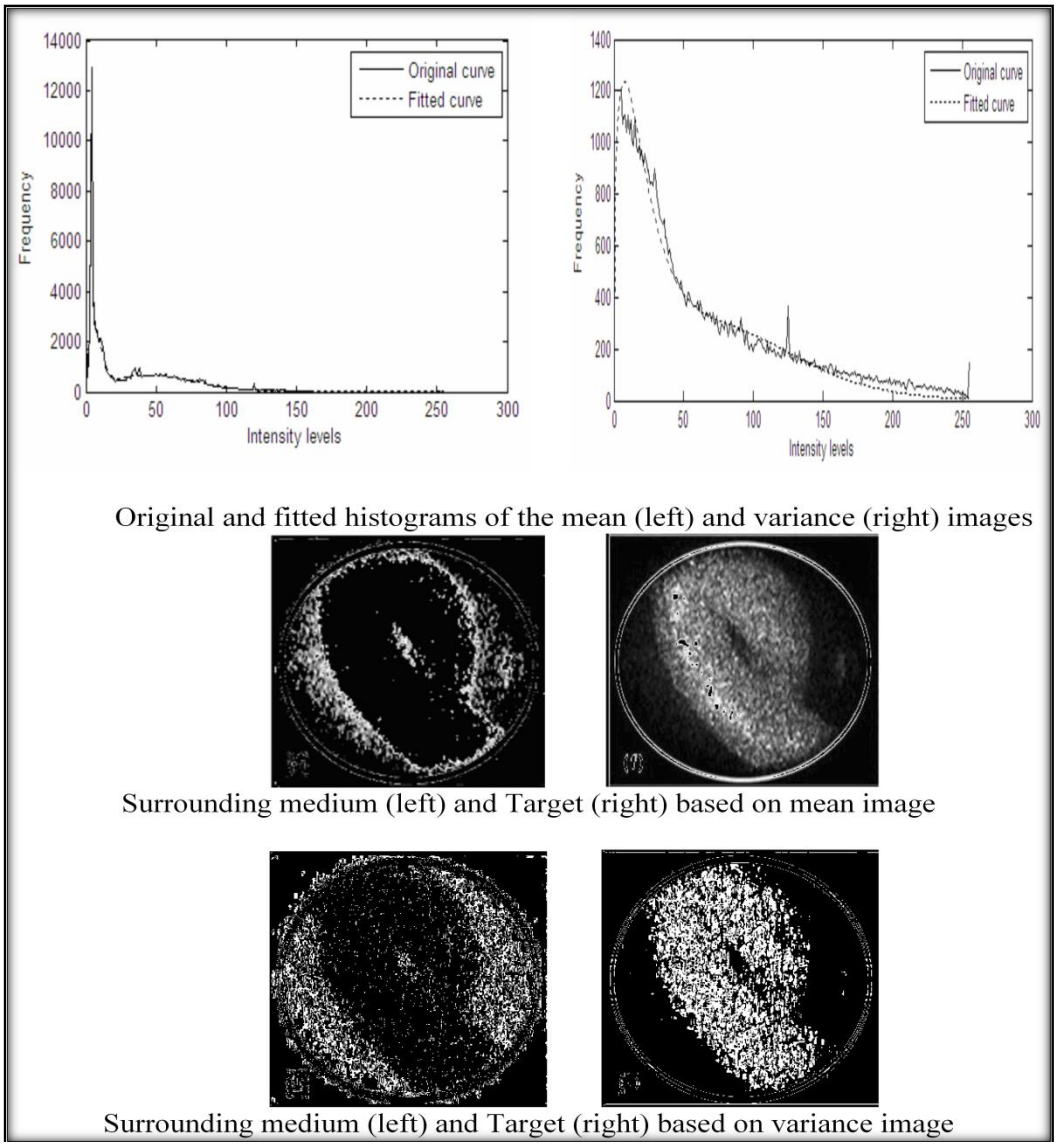

Figure 2.8 First experiment: Original and fitted curves for mean and variance images (first row), along with discriminated image regions for the mean and variance images (second and third rows, respectively)

2.1.3. Tissue characterization utilizing polarimetry

The primary goal in molecular imaging is to obtain the highest signal, accurately localized with high temporal resolution, using the least amount of molecular probe as possible. Optical imaging on the molecular scale provides a safe, accurate, and low-cost alternative to other methods described. The sensitivity offered is excellent, possibly up to 10^{-17} mole/L, thereby decreasing the need for large probe amounts. Another advantage is the option of injecting multiple probe types for multichannel imaging. Optical techniques span spatial scales from subcellular to organ level, yet rely on a disease specific source of contrast as it affects a measurable property of light. Contrast enhancement of optical images has been an active area of research recently, as decoupling diagnostic information from nonspecific background proves to be a challenging problem.

Imaging systems have provided clinicians and researchers noninvasive methods for observation of internal bodily structures, determination of functional tissue characteristics, and identification of diseases and conditions. As technology advances, short data acquisition time, reduced cost, high spatial resolution, high contrast resolution, and high specificity images, at a decreased radiation dose are realized, offering patients efficient diagnosis and decreased morbidity.

Optical imaging provides a detailed description of biological tissues [19, 22]. For instance, it allows the characterization of a variety of diseases, such as breast cancer, skin cancer, lung cancer, cancer of the bladder and the analysis of molecular pathways leading to diseases. In addition, optical polarimetry provides enhanced imaging and spectral polarimetric information regarding the metabolic information of the tissue, as well as the molecular mechanism of a biological function advertising its non-invasive nature. Image formation through detection of the polarization states of light offers distinct advantages for a wide range of detection and classification problems and has been explored by a number of authors, due to the intrinsic potential of the optical polarimetry to offer high-contrast, high-specificity images under low-light conditions. Backscattered optical polarimetric signatures from a target contain information not only related to the target composition, structure, texture, geometry but also to chemistry, biological functions and metabolism. Typically, cancerous cells exhibit structural, biochemical and metabolic anomalies [35]. Different tissues exhibit different indices of refraction and offer unique polarimetric, scattering and absorption characteristics [36]. For instance, precancerous lung epithelial tissues exhibit higher reflectance, increased DOP and larger retardance characteristics than healthy tissue [37], unlike other types of lung cancers of invasive nature. Similarly, different lung cancer types and subtypes appear distinct optical differences.

Having introduced the polarimetric system of the University of Akron in the previous sections along with the preliminary findings of the application of polarimetry to simulating materials, lung tissue samples are utilized within the experimental procedure, directly connecting Stokes parameter imaging to biomedicine. Specifically, combining polarimetric analysis with exploratory statistical analysis and modeling would offer the opportunity to relate a physical procedure to discriminant signatures by separating different parts of

the histograms and applying curve fitting to different statistical distributions. An attempt for complete characterization of the tissue sample in terms of contrast, dynamic range (DR), discrimination and specificity could prove beneficial, leading to discrimination of healthy, precancerous and cancerous lung pathologies that could possibly facilitate accurate diagnosis of lung cancer. Appendix contains a number of relevant publications of the author on this extremely promising area for a more detailed investigation.

In [37], Giakos et al evaluated backscattered signal contributions from healthy tissue, precancerous tissue (carcinoma *in situ*) and stage I cancerous tissue from lung under co-polarized and cross-polarized geometry. The findings indicate that backscattered intensities from stage I lung adenocarcinoma are higher than those of normal tissue, stage I lung adenocarcinoma depolarizes incident photons less than normal tissue and backscattered photons maintain their original linear polarization state at a higher degree with respect to the normal tissue. A characteristic difference of optical parameters between normal lung tissue and stage I carcinoma is illustrated in Figure 2.9, revealing the potential of tissue discrimination through the proposed polarimetric imaging scheme.

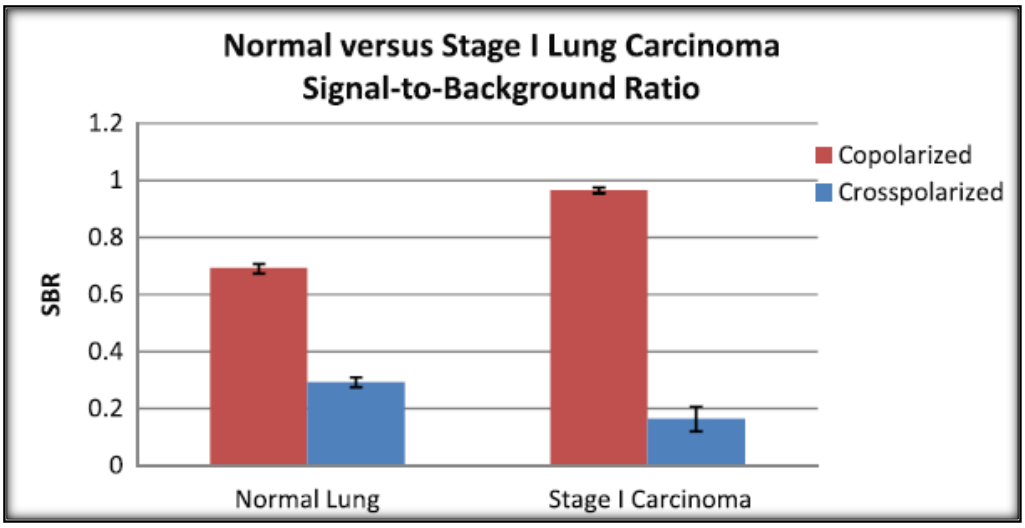

Figure 2.9 Normal versus stage I lung tissue signal-to-background under co-polarized and cross-polarized geometries

The key objective and hot prospect of our study is to determine how lung anatomy and pathology relate to the optical parameters of lung cancer. A preliminary finding is that the formation of clustered large-size cells in precancerous cancer stages prevents light from penetrating the tissue as deeply as it would in normal tissue, giving rise to high photon backscattering. In addition, because of the reduced amount in collagen, the early-stage cancerous epithelial structure tends to depolarize the light less than normal tissues. Further validation with repeated experiments and expansion to other types of cancer is necessary in order to make the conclusions derived more robust and internationally acceptable, yet the first step of the innovation has taken place.

2.2. Histology and microscopy fundamentals

Histology is the branch of medicine that studies the texture of biological material, namely the elements it consists of and the way these are connected with each other, structurally and functionally. The knowledge of physiological histology is fundamental in order to identify the nature and the origin of each disease, to estimate the degree an ailment is caused by an alteration in the tissue structure or by a malfunction of the tissue biochemistry. Using simple medical techniques, mostly painless for the patient, tissue sections are obtained (biopsy) and examined under a microscope. Such procedures include:

- Lancet incision in directly accessed tissues, such as skin, mouth e.t.c.
- Needles, in the case of compact organs (FNA)
- Endoscopic tubes in body hollows (gastrointestinal system)
- Flexible catheters in blood vessels

The structure and function of all live organisms are based on cells. The cells of a multicellular organism vary significantly among each other. Although they originate from one milted ovum, each of the cells eventually builds up the morphology that is appropriate for its operation through the process of differentiation. This procedure results in the grouping of cells with common functional properties and their adaptation to the needs of a continuously varying environment (e.g. the replacement of a heart muscle by a potent fibrous connective tissue). Depending on the main function they perform, cells are classified into groups. Frequently, though, a cell may participate in various operations, thus it can belong to more than one group. The most important categories of cells are:

- Epithelial ones, having as their common role to form barriers, absorb and exude
- Connective tissue ones, having as their common role to brace and organize the body
- Systole ones, having as their common role the movement
- Nerve ones, having as their common role the communication between the cells
- Genital ones, having as their common role the reproduction
- Blood cells, having as their common role the transfer of oxygen and the defense
- Immunization system cells, forming the defense mechanism of the organism
- Hormone producing cells, aiming at the indirect communication of the cells

A ***tissue*** constitutes a union of cells ordered in a specific mode. When the cells forming the tissue follow the same structure (morphology-construction) the tissue is characterized as "simple tissue" (e.g. lipoid tissue),

while the tissue that consists of mixed cellular population, extracellular substance and cellular products (e.g. nerve tissue) is named as "composite tissue". An anatomically distinct cluster of tissues, of different kind yet presenting common special functionality, forms an ***organ***, while as a ***system*** we consider a group of organs having common functional roles or related with each other.

The simplest method to study cells and tissues is the use of photon microscope. Thin slices of tissues are laid on glass tiles, stained with the appropriate pigment, lighten by common light and observed in the microscope. The use of electron microscope improves discrimination ability, overcoming the drawback of photon microscope to visualize thin and small structures inside the cell. Immunohistochemistry (IHC) and fluorescence in situ hybridization (FISH) are techniques that have proved extremely useful tools for improving the visual result of microscopy. IHC utilizes antibodies against specific cellular elements, while FISH aids in the study of DNA or RNA [39], extracting significant information in molecular level. In this way, structures that couldn't be visible with other techniques are now observable in the photon and electron microscope.

Prior to their observation and analysis in microscope, tissues need to be appropriately prepared [40]. This procedure is the key part of the entire histological analysis process and directly affects the final optical result and the applicability of microscopy and image processing methods for extracting accurate conclusions. The scientific training of the laboratory staff that performs the tissue preparation, the precise execution of the intermediate steps and the strict compliance with the time intervals of tissue handling are prerequisites for the validation and analysis of the results. The preparation process can be analyzed into the following basic steps:

1. **Stabilization (fixation):** This step aims at preserving the tissue as well as possible in order to stabilize its elements, as if it was live, increasing its stiffness so as to be cut in thin slices and killing all the bacteria and virulent factors present on the tissue. Among a variety of stabilization materials we emphasize on formalin (the most common and inexpensive stabilization material), alcohol (not pure alcohol as it causes abrupt dehydration and crimping of the tissue) and dichloride mercury (it stabilizes quickly but reposes salts in the tissue). Having been stabilized, the tissue is sliced into small pieces using a common lancet. Slices containing ossified tissue or bone pieces need to be desalinated in order to soften and be sliced in the microtome. The slighter the bone pieces, the easier they are demineralized. The duration of this procedure depends on the tissue stiffness and the size of the slice and varies from a few hours until 1-3 days. Continuing, the slice is washed in regulative solution and is entirely stained.
2. **Dehydration:** This procedure is automatically performed with the aim of a dehydrating/ embedding system and endures 24 hours. Tissue slices are gradually dehydrated using alcohol solutions of increasing concentration (60%, 70%, 90% and 100%) until all water (endogenous tissue water and stabilization liquid water) is removed. The dehydration procedure must be executed cautiously and precisely, aiming at both stiffing the tissue and removing all of its components

that are diluted in alcohol. Numerous technical errors can take place during this process, such as breaking or shrinking the tissue, thus processing times must be accurately followed. Continuing, the procedure of clarification takes place, where alcohol is replaced by an organic solvent (xylene or toluene), which can be mixed with both alcohol and paraffin in liquid form. Finally, the tissue is enclosed in melted paraffin (paraffin confinement or impregnation in paraffin, lasting 8-10 hours) and left until it's cooled down so as the paraffin gets solid.

3. **Skinosis (paraffin embedding):** Once the material is cooled and the paraffin is fixated, the structure is placed in fixative fluid (paraffin in liquid form) in order to mold a tissue-paraffin "block", which will be able to be sliced in thin incisions (2-7μm) without causing deformation of the cellular structure and the tissue architecture. The precise and correct placement of the tissue sections in the paraffin block is of fundamental importance as this will define the slice that will be mounted on the tile.
4. **Slicing on the microtome:** The tissue-paraffin block is placed on the microtome, where it is cut in slices 5-8μm thick. These slices are inspected for their completeness in a special "cool water bath" and spread on glass tiles (slides) using leucoma, made up by albumen, whipped up with distilled water and glycerin, adding crystals of carbolic acid in order to prevent growth of funguses. A drop of this solution (well preserved in a bottle to be protected from dust) is spread on the slide surface by finger, smoothly, without plaiting and sheathing of the slice so as to eliminate errors inserted by artifacts for the observation under the microscope. Slides must dry before pigmentation (desiccation procedure), usually by being passed in a furnace under 37^{o}-40^{o} C for 30-45 minutes. Higher temperatures insert the risk of tissue damage.
5. **Hydration:** After the plating of the slices on the tiles, the procedure of deparaffinization takes place, where paraffin is removed with the aid of an organic solvent (e.g. xylene). Consequently, the hydration of the slices in successive solutions of increasing dilution of alcohol in water is performed and the incisions are stained using the appropriate pigments. Generally, in a routine laboratory, the preparation of a paraffin section for histological analysis requires a whole day to be completed.
6. **Staining:** Staining of the tissue sections can be performed in two ways:
    - The tissue section remains in the pigment as long as needed for the staining of the special element that occludes the substance in the desirable degree.
    - The tissue section remains in the pigment for a longer time interval. In this way, both the special element and the rest tissue ones are overstained and the surplus of the pigment is removed using another liquid. This stage of the staining procedure, which is the most commonly adopted, is called differentiation and the liquid used is named differential liquid (usually acidized alcohol of appropriate concentration as a

weak solution does not discolor the slice and a strong one completely discolors the tissue sections). It is advised that the differentiation procedure be performed by immersing the sections into the differential liquid (and not continuously leaving them in it) and be terminated by rinsing with plentiful common water. Advanced staining techniques (such as immunohistochemistry) can be further adopted depending on the quality of the extracted results required and the nature of the special element to be detected and analyzed by the specialist.

7. **Dehydration – clarification – covering:** Dehydration, already mentioned in previous stages, is performed in the same manner as in the paraffin-embedding procedure using a series of alcohol solutions of increasing concentration (70^o-100^o). Clarification of the sections is achieved by immersing them into two xylene baths for two and five minutes respectively. The precision and quality of the dehydration procedure is fundamental for the future analysis procedure, as poor dehydration results in blurring effects on the slides under microscope observation. After the clarification in xylene, slices are caped with a special coverslip that is attached with the aid of a drop of Canadian balsam, natural or artificial, paying high attention to the complete removal of the air bubbles between the coverslim surface and the slice. Finally, the slide is cleaned with a xylene immersed wipe.

The discriminating ability of the photon microscope can be further increased utilizing thinner slices of paraffin (0.5-2μm), which is achieved with the consolidation of the tissue in acrylic or epoxy resin. Most acrylic resins are widely used as a consolidation medium, being stiffer substances than paraffin and better prop means for the tissue. Comparing with paraffin they offer thinner incisions, thus better discriminating ability under the microscope and produce more qualitative slices taken from highly dour tissues, such as calcified bone.

Epoxy resins constitute the toughest prop consolidation mediums. The utilization of specialized microtomes may extract very thin incisions (0.5-1μm) of advanced optical quality and compound specific, fine slices, proper for electron microscopy, since they are resistant to the destructive action of the electron beam emitted by the microscope, contrary to other substances. Another characteristic of the epoxy resins is their ability to prevent pigments from penetrating into the tissue section, leading to the adoption of another substance, toluidine blue, which stains the various biological elements in different tones of blue.

Electron microscope facilitates the discrimination of detailed subcellular structures. Tissue processing necessitates specially stabilized/fixated, thin sections (<2mm) within particular fixation liquids, such as gluteal and bromium tetroxide, in order to avoid electron dispersion. The stains utilized contain a heavy metal (usually uranium or lead).

2.2.1. Immunohistochemistry fundamentals

Immunohistochemistry (IHC) is the localization of antigens in tissue sections by the use of labeled antibody as specific reagents through antigen-antibody interactions that are visualized by a marker such as fluorescent dye, enzyme, radioactive element or colloidal gold [41]. It is a method for detecting specific antigens in tissues or cells based on an antigen-antibody reaction. The initial technique was developed in 1940s using immunofluorescence on frozen tissue. Enzyme-based IHC was introduced in 1970s. A series of advancements in the technology, particularly during late 1980s and 1990s, led to the development of antigen retrieval techniques to make IHC possible on nearly all archival tissue. This, coupled with sensitive detection systems, and better antibodies has made this technique routine in surgical pathology and research. With the expansion and development of immunohistochemistry technique, enzyme labels have been introduced. Other labels include radioactive elements, and the immunoreaction can be visualized by autoradiography.

Since immunohistochemistry involves specific antigen-antibody reaction, it has apparent advantage over traditionally used special enzyme staining techniques that identify only a limited number of proteins, enzymes and tissue structures. Therefore, immunohistochemistry has become a crucial technique and widely used in many medical research laboratories as well as clinical diagnostics [42].

There are numerous immunohistochemistry methods that may be used to localize antigens. The selection of a suitable method should be based on parameters such as the type of specimen under investigation and the degree of sensitivity required. Electron microscopic (EM) immunohistichemical techniques can be divided into two groups: Those where the immunostaining takes place prior to resin embedding are referred to as pre-embedding. Those methods where the immunolabeling is undertaken after resin embedding are known as post-embedding. The choice of whether to apply pre- or post-embedding method to the detection of an antigen in any particular location depends on a large extent upon the distribution and liability of the antigen and the characteristics of the primary antibody. Before starting immuno-EM labeling, a test for the characteristics and dilution of the primary antibody should be performed at light microcopy level. Several recently developed methods rely on labeling with colloidal gold particles. These methods were originally introduced for electron microscopy as the gold particles are easily visible under the electron microscope, but they are also useful for light microscopy. Since gold particles can be made in different size from 5 to 30 nm, it is possible to carry out multiple staining at the electron microscopic level, most easily by direct labeling of several first layer antibodies with different sized particles. The indirect techniques can also be used in double or triple labeling by parallel approach if the primary antibodies are from different species and by sequential approach if the primary antibodies are from same species [43].

Tissue preparation is the cornerstone of immunohistochemistry. To ensure the preservation of tissue architecture and cell morphology, prompt and adequate fixation is essential. However, inappropriate or prolonged fixation may significantly diminish the antibody binding capability. There is no

universal fixative that is ideal for the demonstration of all antigens. However, in general, many antigens can be successfully demonstrated in formalin-fixed paraffin-embedded tissue sections. The discovery and development of antigen retrieval techniques further enhanced the use of formalin as routine fixative for immunohistochemistry in many research laboratories.

The Her-2/neu gene can be screened by using molecular and immunological probes that vary in their complexity, sensitivity and specificity. In the beginning, Her-2 amplification was evaluated by **Southern blotting**, which was supplanted by a sensitive and rapid quantitative polymerase chain reaction method [39]. Fluorescence in situ hybridization **(FISH)** is a more recent technique that enables Her-2/neu amplified cells to be visualized within a tumor slice. In addition, Her-2/neu overexpression can be detected with various methods, including **Northern blot** and **in situ hybridization** for Her-2 RNA, **Western blot** and **immunoassays** for Her-2 protein, but he most widely used method is **immunohistochemistry** (IHC). FISH is a more recently developed method that can visualize the number of gene copies present in tumor cells and provide a sensitive and accurate measure of Her-2/neu gene amplification while IHC can be easily carried out on formalin-fixed, paraffin-embedded tissue, is more familiar, less expensive and simpler compared with FISH. FISH measures Her-2/neu amplification in DNA level while IHC measures gene overexpression in protein level and identifies cases in which the gene product is overexpressed even without being amplified. Yet, the results produced cannot be fully objectively accepted by all researchers and are complex and subject to considerable variations in the hands of different teams and laboratories. The advantage of FISH versus IHC is the ability to analyze gene integrity and protein expression on two consecutive tumor sections, thus manipulating the same cells [39]. IHC has the drawback that produces results that are conflicting due to different sensitivity and specificity of the primary antibodies used, there is variability in IHC interpretation and technical artifacts can be introduced [44].

In immunohistochemistry, positive reactions with DAB (diaminobenzidine) are identified as a dark brown reaction product on the cell membrane and the specimens are graded as negative, low, medium, and high positive, based on both the percentage of positively stained cells and the staining intensity according to a scoring protocol. The specimens with high or medium IHC positivity are considered to have Her-2/neu overexpression, compatible with FDA approved criteria for Herceptin treatment. An arbitrary scoring system needs to be assigned for Her-2/neu protein levels, which in reality cover a continuous spectrum. In fact, different scoring systems have been used. Recent pilot studies use graded values, including high, medium, and low positive and negative, whereas HercepTest uses 3+, 2+, 1+, and negative score. Another scoring approach is mentioned in [45]: categorization as 3+, 2+,1+ or 0+. When membrane staining, whether incomplete, complete, strong or weak, is absent in less than 10% of the cells, the score is negative or 0. Staining is scored as 3+ when the surface of the tumor cell has strong intensity, 2+ when it has moderate intensity and 1+ when the membrane has weak intensity and is incompletely stained. However, other studies have used strong positive (2+), weak positive (1+), and absent (0),or a positive versus negative system, where "positive" was defined as the relative difference in

cytoplasmic membrane staining between tumour cells and normal epithelial cells. Therefore, it is inevitable that some interlaboratory discrepancies may exist for at least some of the cases, especially medium or low positive ones.

In general, the HercepTest scoring is adopted. According to this, **negative** results are 0 and 1+ intensity (no or barely perceptible membrane staining in >10% of tumor cells) and **positive** results are 2+ (moderate complete membrane staining in >10% of tumor cells) and 3+ (strong complete membrane staining in >10% of tumor cells) respectively. The description is summarized in the following tables, where the adopted scoring system is described in Table 2.2 and summarized in a standardized form in Table 2.3 according to practical measurements, keeping up with the majority of bibliography.

Table 2.2 Generalization of IHC score

Scoring of IHC staining	
0	**No slides returned.**
1&2	**Considerably less invasive tumor nuclei staining than expected, when compared to the test slides stained by the organizing laboratory.**
3	**Demonstration of less invasive tumor nuclei staining than expected to stain or/and the intensity of staining is considerably weaker than expected.**
4&5	**Demonstration of the proportion of nuclei of invasive tumors expected to stain, with roughly the expected staining intensity.**

Table 2.3 Standardized IHC score based on practical measurements

Score	HER2 Status	Staining Pattern
0	Negative	**No staining observed, or membrane staining in less than 10% of tumor cells.**
+1	Negative:	**A faint/barely perceptible membrane staining detected in more than 10% of tumor cells. The cells are only stained in** *part* **of the membrane.**
+2	Borderline	**A weak to moderate complete membrane staining observed in more than 10% of tumor cells.**
+3	Positive:	**A strong complete membrane staining observed in more than 10% of the tumor cells.**

It is not known if there is a real difference between 10% and 100% staining from a clinical point of view. Studies on HER2 do not address the percentage of positive staining in detail. In this regard, it is difficult to compare different studies, because of different definitions of positivity.

Immunohistochemistry is a purely medical issue of deep theoretical background and the detailed explanation of its rules and procedures is not of

our main interest. Our goal is to attempt to process the extracted IHC images of breast tissues and automatically determine/define the extent of HER-2 overexpression on the examined breast tissue. This is not an easy part, as very few image analysis methods have been developed and, most of all, there is not a totally and, generally accepted, subjective method to define the degree of malignancy. In addition, the visual processing of the prepared tissue is directly dependent on the quality of the laboratorial technique. The tissue evaluation is achieved by counting, through a standardized procedure, the total percentage of staining of the membranes of the cells forming the tissue section. If the percentage exceeds a specific value, defined according to a "scoring method", we consider this tissue part as "affected", so the "patient" has to proceed to the next step, which is targeting the HER2 antibody with anti-HER2 therapy.

We focus on, and try to exploit, the fact that IHC "stains" the membranes of HER2 overexpressed cells, which monitors them with a characteristic brown color (adopting the DAB staining protocol) or red color (adopting the PAP staining protocol) in the extracted microscope images, while the cell nuclei are highlighted with a pure blue coloring. The percentage of staining along each membrane contour, the percentage of "stained" cells with respect to all cells and the "darkness" (the intensity of brown/red color) at each membrane are factors that reveal if a tissue is healthy or not. The difficult part is to accurately define these factors and safely interpret them according a well-established scoring system. We have to be very careful within this procedure. Determining a healthy tissue as "containing malignant cells" would saddle the patient with the heavy load of carrying the disease and introduce him/her to unnecessary, extremely costly and potentially dangerous targeted treatment with Herceptin, which has been found suspicious of causing cardiovascular abnormalities. Considering a defected tissue as healthy would prevent the patient from following an instantly needed therapy, thus putting his/her own life in danger!

The effect of IHC testing on the tissue sample is to stain the membranes of tumor cells, partially or completely. The percentage of tumor cells that have completely-stained membranes and the intensity of that staining were used, so far, by an experienced pathologist to derive a score. Our goal is to develop an algorithm/procedure to contribute to the specialist's evaluation by segmenting the input IHC image to regions forming the tissue cells, count their number, define their contour borders associated to the cytoplasmic membrane and deliver quantitative measurements on the distribution of membrane staining values that are relevant to deriving a score.

Generally, the membranes are assumed to be stained brown or red, according to the staining protocol implied by the utilized antibodies while the nuclei are assumed to be stained blue. An important feature of the developed algorithm is to be able to logically connect membranes that are not completely stained. This is necessary in order to determine the completeness (percentage) of membrane staining for each and every tumor cell. There should be a high degree of concordance between algorithm cell boundaries and biological membranes (it is generally accepted that no algorithm will perfectly perform this task).

A continuous and qualitative co-operation with a medical specialist is needed in order to accurately define the parameters of the problem and insert them, step-by-step, into the image processing procedure. It is also important to mention the undoubtedly essential contribution of the anatomy expert to the tissue evaluation, recognizing that no automated or semi-automated algorithmic procedure can totally substitute the expert's tutoring and observation.

Closing this introductory section and before entering in the pure immunohistochemical image processing theory and segmentation, an optical demonstration of nature of IHC microscope samples is depicted in Figure 2.10.

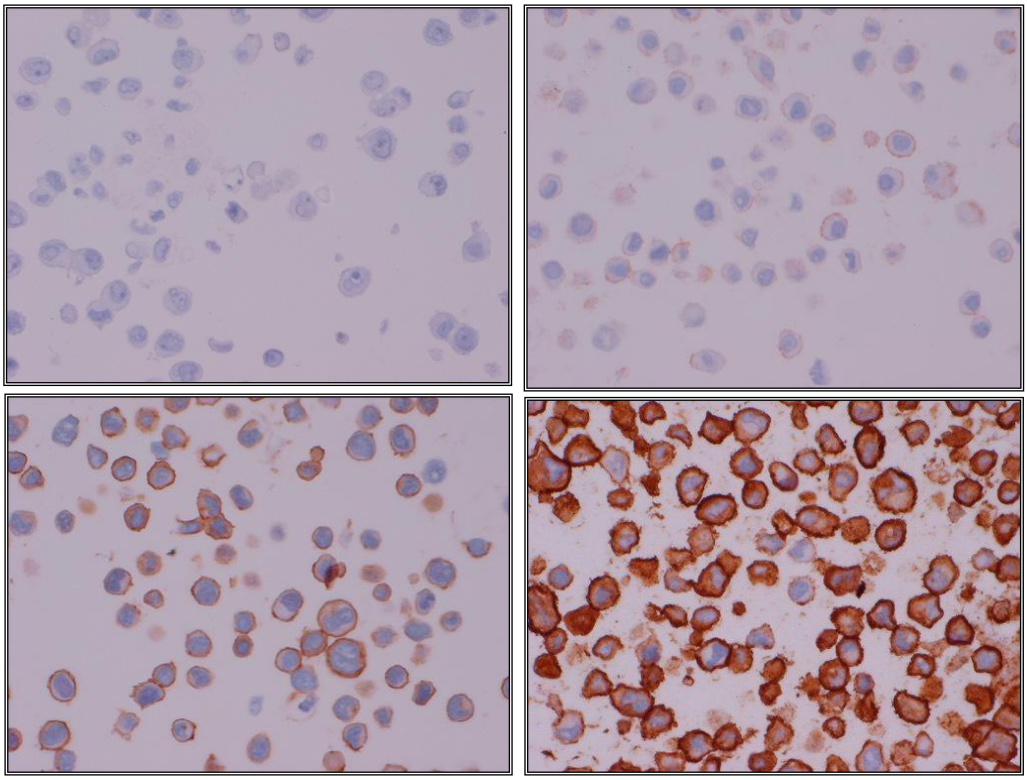

Figure 2.10 Upper left - IHC score 0 image (totally normal and healthy tissue, no HER2 overexpression), Upper right - IHC score+1 image (healthy tissue with controlled HER2 overexpression), Down left - IHC score+2 image (healthy but potentially suspicious tissue, augmented HER2 overexpression), Down right - IHC score +3 image (affected tissue)

3. Image processing background

Image segmentation aims at extracting attributes of interest from an image considering its common properties, such as discontinuities and similarities, within the different object classes forming the captured scene. Points, lines, regions, boundaries are among the key features to be evaluated through this procedure. Several approaches have been introduced in international bibliography; point and line detection techniques where the detected edges are linked in order to accurately represent the shape of each object, thresholding methods (histogram, adaptive, multi-level) which divide the image into segments according to distinct bands of pixel intensities and region growing/splitting methodologies which iteratively classify neighboring pixels of "seed-points" into a region through appropriately selected similarity criteria [46]. The efficiency of a segmentation method highly depends on the properties of the processed image (colors, size, contrast, texture, presence of noise), the possible prior knowledge on it (number of key objects, region overlapping) and the expedient feature to be extracted (contours, regions, edges). Edge segmentation methodologies appear very sensitive to noise, thresholding techniques lead to ambiguous boundaries and prerequisite homogenous, few and non intersecting regions, while region based segmentation approaches introduce computational complexity and are sensitive to the initialization of seed-points. Thus, key image feature extraction can be characterized as a complex, application-dependent yet challenging scientific area.

3.1. Color models

The RGB color model is an additive color model in which red, green and blue light are added together in various ways to reproduce a broad array of colors and is widely used in screening application. The name of the model comes from the initials of the three additive primary colors, red, green, and blue. Pure color information is described as a linear combination of all the three components. The term RGBA is also used to mean Red, Green, Blue, Alpha. This is not a different color model, but a representation, where Alpha is an additional channel (not component) used for transparency. For an 8-bit image, each component value ranges from 0-255, defining the extent of the basic color it contains. It is represented as a cube in the Cartesian space with each axis representing each color component.

In the HSV (Hue, Saturation, Value) model, also called HSB (Hue, Saturation, Brightness) or HIS (Hue, Saturation, Intensity), color is represented by three components; a) Hue (H), defining the pure color type (such as red, green) and ranging from 0 to 360 degrees (with red at 0 degrees, green at 120 degrees, blue at 240 degree etc), b) Saturation (S) or “purity” ranging from 0 to 100% and defining the amount of white color present (the lower the saturation of a color the more faded the color will appear) and c) Value (V) or Brightness (B) or Intensity (I), ranging from 0 to 100%. It is a nonlinear transformation of the RGB color space. In order to process images aiming at extracting color information and features, it is preferable to use the HSV color model over alternative models such as RGB, because of its advantage to emulate the human color perception system. In addition, pure color features are independent on the intensity channel, which plays a key role in color segmentation as only the Hue channel is processed for color determination. RGB is an additive color space, modeling the way that primary color lights combine to form new colors when mixed.

In the Lab color space, also known as CIE or CIELAB, color is represented by dimension L standing for lightness and the a, b channels for the color-opponent dimensions, having the color variable independent of the color intensity. Lab color is designed to approximate human vision and its L component closely matches human perception of lightness. Thus, it can be used to make accurate color balance corrections by modifying only the a and b components, or to adjust the lightness contrast using only the L component. The L*a*b* color space includes all perceivable colors, exceeding the capabilities of the RGB color model. One of the most important attributes of the L*a*b*-model is device independence, meaning that the colors are defined independent of the nature of their creation or the device they are displayed on.

The representation of the three color spaces is depicted in Figure 3.1

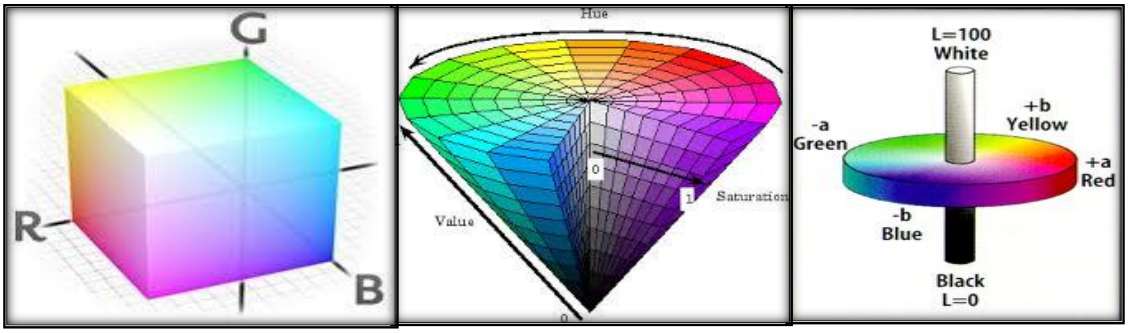

Figure 3.1 Representation of RGB, HSV and LAB color model [www.mathworks.com]

The conversion from the RGB model to the HSV is achieved using the following formula:

$$H = \frac{360}{2\pi} \cdot \arctan\left(\frac{\sqrt{3}}{2}[G-B], R - \frac{[G+B]}{2}\right) \cdot \frac{240}{360}$$

$$S = \sqrt{R^2 + G^2 + + B^2 - RG - RB - GB} \cdot \frac{240}{255} \qquad (3.1)$$

$$I = \frac{R+G-B}{3} \cdot \frac{240}{255}$$

3.2. Image clustering

Cluster analysis or clustering is the process of grouping a set of objects into classes (clusters) according to a matching criterion (distance function) in such a way that the inter-cluster similarity between the elements along with the extra-cluster separability are increased. It is a common technique for statistical data analysis with numerical application including machine learning, pattern recognition, image analysis, information retrieval and bioinformatics.

Clustering can be achieved by various algorithms that differ significantly in their notion of what constitutes a cluster and how to efficiently represent and find classes, making feature extraction and definition a key part of the whole process. Popular representation of clusters include groups with small distances among the cluster members, dense areas of the data space, intervals or particular statistical distributions. The appropriate clustering algorithm and parameter settings (including values such as the distance function to use, a density threshold or the number of expected clusters) depend on the distinct input data set and expected use of the results. Cluster analysis is not an automatic task but an iterative process of information searching and extraction through an interactive optimization procedure that involves initialization, random in the majority of the cases, trial and failure. Data preprocessing is also needed along with model parameters determination and convergence criteria in order the result to achieve the desired properties.

Clustering has been widely used in computer vision for partitioning a digital image into multiple segments (sets of pixels) with common characteristics such as color, intensity or texture or even locate objects and boundaries (lines and curves). The objective is to assign a label to every pixel in an image such that pixels with the same label share certain visual characteristics. The classic K-means algorithm and the recently re-emerged and promising Mean-Shift algorithm are two representative methodologies for image clustering segmentation.

K-means clustering [47] is an iterative technique that is used to partition an image into K clusters and constitutes one of the simplest, quickest, yet representative unsupervised learning algorithms that solve classification problems. The main idea is to define K centroids, one for each cluster, having the limitation that the classes must be known a priori. Different location of centers causes different results, thus the algorithm suffers from initialization. The better choice is to position them as far from each other as possible. The next step is to take each point belonging to a given data set and associate it to the nearest centroid, according to a well defined criterion. Squared Euclidean distance, where each centroid is the mean of the points in that cluster and Cityblock Distance where each centroid is the component-wise median of the points in that cluster are the two dominant distance metrics, defined in the following equations:

Squared Euclidean Distance $$E_{ij} = \sum_{i=1}^{n} (X_i - C_j)^2 \quad (3.2)$$

Cityblock distance $$E_{Cij} = \sum_{i=1}^{n} | X_i - C_j | \quad (3.3)$$

where n is the total number of points, X_i and C_j represent the candidate point i and centroid of cluster j resprectively.

When all points have been connected with a cluster center , the first step has been completed and a preliminary classifications has been achieved. At this point k new centroids as barycenters of the clusters resulting from the previous step need to be re-calculated. After this update of the k centroids, a new binding has to be done between the same data set points and the nearest new centroid, forming an iterative procedure. As a result of this loop we may notice that the k centroids change their location step by step until no more changes take place. In other words centroids do not move any more.
The basic algorithmic steps are summarized in the following scheme:

1. Pick K cluster centers, either randomly or based on some heuristic
2. Assign each pixel in the image to the cluster that minimizes the distance between the pixel and the cluster center according to a selected distance function
3. Re-compute and update the cluster centers by averaging all of the pixels in the cluster
4. Repeat steps 2 and 3 until convergence is attained (i.e. no change in pixel classification is observed)

In this case, distance is the squared or absolute difference between a pixel and a cluster center. The difference is typically based on pixel color, intensity, texture, and location, or a weighted combination of these factors. K can be selected manually, randomly, or by a heuristic. This algorithm is guaranteed to converge, but it may not return the optimal solution as the quality of the solution highly depends on the initial set of clusters and the value of K. The way to initialize the centroids is not specified and it frequently happens that suboptimal partitions are found. This poor initialization can be improved by multiple runs of the algorithm or the clustering of one or more samples first for "training" the algorithm. Another drawback is the handling of empty partitions and the productions of outliers, especially in the cases of different size of the regions to be segmented. The prerequisite of the algorithm for known number of classes is particularly troublesome, since in most application there is not such knowledge. A segmentation example applying k-means clustering to a immunohistochemical image sample is illustrated in Figure 3.2. The nature of the biomedical input image and the objective to segment cell nuclei implies the existence of three color classes within the image (yet the selection of K=3): a) the "blue" area of the cell nuclei, b) the "brown" area of the membrane staining and c) the remaining tissue area. Selecting as a feature input the color information derived from the S and V channels of the converted RGB image to the HSV color space and the Euclidean distance as a similarity criterion, the segmented color components are extracted.

The basic limitation of k-means clustering for a priori knowledge on the number of candidate classes and the shape of their distribution is overcome utilizing the Mean-Shift clustering algorithm. Mean Shift (MSH) is a robust technique which has been applied in many computer vision tasks, including image segmentation and visual tracking. It was proposed in the middle 70’s [48] but was not widely used till Cheng [49] and Comaniciu [50] applied the algorithm to Computer Vision and woke up the interest on it. In essence, MSH is an iterative mode detection algorithm in the density distribution space based on the moving to a kernel-weighted average of the observations within a smoothing window. This computation is repeated until convergence is obtained at a local density mode. The

steps are: (1) estimate the density, (2) find the modes of the density and (3) associate each data point to one mode.

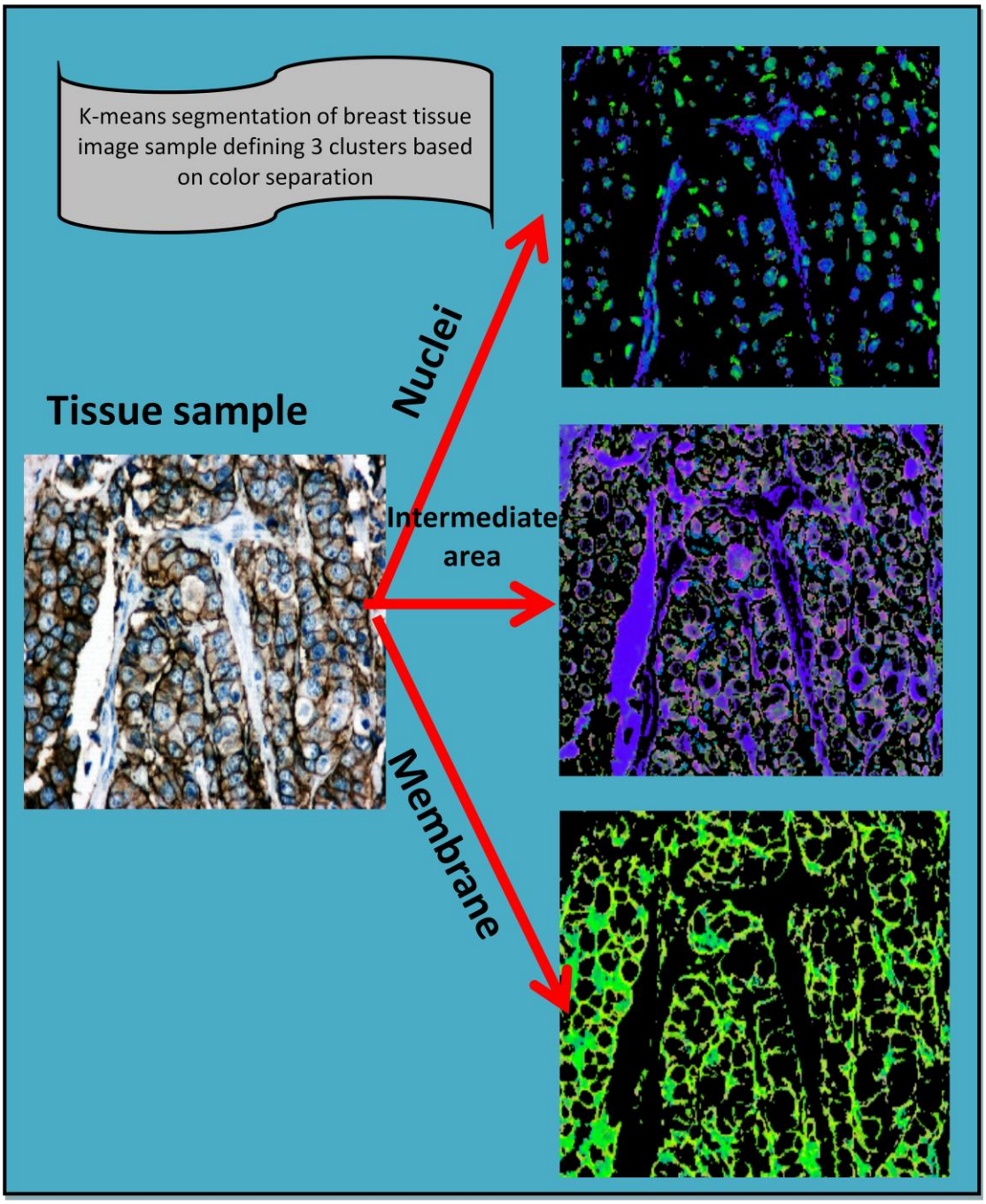

Figure 3.2 Example of immunohistochemical image segmentation applying the k-means clustering algorithm

The main idea beyond mean shift is to treat the points in the d-dimensional feature space as an empirical probability density function where dense regions in the feature space correspond to the local maxima or modes of the underlying distribution. For each data point in the examined sample, a gradient ascent procedure is performed on the local estimated density until convergence. The stationary points of this process represent the modes of the distribution. Thus, the data points associated with the same stationary point are considered members of the same cluster. This procedure is schematically represented in Figure 3.3.

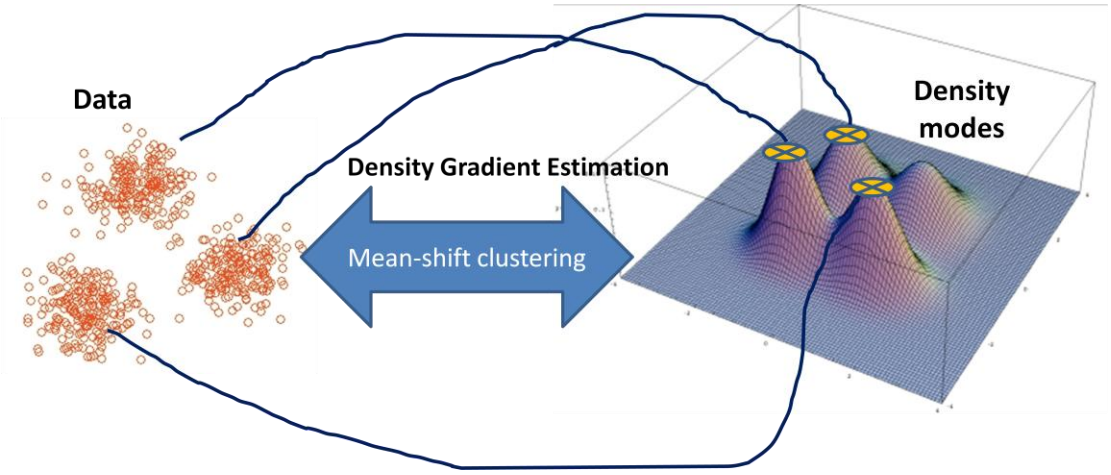

Figure 3.3 Schematic representation of mean-shift algorithm

Each data point is associated with the nearby peak of the dataset's probability density function. Mean shift defines a window around each point and computes its mean. Then it shifts the center of the window to the mean and repeats the algorithm till it converges. After each iteration, the window shifts to a denser region of the dataset. Yet, the algorithmic steps include:

1. Fix a window around each data point
2. Compute the mean of data within the window
3. Shift the window to the mean and repeat till convergence.

A summary of the basic mathematical background of the algorithm takes place in the following lines. A kernel φ(x) is a function that satisfies the following requirements:

$$\int_{R^d} \phi(x)dx = 1 \quad \text{and} \quad \varphi(x) \geq 0 \tag{3.4}$$

Some examples of kernels include:

$$\textbf{1. Rectangular} \quad \varphi(x)=\begin{cases} 1 & a \leq x \leq b \\ 0 & \text{else} \end{cases}$$

$$\textbf{2. Gaussian} \quad \varphi(x)=e^{-\frac{x^2}{2\sigma^2}} \tag{3.5}$$

$$\textbf{3. Epanechnikov} \quad \varphi(x)=\begin{cases} \frac{3}{4}(1-x^2) & |x| \leq 1 \\ 0 & \text{else} \end{cases}$$

Kernel density estimation is a non parametric way to estimate the density function of a random variable. This is usually called as the Parzen window technique. Given a kernel K, n data points $\{x_1, x_2, \ldots, x_n\}$and a bandwidth parameter h representing the window size, the Kernel density estimator for a given set of d-dimensional points is given as

$$\hat{f}(x) = \frac{1}{nh^d} \sum_{i=1}^{n} K\left(\frac{x - x_i}{h}\right) \tag{3.6}$$

Mean shift can be considered to be based on gradient ascent on the density contour. Applying gradient to the kernel density estimator we obtain

$$\hat{f}(x)=\frac{1}{nh^{d}}\sum_{i=1}^{n}K(\frac{x-x_i}{h})\Rightarrow\nabla\hat{f}(x)=\frac{1}{nh^{d}}\sum_{i=1}^{n}K'(\frac{x-x_i}{h}) \qquad (3.7)$$

Using the kernel form

$$\mathbf{K(x-x_i)=ck(\left\|\frac{x-x_i}{h}\right\|^2)} \qquad (3.8)$$

, where c is a constant, the gradient of the density estimator becomes

$$\nabla\hat{f}(x)=\frac{2C}{nh^{d}}\sum_{i=1}^{n}(x-x_i)K'(\left\|\frac{x-x_i}{h}\right\|^2) \qquad (3.9)$$

Setting g(x) = - K'(x) we have

$$\nabla\hat{f}(x)=\frac{2C}{nh^{d}}\sum_{i=1}^{n}(x_i-x)g\left(\left\|\frac{x-x_i}{h}\right\|^2\right)=$$

$$=\frac{2C}{nh^{d}}\left[\sum_{i=1}^{n}g\left(\left\|\frac{x-x_i}{h}\right\|^2\right)\right]\underbrace{\left[\frac{\sum_{i=1}^{n}x_i g\left(\left\|\frac{x-x_i}{h}\right\|^2\right)}{\sum_{i=1}^{n}g\left(\left\|\frac{x-x_i}{h}\right\|^2\right)}-x\right]}_{\textbf{mean shift vector}} \qquad (3.10)$$

Finally, we obtain the formulas-definitions:

$$\textbf{KDE of f with Kernel g :}\quad \hat{f}(x)=\frac{2C}{nh^{d}}\left[\sum_{i=1}^{n}g\left(\left\|\frac{x-x_i}{h}\right\|^2\right)\right]$$

$$\textbf{Mean Shift Vector}\quad :\quad \mathbf{m(x)}=\frac{\sum_{i=1}^{n}x_i g\left(\left\|\frac{x-x_i}{h}\right\|^2\right)}{\sum_{i=1}^{n}g\left(\left\|\frac{x-x_i}{h}\right\|^2\right)}-x \qquad (3.11)$$

$$\textbf{Gradient at x}\quad :\quad \nabla\hat{f}(x)=\frac{2C}{nh^{d}}\hat{f}(x)\mathbf{m(x)}$$

Equation (3.11) indicates that the mean shift is proportional to the local gradient estimate, yet it can define a path leading to a stationary point of the estimated density, the mode of the distribution (the cluster centroid). It is also noticed that the mean shift step is large for low density regions corresponding to valleys and decreases as *x* approaches a mode (becomes zero if the point identifies with the mode).

It is remarkable that the only parameter of the algorithm is the bandwidth h. The number of classes is internally evaluated as the mean shift vector determines if the newly calculated centers will merged with the existing ones or will be the barycenter of a new cluster. The basic drawback of the algorithm is the

low speed of convergence but there exists a lot of research regarding implementation for speed-ups and improvements. In addition, a limitation of the standard mean shift procedure is that the value of the bandwidth parameter is unspecified and application dependent [51]. An example of Mean Shift clustering segmentation performed on the Hue color band of an immunohistochemical image sample is illustrated in Figure 3.4.

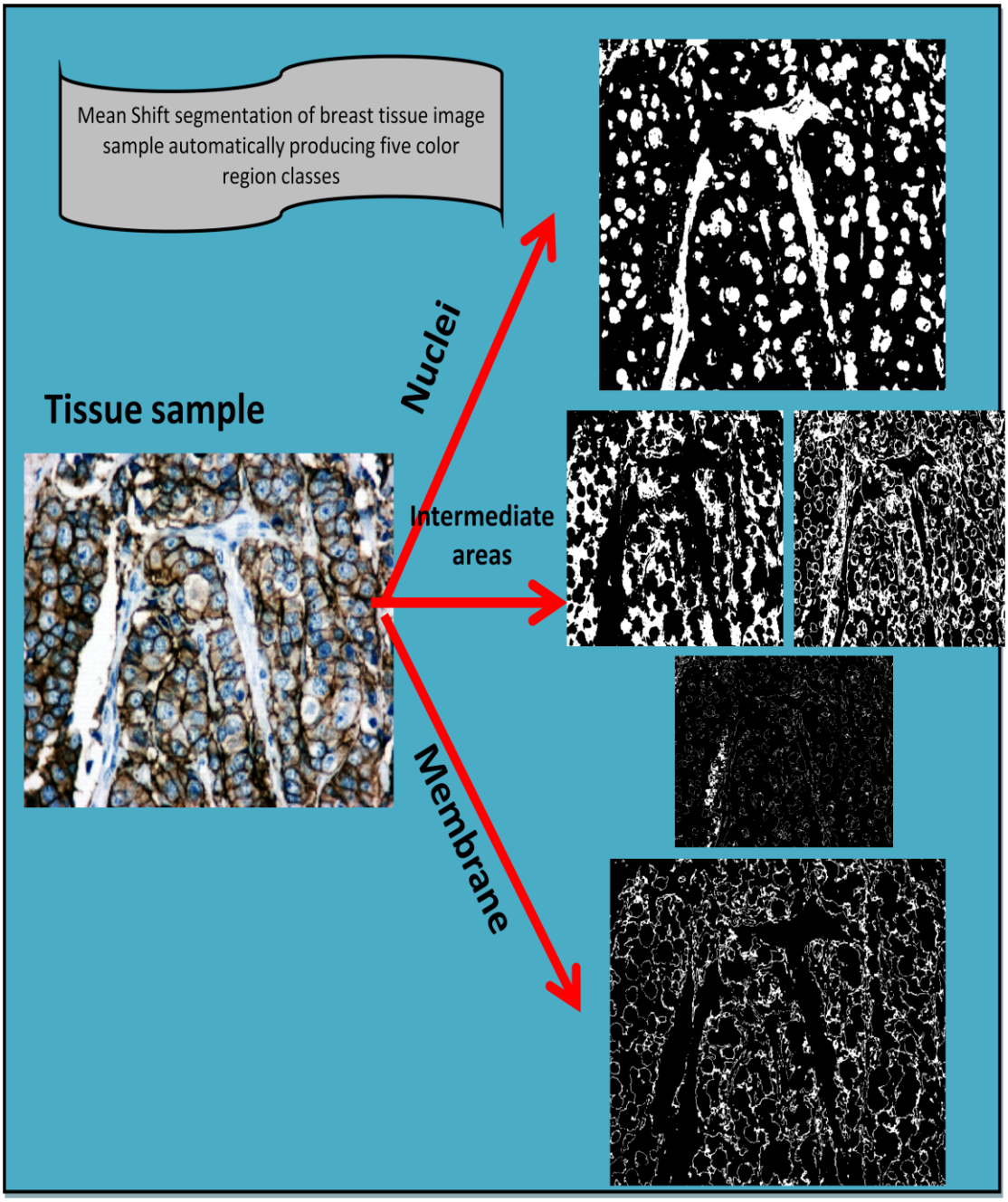

Figure 3.4 Example of immunohistochemical image segmentation applying the Mean-Shift clustering algorithm

3.3. Watershed transform

Watershed transform constitutes one of the reference methodologies regarding image segmentation. The major idea beyond watershed transformation is based on the concept of topographic representation of image intensity, fused with other principal image segmentation methods including discontinuity detection, thresholding and region processing. Because of these factors, watershed segmentation displays more effectiveness and stableness than other segmentation algorithms, producing closed contours and separating intersecting regions.

When reporting on watershed transform, three fundamental notions arise; minima, catchment basins and watershed lines. These definitions are illustrated in Figure 3.5. If we imagine that bright areas of an image have “peaks” and dark areas have “valleys’, then it might look like the topographic surface illustrated above. We may observe three types of points: (1) minima, points belonging to the different minima; (2) catchment basins, points at which water would certainly fall in a single minimum; and (3) watershed lines, the highest intensity level points at which water would have equal probability to fall in more than one minimum. The goal of this segmentation scheme is to detect all of the watershed lines (the highest gray level).

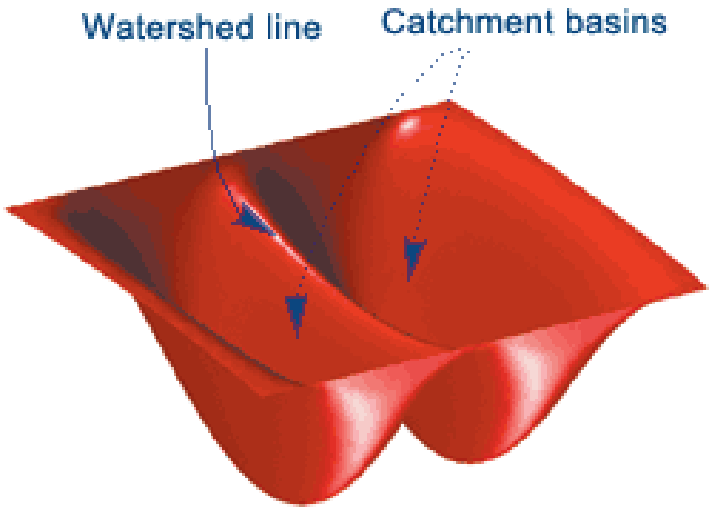

Figure 3.5 Fundamental definitions of the Watershed transform (www.mathworks.com)

The scenario underlying this method comes from geography: it is that of a landscape or topographic relief which is flooded by water, with watersheds being the separation lines of the domains of attraction of rain falling over the region. Alternatively, we may imagine the landscape being immersed in a lake, with holes pierced in local minima. Basins will form the water tanks filled up with water starting at these local minima, and, at points where water originated from different basins is crossed, dams are built. When the water level has reached the highest peak in the landscape and only the watershed lines are obvious, the process is stopped, yet the landscape has been partitioned into clearly separated water tank regions [52]. This procedure is illustrated in the Figure 3.6:

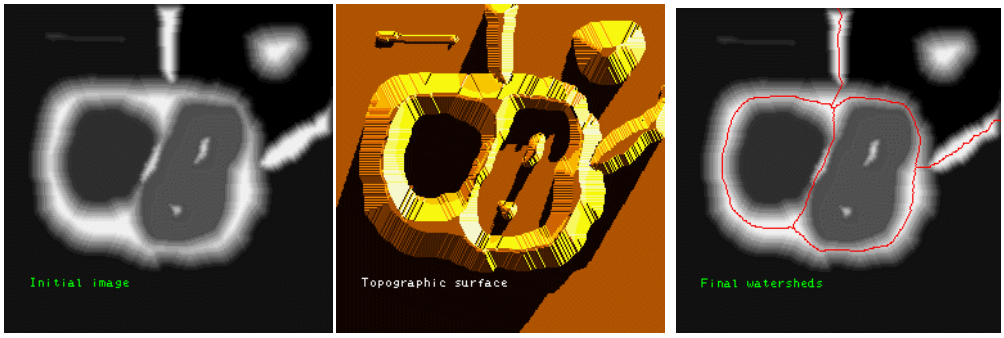

Figure 3.6 Initial grayscale image, topographic surface and finally segmented watershed image (http://cmm.ensmp.fr/~beucher/wtshed.html)

In order to apply this scenario to image segmentation, two approaches may be used: either one starts from locating the basins and then finds the watersheds by taking a set complement of them or one computes a complete partition of the image into basins, and subsequently extracts the watersheds by boundary detection. The segmentation procedure also includes an appropriate labeling of the resulting regions, implying that all points belonging to a given catchment basin have the same unique label, which is distinct from all the other assigned labels of the catchment basins. Sometimes the watershed transform is not applied directly to the original image, but to its (morphological) gradient [53], producing watersheds at the points of grey value discontinuity (edges). The watershed algorithms can be generally divided into two classes, one based on alterations of a recursive algorithm by Vincent & Soille [54], and another based on distance functions by Meyer [55].

Assume that the image f is an element of the space C(D) of real twice continuously differentiable functions on a connected domain D with only isolated critical points. Then the topographical distance between points p and q in D is defined by:

$$T_f(p,q) = \inf_{\gamma} \int_{\gamma} \|\nabla f(\gamma(s))\| ds \qquad (3.12)$$

where the infinum is over all paths (smooth curves) inside.

Let have $f \in C(D)$ have k minima$\{m_{k\in I}\}$ (roots of its gradient producing positive second gradient) for some index set I. The catchment basin $CB(m_i)$ of a minimum m_i (i=1,2,…,k)) is defined as the set of points which are topographically closer to m_i than to any other regional minimum m_j:

$$CB(m_i) = \left\{ x \in D | \forall j \in I \setminus \{i\} : f(m_i) + T_f(x, m_i) < f(m_j) + T_f(x, m_j) \right\} \qquad (3.13)$$

The watershed of f is the set of points which do not belong to any catchment basin:

$$Wshed(f) = D \cap \left(\bigcup_{i \in I} CB(m_i) \right) \qquad (3.14)$$

So the watershed transform of f assigns labels to the points of D, such that different catchment basins are uniquely labeled and a special label W is assigned to all points of the watershed of f. Thus the Meyer's flooding algorithm is summarized as

Label the regional minima with different colors

1. Select a pixel p, not colored, not watershed, adjacent to some colored pixels, and having the lowest possible gray level
2. If p is adjacent to exactly one color then label p with this color
3. If p is adjacent to more than one color then label p as watershed
4. Repeat steps 1-3 until all pixels have been processed

There exist a lot open issues concerning the watershed transform. A detailed and thorough analysis and review of the existing watershed transform approaches can be found in [52]. Firstly, there is the question of accuracy of watershed lines. In general, the result should be a closed contour, so the distance metrics adopted in the watershed calculation should approximate the Euclidean distance. The main drawback of the watershed method in its original form is that it produces a severe oversegmentation of the image, many small regions are extracted due to calculation of numerous local minima in the input image. The most appropriate solution is the use of markers, key sub-regions or single points within each basin that significantly differ from the remaining basin region (e.g. the brightest points derived by the h-maxima transform), resulting to the so-called marked-watershed transform [56]. Each initial marker has a one-to-one relationship to a specific watershed region, thus the number of markers will equal the final number of watershed regions. The markers can be manually or automatically selected, saving computational time and improving segmentation accuracy.

An example of application of the watershed transform is illustrated in the following scheme. Detailed analysis of the implementation steps will be given in the next section. In the first application of the transform (upper image) the input image was directly the blue color channel of the original image. We can notice that the result is not accurate as oversegmentation has taken place. Extracting markers applying the h-domes (see Section 4) and using as an input the difference of markers from the blue channel of the original image the segmentation accuracy is significantly increased.

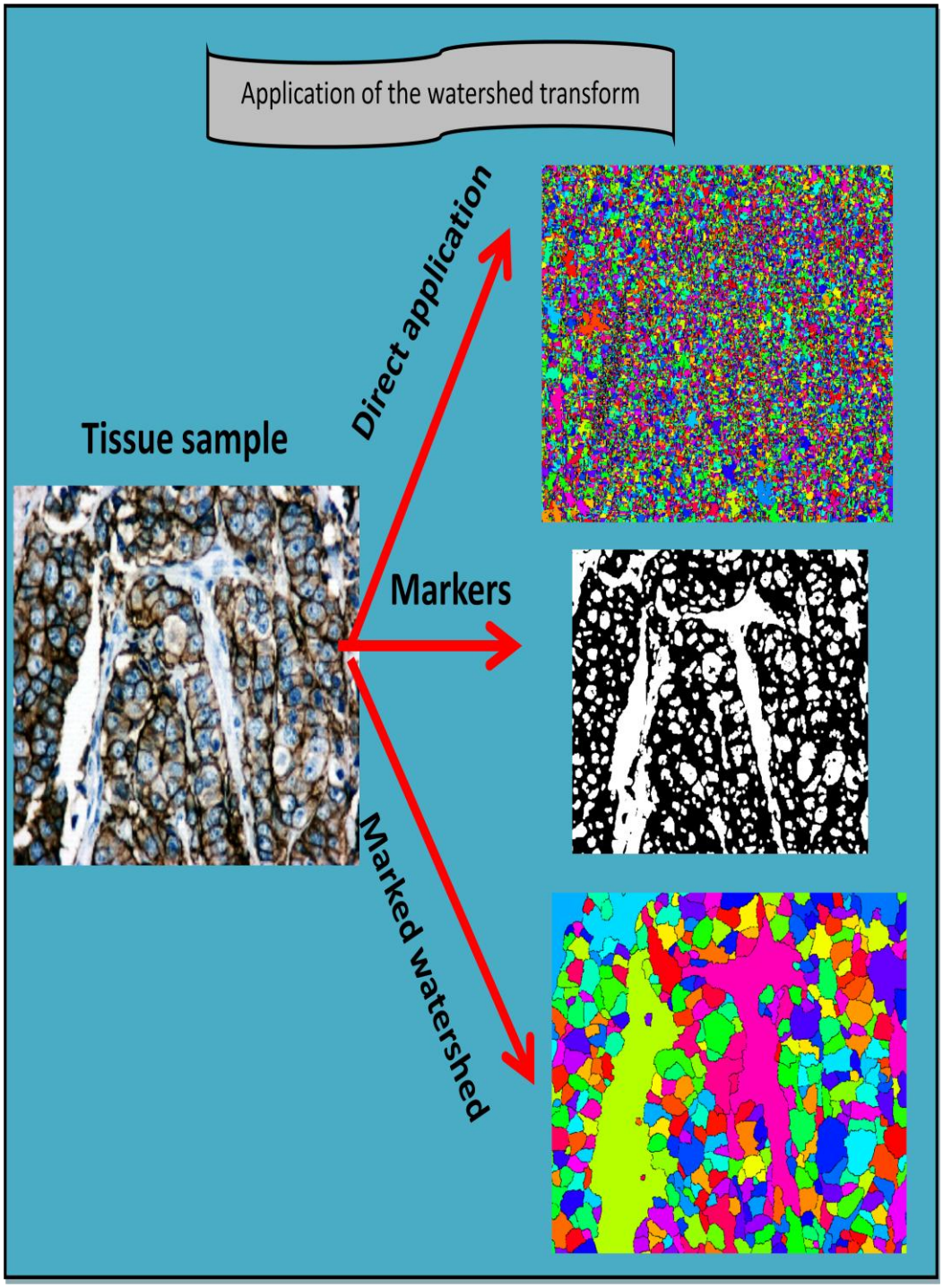

Figure 3.7 Application of watershed transform and the marked-watershed transform to an immunohistochemical image

3.4. Active contours model

Contour-based techniques are well established in international bibliography, providing accurate and robust results even in noisy environment, having the drawback of suffering from initialization, local minima and stopping criteria problems. The principle of these techniques lies on the linking of edge points extracted via an edge detection scheme, attempting to exploit curvilinear continuity in order to iteratively approximate the object borders starting from an initialized closed curve [57]. Global minimum energy searching methods have been proved generally effective in overcoming local minima problems due to the presence of artefacts introduced within the image, leading to robust convergence regarding the final contour extraction.

Chan and Vese [58] proposed a powerful and flexible methodology for active contours object detection combining curve evolution techniques, level sets and the Mumford-Shah functional, accomplishing to detect corners and any topological change. The model begins with a contour in the image plane defining an initial segmentation and then this contour gradually evolves according to a level set method until it meets the boundaries of the foreground region. According to the model, a curve C is represented via a function φ (the level-set function) as $C=\{(x, y)|\varphi(x, y)=0\}$, where (x, y) are coordinates in the image plane while the evolution of the curve is given by the zero level curve at time t of function φ(x, y, t) . Negative values of φ denote points outside the curve while positive values of φ originate from points belonging to the internal area of the curve, as depicted in the following scheme:

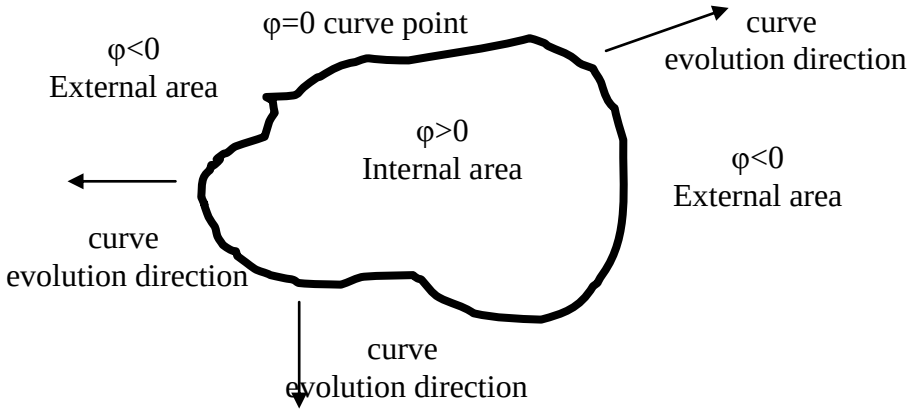

At any given time, the level set function simultaneously defines an edge contour (φ=0) and a segment of the image (φ≠0) and is being evolved according to the partial differential equation (3.15), iteratively converging to a meaningful segmentation of the image.

$$\frac{\partial \phi}{\partial t} = |\nabla \phi| F, \quad \varphi(x,y,0)=\varphi_0(x,y) \qquad (3.15)$$

where F denotes the speed of the curve evolution and $\varphi_0(x,y)$ defines the initial contour the algorithm started to be generated from.

A particular case is the motion by mean curvature, when F becomes the curvature of the level-curve of φ passing through (x,y) according to the formula:

$$F = div\left(\frac{\nabla\phi(x,y)}{|\nabla\phi(x,y)|}\right) \tag{3.16}$$

The speed of the evolving curve becomes zero on the points with highest gradients, therefore the curve stops on the desired boundary, which appears strong gradients.

Chan and Vese updated the classic snake model described above, introducing the energy functional term. Assuming that the image I consists of two regions of approximately constant distinct intensities I^1 and I^2 and that the object of interest is represented by the region of value I^1 (inside curve C), the "fitting energy functional" is denoted according to equation (3.17):

$$\begin{aligned} F_1(c_1,c_2,C)+F_2(c_1,c_2,C) = \lambda_1\cdot\int_{insideC}|I(x,y)-c_1|^2\,dxdy + \lambda_2\cdot\int_{outsideC}|I(x,y)-c_2|^2\,dxdy \\ +\mu\cdot Length(C)+\nu\cdot Area(inside\ C) \end{aligned} \tag{3.17}$$

where C is any variable curve except for the object boundary C_0, constants c_1 , c_2, are the averages of I inside and outside C respectively, and $\mu,\nu,\lambda_1,\lambda_2$ are non-negative fixed user defined parameters. If $F_1(C)>0$ and $F_2(C)\approx 0$ the curve is outside the object, if $F_1(C)\approx 0$ and $F_2(C)>0$ the curve C is inside the object and if $F_1(C)>0$ and $F_2(C)>0$ then the curve is both inside and outside the object, intersecting with its boundary. The contour of the foreground region is the solution of the minimization problem $\inf_C (F(c_1, c_2, C)) \approx 0 \approx F(c_1, c_2, C_0)$. Using the Heaviside function *H* and the one –dimensional Dirac measure δ_0 , defined, respectively by

$$H(z)=\begin{cases}1, & if\ \ z\geq 0\\ 0, & \text{if } z<0\end{cases}, \quad \delta_0(z)=\frac{d}{dz}H(z) \tag{3.18}$$

we can calculate component Length, Area and the means c1, c2 of equation (3.17) following the formulas:

$$\begin{aligned} &Length(\phi=0)=\int_c|\nabla H(\phi(x,y))|dxdy=\int_c\delta_0(\phi(x,y))|\nabla(\phi(x,y)|dxdy \\ &Area(inside\ \varphi\geq 0)=\int_c H(\phi(x,y))dxdy \\ &c_1(\phi)=\frac{\int_C I(x,y)H(\phi(x,y))dxdy}{\int_c H(\phi(x,y))dxdy} \\ &c_2(\phi)=\frac{\int_C I(x,y)[1-H(\phi(x,y))]dxdy}{\int_c [1-H(\phi(x,y))]dxdy} \end{aligned} \tag{3.19}$$

A detailed description of the complete mathematical background can be found in [59]. Chan and Vese proposed the fixed values $\lambda1=\lambda2=1$ and $\nu=0$. Parameter μ defines the update weight factor for curve evolution owing to the perimeter size of the already evaluated regions, while $\lambda1$, $\lambda2$ are the update weight factors owing to the variations of the image in the external and internal area, respectively, of the curve.

In order to reveal the efficiency of the Chen and Vese Active Contours scheme, an illustration of the application of our contour based segmentation technique to an immunohistochemical image sample follows. Further analysis of our implemented algorithm along with enriched results will be presented in the following section of the thesis.

The algorithm was fed with the image sample in the LAB color space (upper left corner), marked with the cell area contours derived from the watershed transform, as an input. The initial contour $\varphi_0(x,y)$ (upper right corner) was extracted via mean-shift clustering. The curve calculated after the convergence of the algorithm and the segmentation result after 969 iterations are depicted in the second row of figure 3.8, in its left and right part respectively.

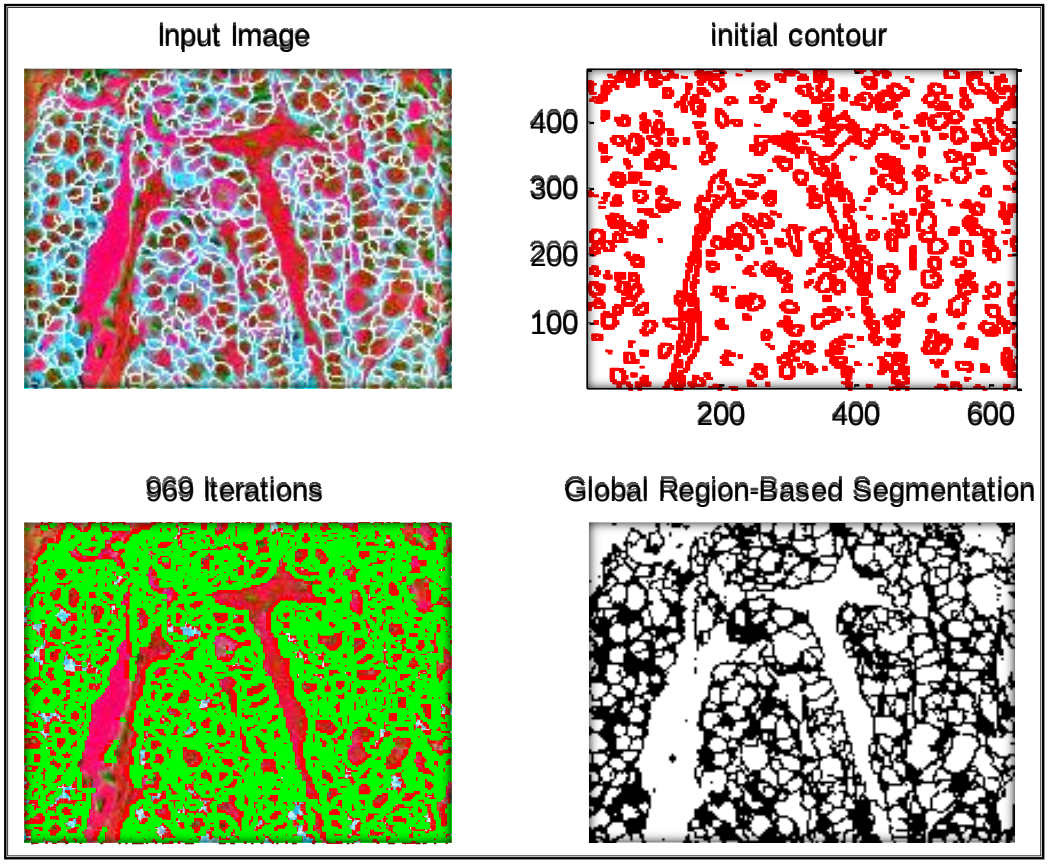

Figure 3.8 Application of active to an immunohistochemical image

4. Tissue evaluation algorithm

4.1. State of the art

In international bibliography, there are few references for individually developed, pure image processing algorithms for microscopic slides derived from immunohistochemistry (IHC). In laboratories, where a serious, precise and secure study must be worked out as the results of immunohistochemistry are directly related to disease treatment issues and health survival, the extraction of the results and the interpretation of the results are made by experts. One approach is the interpretation by a group of pathologists in order to score the immunohistochemical result by their experience and by their visual ability. Of course, this approach is fully subjective and dependent on the specialist's ability. The common approach is to use commercial software. This approach, based on automation and fully commercially developed programs, extracts more objective results with the cost of increased demands for hardware, software and calculation time. Yet, this algorithmic procedure is not open for further analysis. Another approach is the pure image processing algorithmic approach, where individual researchers suggest their own methodology, implementation and study for the analysis of immunohistochemical slides. The drawback of this approach is that it cannot be generally adopted and accepted as it is based on intuition and needs a great number of trials, tests, data processing and further investigation to correlate the results and evaluate their efficiency. Unfortunately, there is very limited bibliography in this section. The third and most common approach is a combination of the two approaches above: algorithmic implementation based on researcher's proposals implemented by simple, low-cost software, "the semi-automated approach". Most publications are based on this approach.

Pure image processing techniques can be classified in three main categories: a) thresholding techniques, b) color transformation techniques and c) histogram based techniques. Comparing these three main categories, we could mention that they are simple, in general, as they process data at their raw form. This has the cost of potentially high computational load depending on the amount of data processed. Thresholding techniques have the drawback of "subjectiveness", as the success of the method is highly dependent on the selection of the appropriate threshold. This process is not an easy and fixed part, as the selection can be made by automated techniques/programs or manually, by the test and reject procedure, which may not converge quickly and accurately. Color transformation requires a respectable computational time, especially for large images but can accurately estimate the characteristic "brown" membrane staining of IHC, surely knowing that red and yellow colored pixels correspond to brown shades of immunohistochemical reaction. Finally, histogram based techniques provide information about the distribution on intensities in the whole image or in specific regions but require a somehow pre-knowledge of the information illustrated.

Computer assisted methods of assessing immunohistochemical staining have been available for some time but, due to their expense and requirement for significant computer skills, have not gained widespread usage. In [60], the authors attempted to assess oestrogen receptor positivity by using digital image analysis. One hundred and fifty six sections were studied of which only forty one were ER

negative. The results showed a close correlation between the digital method (H-score), the optical result (median optical density of the nuclear mask) and the manually assessed oestrogen positivity. In [61], an attempt to quantitatively evaluate Her-2/neu expression using Photoshop was made. Forty breast cancer cases were examined and statistical analysis was performed. The results showed high correlation between the proposed method and the semi-quantitative HER-2/neu immunostaining score.

Pure image processing techniques is the main and desired category of IHC image processing techniques, an open research process. The existed methods in international bibliography are very limited. This category offers flexibility in implementation, yet needs a great number of validation tests to approve the extracted results. In [62], a respectable and complete implementation of specific algorithms was introduced. Unfortunately, the presentation contains only visual and non-comparable results.

In [63] an application of automatic thresholding in image analysis scoring of cells in human solid tumors was introduced. Thresholding is a common, computationally efficient segmentation technique. Interactive thresholding may be subjected to errors due to investigator bias and inconsistencies, while automatic thresholding may be subjected to errors due to computer failure to judge the accuracy of the selected threshold. The success of a particular method is dependent on the detail and complexity of the image and on the uniformity in the classifying pixel property among objects. The first goal was to distinguish nuclei from non-nuclear objects and cellular debris. According to the results, the gray-level threshold algorithm achieved to distinguish the nuclei that were darkly stained brown or blue and therefore had low gray-level values from the lightly stained background material and cytoplasm with high gray-level values. Overlapping nuclei were not recognized. The results also showed that the automatic selection of the threshold required less time than selecting it individually for both gray-level threshold and hue threshold. In addition, the automatically selected thresholds remained identical between days while investigator-selected thresholds were subjected to human error. Three investigators extracted results, which showed a high correlation between automatically and individually selected GLT but significant differences in the HT selection. The authors propose both the automated GLT and HT selection method because the image routine results were indistinguishable from their visual counterparts, had less variation than that of visual analysis and had supremacy against the corresponding individually defined ones. Errors due to automatic thresholding altered the size and shape of objects but had little impact on the selection of objects for analysis, thus the number of objects determined will not be affected. Instead, object properties (e.g. optical density, size) might be altered, thus automatic thresholding should be carefully used for purposes such as morphometry or DNA ploidy measurements. Finally, optimal sample preparation for accurate image analysis results is critical.

Semi-automated approach to IHC image processing relies on commercially available software, of varying capabilities and cost, which generally provides a simple and complete interface and a variety of implemented routines in order to extract numerical data (e.g. histogram extraction, thresholding, pixel counting, contrast and brightness manipulation). The IHC interpretation is then supplemented by other numerical calculations, dependent on the researcher. This

approach is a simple, flexible and secure method as the results of the software are precise, reliable and quick. The flexibility of the various proposed methods depends on the researcher's intuition and the availability offered by the software (usually Matlab and Photoshop).

Currently available algorithms are best suited to counting pixel number or to measuring area. Although these approaches are adequate for comparative assessments, they do not allow quantification of the absolute amount of chromogen present in an image or a portion of an image. Because pixels have dimension, algorithms based on pixel counting generate information concerning area. Therefore, the area occupied by any particular color range can be specified and compared in a relative manner, but it is not possible to determine the absolute amount of chromogen present. On the other hand, algorithms based on color thresholding or counting pixel number within a color/brightness range preassume the presence of information within a specific range. In general, the DAB-generated "brown" color in IHC must be calculated. This has the limitation that coefficients in the basic equation must be determined, the range of the brown color is not known to the viewer and needs to be determined and finally that this approach counts only for systems generating chromogen of identical brown color and not of any other color.

In [64], a method of segmentation and classification of nuclei is presented. As regards the segmentation part, the key point is the window size selected in order to recognize all nuclei. A small window size will not recognize large nuclei with the benefit of quicker segmentation result extraction. As regards the classification part, the visual determination of the result is highly subjective so the statistical pattern recognition scheme used must have a well defined training set in order to exactly recognize the nuclei.

In [65], a brightness-area-product-based-protocol was introduced in order to quantitatively assess the brightness of a single channel immunofluorescent histological image. The results revealed a very close correlation between individual observer interpretation of B-gal expression intensity scored as 0-3 and the interpretation of the brightness calculated by the proposed procedure. As regards the pure image processing part, adequate control for background is a vital consideration. There are several ways to report the brightness of an image, such as optical density and mean pixel intensity or average grey level in fluorescence and chromogen stained images. To detect the most abundant of epitopes, the vast majority of pixels within a region of interest will be of low pixel intensity swamping the averaging process and giving a low mean intensity. Thus, thresholding is critical but once a threshold is introduced and a mean pixel intensity is calculated, information about brightness abundance is lost. Integrated optical density is more sensitive to abundance, however the inclusion of background.into the number calculated means that differences between regions cannot be eliminated because the majority of pixels will generally be of lower intensity. Concluding, the technique cannot give absolute quantitative information as to the amount of antigen present in an area but can provide a simple means to objectively compare the intensity of staining in identical anatomical regions. A threshold BAP provides a simple intuitive measure of the relative brightness of an image which correlates well with human observation.

4.2. Proposed algorithmic scheme

Aiming at accurately segmenting microscope images depicting breast cancer tissue samples, which are prepared by the laboratory method of immunohistochemistry, for the fulfillments of this thesis we developed a novel methodology fusing appropriate image processing techniques, the fundamental aspects of which was analyzed in the third chapter. The proposed algorithm, contrary to the majority of existing approaches, takes minimal amount of prior knowledge on the characteristics of the image and necessitates minimal user intervention in order to guide or train it by manually selecting a point or region of interest. The only calibration needed is the determination of the cell size parameters depended on the magnification used during the image capture via microscopy. In addition, the presented method is capable of segmenting cells stained either utilizing the DAB or the PAP protocol, which was analyzed in section 2.2.2. As a further step, after achieving the relatively accurate segmentation of the cells and contour extraction of their membrane, we attempted to produce quantitative results for evaluating HER2 overexpression according to the internationally established scoring method by measuring the completeness and the intensity of the staining applying thresholding. The classification results produced give rise to further investigation of our proposal, with the prospect of transforming it to an assisting tool for pathologists, contributing to tissue evaluation and cancer diagnosis and treatment.

The presented cell segmentation and tissue evaluation methodology is a procedure resulted from the fusion of three key, successive processes:

- **Image enhancement**, where the sample images are filtered from noise, transformed from the RGB to the HSV and LAB space model and contrast enhanced via histogram equalization
- **Nuclear area estimation**, where the cell nuclei are separated from the whole tissue area via mean-shift clustering of the Hue channel of the enhanced HSV image, taking into account that the areas of interest will be uniquely assigned a characteristic blue color, emerged during the tissue preparation procedure
- **Membrane contour evaluation**, where the membranes of the cells are extracted via the active contours model (snake model), which is, innovatively, initialized by the initial contours derived from the clustering procedure performed in the previous step. The convergence of the cell boundary calculation is controlled by the lines resulted from the watershed transform, securing that the snake evolution will stop to a boundary and will not spread to the whole image area

The schematic representation of the algorithmic steps is illustrated in Figure 4.1. and includes the following basic stages:

1. **Image enhancement**, where the image is converted to the HSV and LAB color spaces in order to enhance the color differences between distinct areas. We noticed that the distance between the blue (nuclei) and brown/red (stained membranes) color is larger in these models than the RGB one. In addition, histogram equalization takes place in order to improve the image contrast

2. **Meanshift clustering**, where the key color regions within the image are extracted processing the pure chromatically informative color band Hue. We focus on the cell nuclei (blue image components) in order to count the cells in a latter stage and feed the segmentation algorithm followed with the appropriate information
3. **Watershed transform with h-domes markers**, where the marked watershed transform, with markers derived applying the h-domes transform, leads to a first estimate of the cell membranes producing closed boundaries that will be used to control the convergence of the segmentation algorithm in the next stage
4. **Active contours segmentation**, which forms the basic segmentation procedure and produces the cell regions and their boundaries. The algorithm is initialized by the result of the clustering method and its convergence is controled by setting borders to the snake evolution originated from the watershed transform

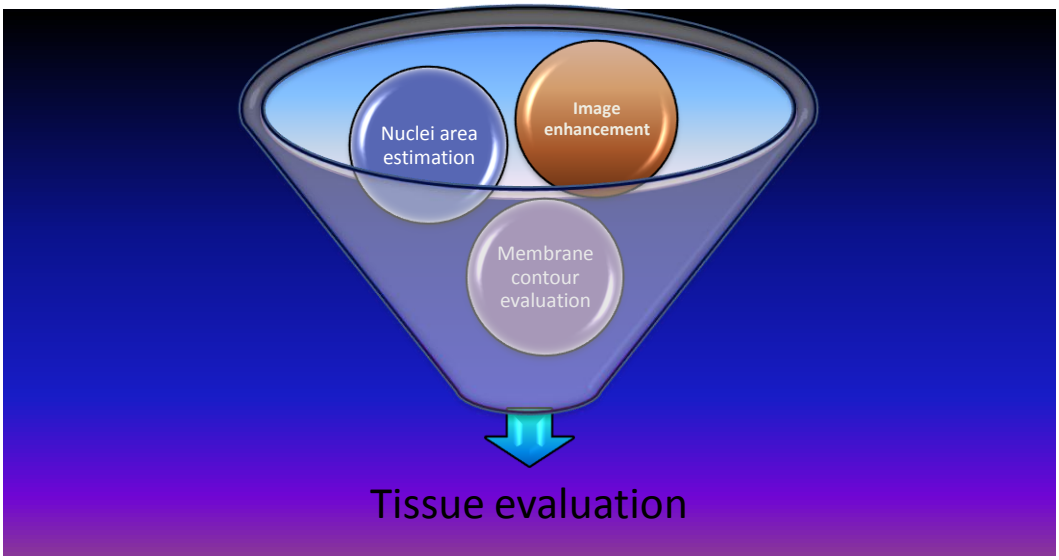

Figure 4.1 Schematic representation of the proposed tissue evaluation algorithm as a fusion of procedures

Having introduced the medical background of breast cancer, the technical aspects of immunohistochemistry and the tissue preparation procedure, the theoretical background of the utilized image processing techniques, we can proceed to the qualitative and quantitative results produced in every intermediate step of our approach.

Forty immunohistochemical tissue slides (33 stained using the DAB protocol and 7 using the PAP protocol), prepared in two different pathological anatomy laboratories, were processed The algorithm was implemented in the Matlab R14 platform and its runnings were performed on a Dell Precision T1600 computer machine, equipped with 8GB of RAM memory, an Intel (R) Xeon (R) CPU E31270 operating at 3.4GHz and NVIDIA Quattro 600 graphics card.

In the following sections, the successive stages of our methodology are analyzed, the contribution of each independent technique is revealed and representative and informative results are presented.

A more detailed representation along with the intermediate images produced in each step of our implementation is depicted in Figure 4.2

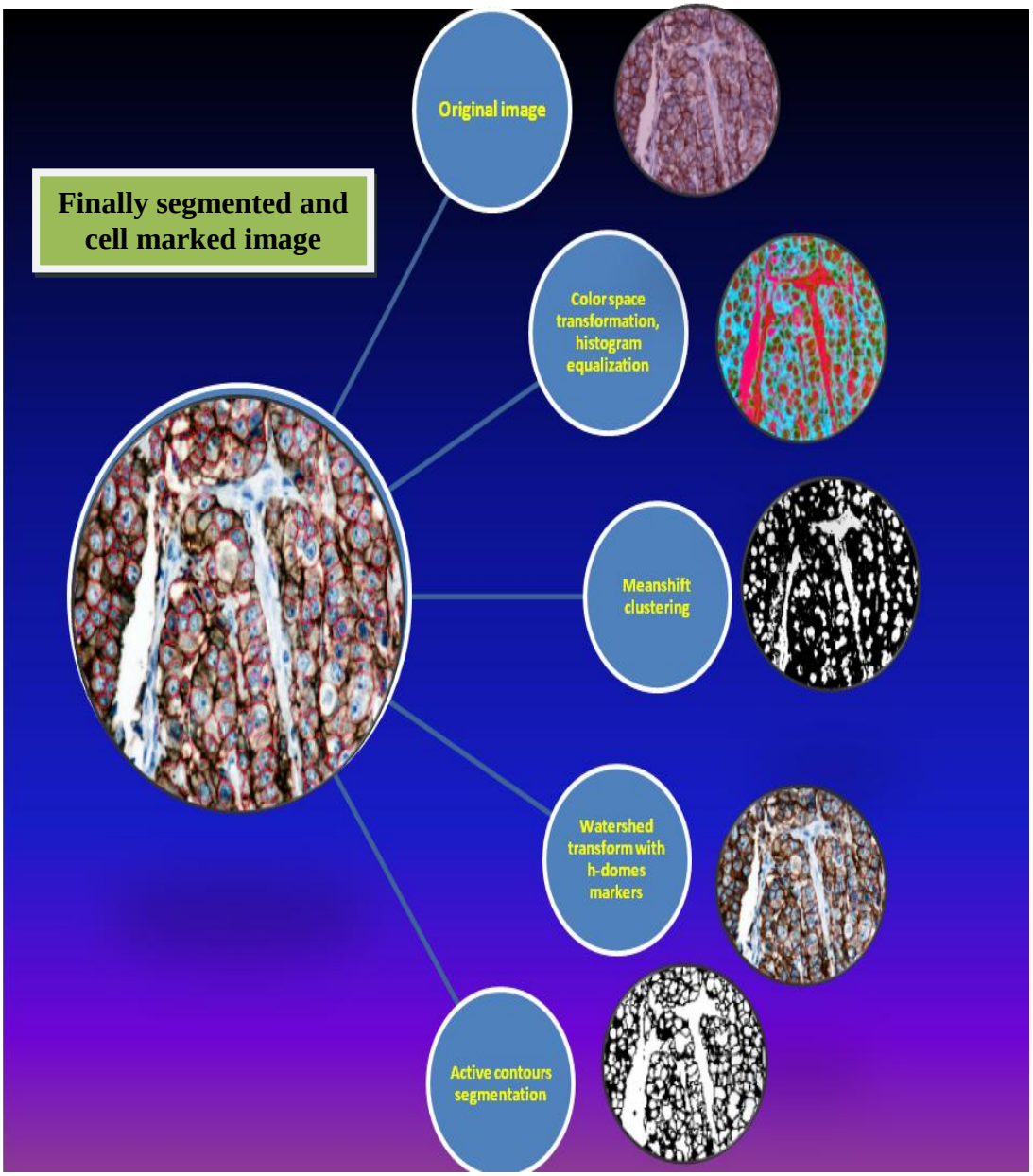

Figure 4.2 Input, output and intermediate steps of the proposed technique

4.3. Color model conversion

As mention in section 3.1, the RGB model is not appropriate for color image segmentation, thus the HSV and LAB color spaces are preferred. In order to improve the quality of the input immunohistochemical images, which suffer from noise and low contrast due to the microscope lens and artifacts due to errors during the tissue preparation, we apply histogram equalization on each color band of the models. In the resulted enhanced images, the key features for image segmentation (cell nuclei and membrane) are more clearly detected through human visualization, an advantage the specialist does not have under the microscope. Color bands before and after contrast enhancement are depicted in Figures 4.3 and 4.4 respectively. As it can be noticed, the Hue and B channels, of

the HSV and LAB space respectively, contain the pure color information necessary for the discrimination of the regions of interest within the segmentation procedure. Value and L channels provide information about the intensity levels of the images, while the Saturation and A bands depict the extracellular area.

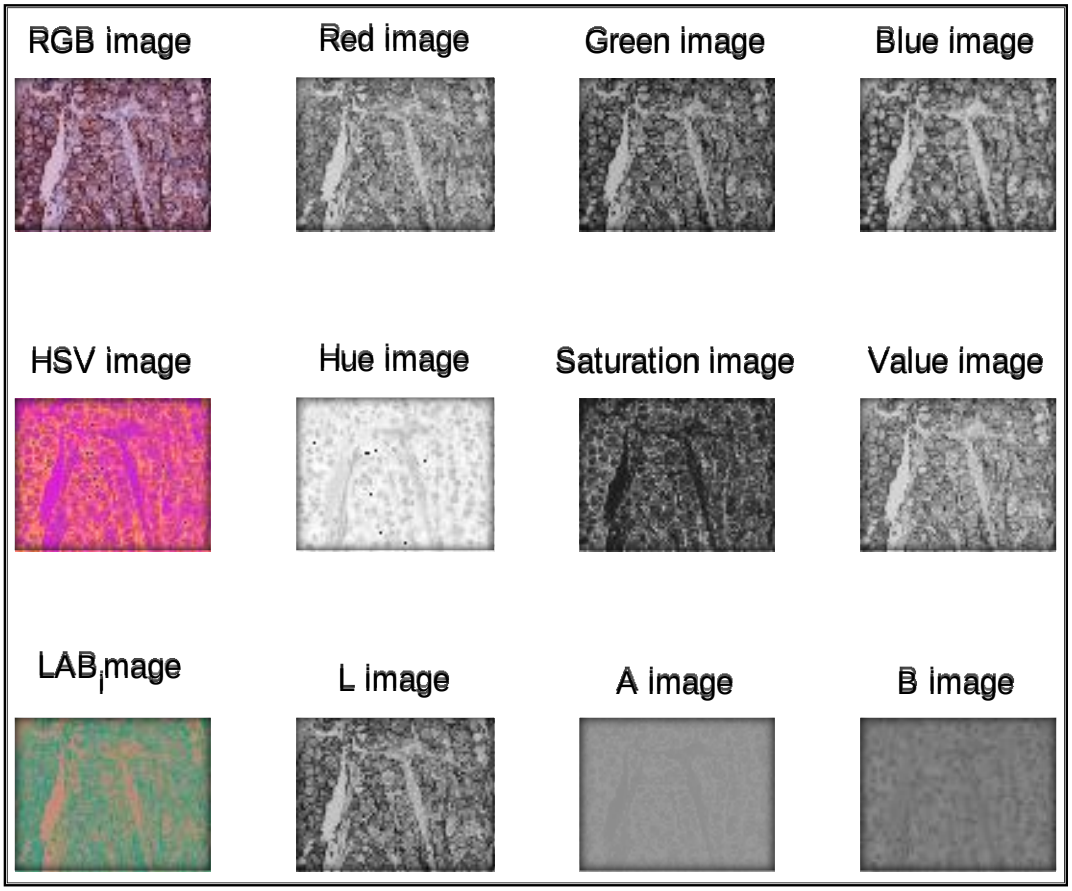

Figure 4.3 Original immunohistochemical image and the three color bands in the RGB (first row), HSV (second row) and LAB (third row) space

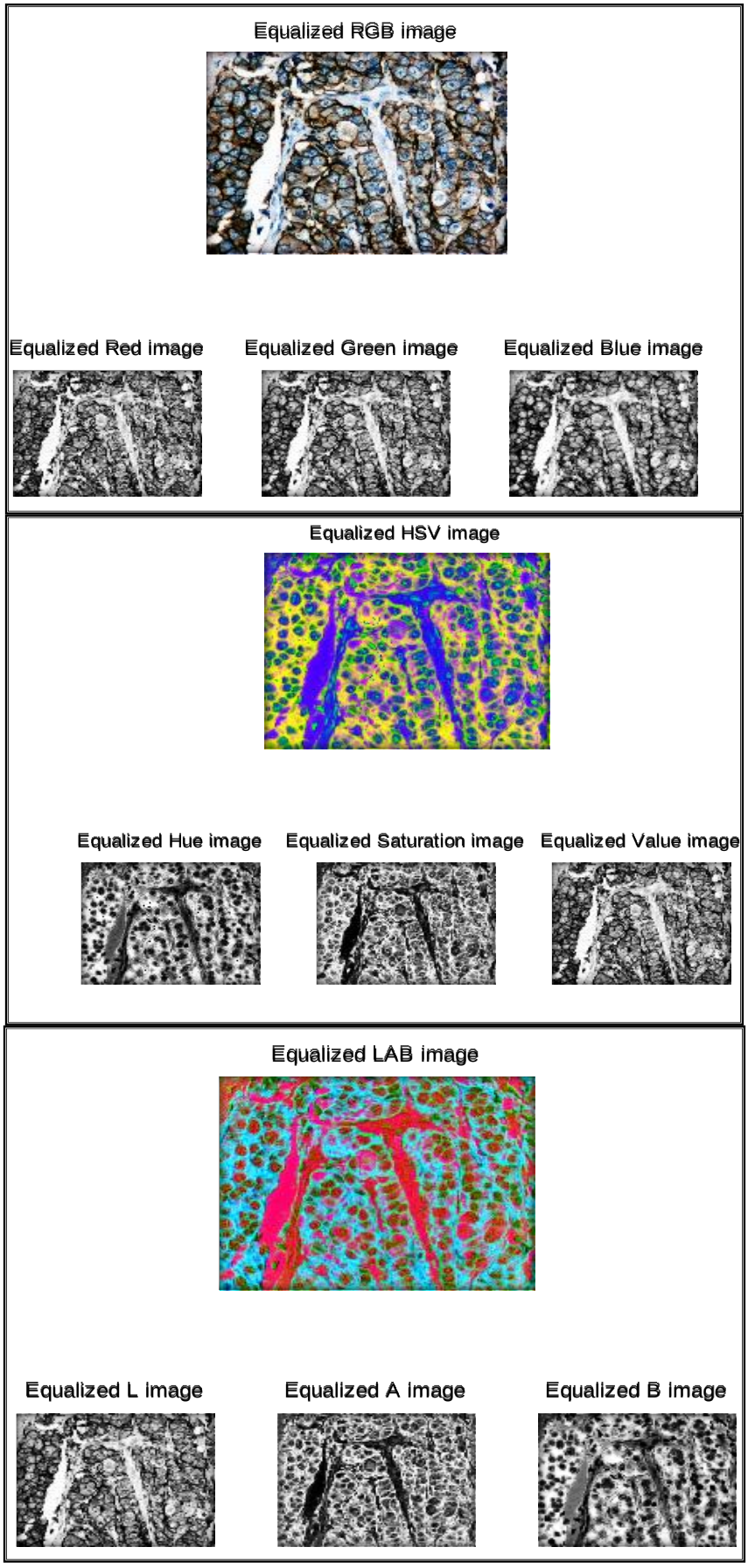

Figure 4.4 Equalized input image in the three color spaces

4.4. Key regions extraction

In this stage of the algorithm, the key regions of the histological image are extracted, namely the cell nuclei and an approximation of their membrane boundary. Assuming that each nucleus is assigned to a cell, the number of candidate cells forming the tissue can be evaluated by isolating the "blue" regions within the image, as implied by the staining protocol. This numbering is the prerequisite for the HER2 positive score evaluation and the tissue classification that will be performed on the final step of our methodology. Since only color information is required to fulfill the nuclei detection, mean-shift clustering of the Hue channel of the contrast enhanced image is performed. The HSV model representation was selected, as only one channel has to be processed, the Hue band, in order to discriminate the different color segments, leading to significantly decreased computational complexity. Color region extraction via clustering facilitates the detection of any color without any prior knowledge on the staining protocol followed, yet brown (DAB protocol) or red (PAP protocol) membrane staining can equally be recognized. In addition, the selection of mean-shift as the clustering method does not require the determination of the known color classes present in the tissue, yet it can detect distinct intermediate zones too. The result of the clustering scheme application is depicted in Figure 4.5. Five clusters were calculated, one representing the candidate cell nuclei, one representing the cytoplasm within the cell regions, one assigned to the candidate cell membrane boundaries and two classes representing the intermediate tissue sections. The bandwidth parameter h of the algorithm was set to 0.15.

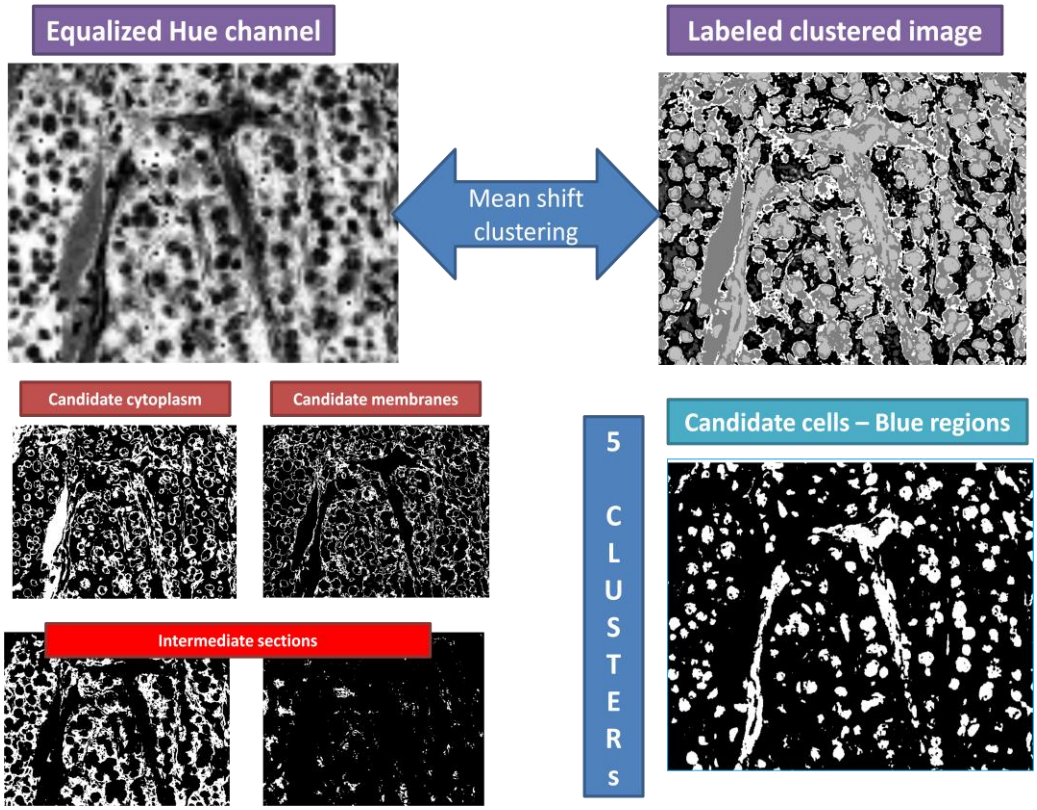

Figure 4.5 Results after applying mean-shift clustering to the IHC image sample

We can observe that the blue regions representing the candidate nuclei areas are accurately determined, as illustrated in Figure 4.6. By utilizing mathematical morphology large regions can be easily eliminated, increasing the detection accuracy of existing nuclei within the tissue. Yet, membrane boundaries cannot be accurately calculated, as many open or semi-closed areas are extracted when the membrane staining is not complete, thus a better technique must be adopted.

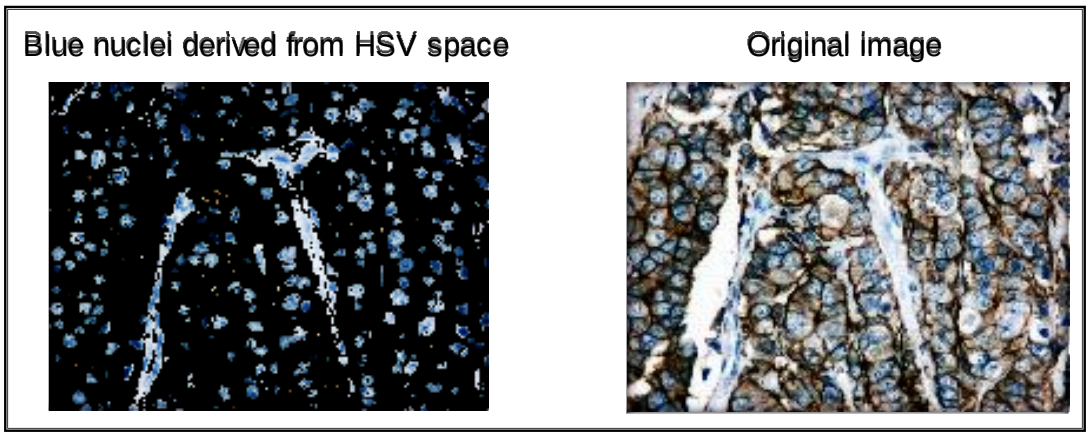

Figure 4.6 Segmented nuclei areas derived from the Hue channel after clustering application along with the equalized original RGB image.

In order to approximate cell membranes, closed boundaries must be produced, implying the use of the watershed transform, which produces segments with complete and non intersecting contours. Direct application of the watershed transform results in oversegmentation, yet the combination of the transform with markers and distance transforms is necessary. In our methodology, the extraction of markers for cell nuclei is achieved utilizing the h-domes transform [66]. The selection of this transform is done as it better enhances the intensity differences between the internal area and its surrounding. In addition, the morphology operators it performs may split marginally intersecting cell nuclei blue areas due the refinement of their size maintaining their original shape.his technique reveals bright structures (maxima) without involving any size or shape criterion. These structures fulfill the following criteria: a) every pixel in the dome has a gray value greater than any of the pixels surrounding it and b) the maximum gray level difference between two pixels in the dome is smaller than or equal to a threshold value h. The h-domes transformation, illustrated in Figure 4.7, can be defined by the formula:

$$M_h(I) = I - \rho_I(I - h) \tag{4.1}$$

where I is the original image, I-h represents the result of subtracting a constant value h from the original image, and ρ_I is the morphological reconstruction of the original image from I-h . The choice of h turns out not to be a critical operation, since a wide range of values yields correct results. For the needs of our implementation it was selected as 80. Since we intend to define markers for the blue regions of cell nuclei, the Blue channel of the enhanced RGB image is selected as the input image I of the transform. Applying the h-domes transform to the Blue color band image we produce the cell nuclei markers. As the nuclei are stained blue, they represent the high intensity regions of the image, yet its regional maxima are revealed via the h-domes transform. By reversing the Blue channel image and subtracting the cell nuclei markers, we produce an image with reversed

minima regions, creating candidate boundaries to surround the nuclei area. This reversed image becomes the input of the watershed transform and acts as a guide for the extraction of the watershed lines, which will form the cell membrane contours. In this way, the transform has enough and useful information to define borders surrounding catchment basins as it can detect intensity differences between compact regions (cells) and their surroundings (membranes). The cell contour extraction result is illustrated in Figure 4.8. The watershed lines superimposed on the original enhanced RGB immunohistochemical image is depicted in Figure 4.9, clearly demonstrated a surprisingly accurate approximation of the cell membranes.

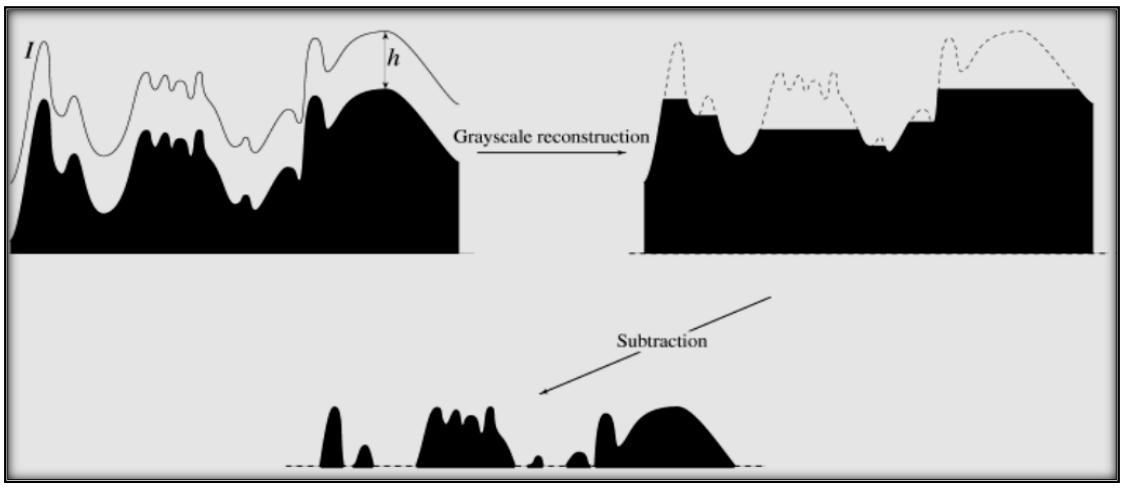

Figure 4.7 Illustration of the h-domes transform of an image I (Reference Halkiotis et al)

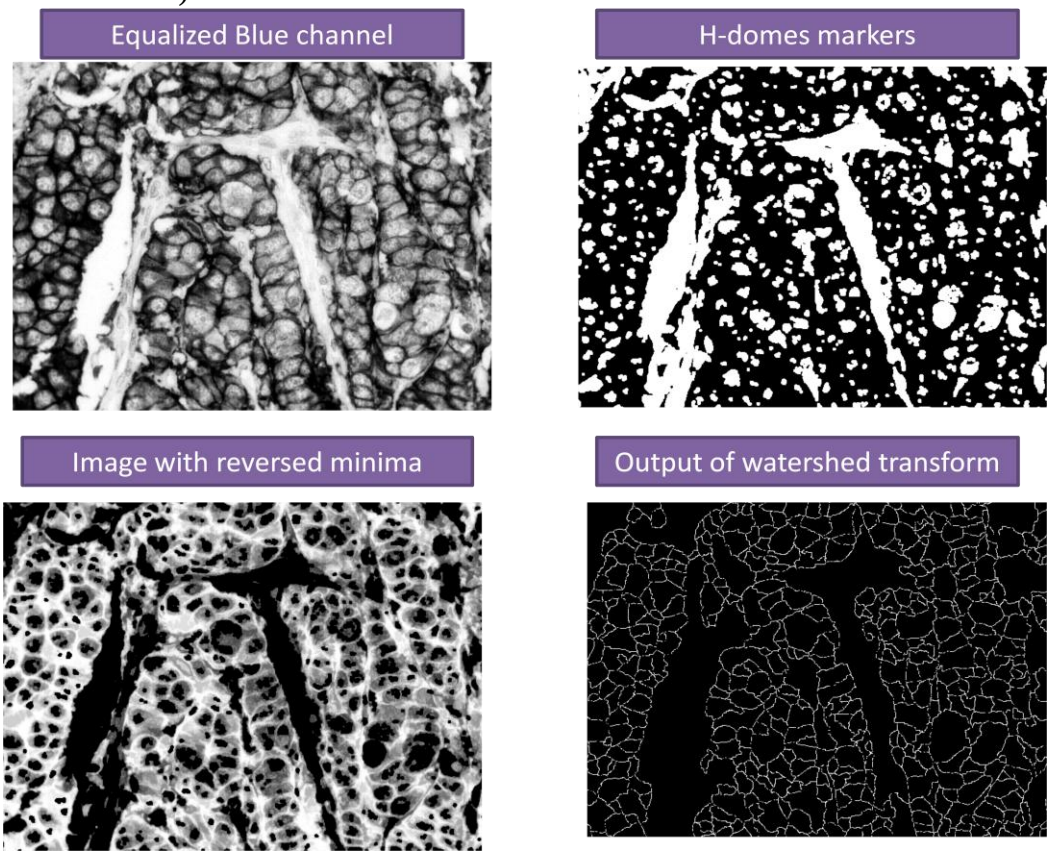

Figure 4.8 Segmentation result after applying the watershed transform to the image after enhancing its minima by reversing its h-domes transform

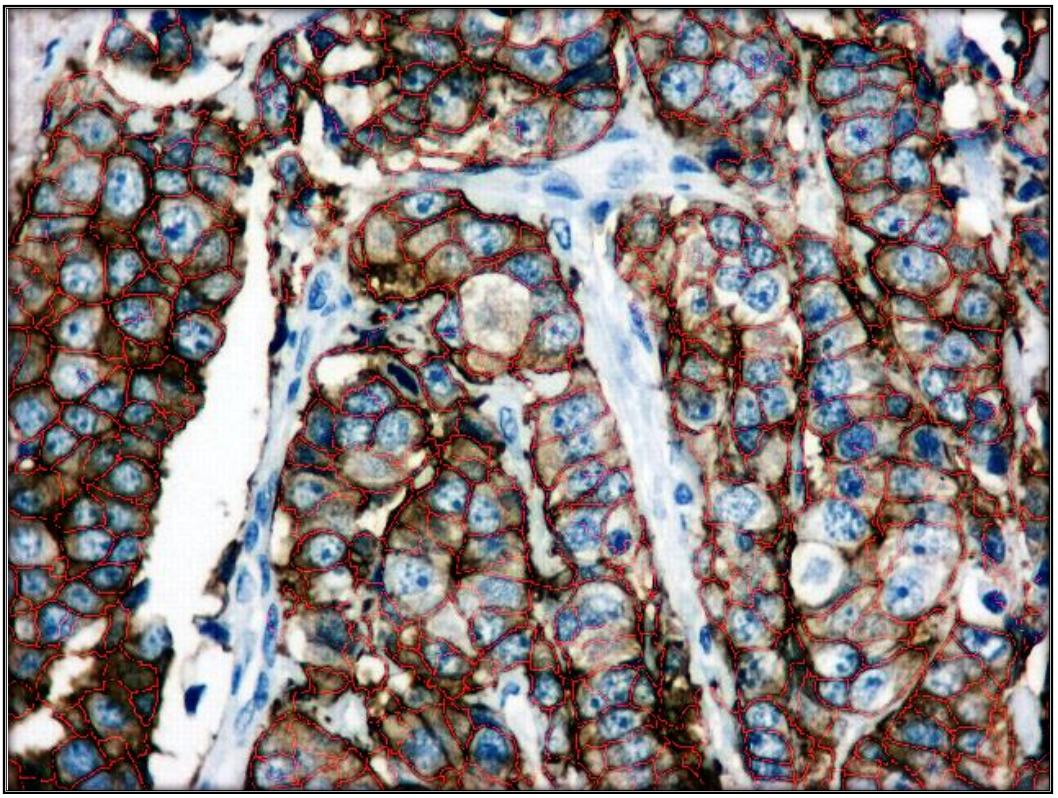

Figure 4.9 Watershed lines superimposed on the enhanced RGB image immunohistochemical image

We may notice that these estimates, in some cell regions, constitute an extension of their real boundary. Keeping the segmentation result of this stage, we may proceed to a more advanced level of evaluation, which is the refinement of the extracted boundaries to an internal area even closer to the exact perimeter of the cells.

4.5. Cell boundary specification

Having already a qualitative estimation of the cell boundaries, we intend to improve the accuracy of the segmentation result. This will be achieved adopting the active contours approach (also known as snakes), which, starting from an initial point or boundary, it repetitively updates and transforms it, forming an evolving contour with the goal of "hugging" all the key objects within the image and being adjusted to their perimeter. The selection of this approach for the last algorithmic stage of our proposed segmentation methodology was based on its advantage to produce closed boundaries, essential prerequisite for cell membrane evaluation and its ability to detect objects irregularly shaped and sized.

The main drawback of the snakes technique is the control of their algorithmic convergence due to pointless initialization (random in most cases), the size and the complexity of the processed image. The innovation of our approach is that the contour evolution is efficiently initialized and a possible terminal of it is supplied as a means of convergence control. More specifically, the initial contour provided originates from the clustering stage, where the cell nuclei have been detected. This selection for the initialization is ideal for accurate cell segmentation as the snakes curve will evolve from the internal area of the cell (each cell always has a nuclei), which has already been found via the Mean Shift algorithm, to its surroundings. Apart from the contribution to improved segmentation accuracy, our proposal significantly reduces the computational cost of the final boundary evaluation, cleverly overcoming the other basic limitation of active contours model, as the "snake" already has the information about the number of regions it will search for. As a further innovative step, we thought of providing the active contours algorithm with an estimate of the final result, in order to secure its convergence. This estimate comes from the result of h-domes marked watershed transform of the previous step of our methodology. By marking the input image of the snakes segmentation procedure with the watershed lines already calculated we prevent the snake from continuously evolving if no obvious border is met. In the immunohistochemical image, this could take place if the staining was too strong and had passed in the cytoplasm of the cell or in the intermediate tissue area. As regards the input image of the active contours algorithm, we selected the channels A and B of the equalized sample image in the LAB color space, since they provide all and only the color information needed for color segmentation.

In Section 3.4, the fundamental aspects of the active contours model were presented along with the Chen and Vese proposing approach. We recall the model description as represented with equation 3.17

$$F_1(c_1,c_2,C)+F_2(c_1,c_2,C)=\lambda_1\cdot\int_{insideC}\left|I(x,y)-c_1\right|^2dxdy+\lambda_2\cdot\int_{outsideC}\left|I(x,y)-c_2\right|^2dxdy$$
$$+\mu\cdot Length(C)+\nu\cdot Area(inside\ C)$$

As already stated, the contour C that will minimize the energy functional will define the boundaries of the regions within the image and its internal area will form the segments detected. In our approach, the parameter ν is set to zero, while the parameter μ, representing the factor that determines the length size update of the contour within the iterative procedure is set to 0.8, as we want a smooth and secure evolution and the regions of interest are not characterized big. In [58] Chen and Vese have processed the images setting parameters λ_1 , λ_2 equal to 1. We differentiate from this consideration and set λ_1=1.5, proposing to change the

weight contribution of the external area to the energy functional, thus the curve evolution step. Since we have started the snake evolution from the compact and intensity smoothed cell nuclei areas, we aim at evolving the curve to the external area of the nuclei and detect the intensity differences of the image from the almost constant mean value intensity within the cell area until we meet the membrane, which differentiates from remaining cell area or its surrounding.

Having determined our active contour model, we proceed to the segmentation of the cells. Convergence is achieved in significantly short time regarding the complexity of the immunohistochemical image, where numerous and irregular regions exist. The segmentation result is refined applying mathematical morphology, rejecting unwanted areas such as segments without nuclei, non circular and non ellipsoidal regions and regions with extremely long or short perimeter and area. These characteristics cannot be assigned to real cells, yet we are able to filter the extracted results and reject incorrectly recognized segments. Threshold values equal to 100, 10000, 0.96 and 4500 were set for small areas, big areas, eccentricity and perimeter respectively.

Figure 4.10 illustrates the input of the active contours algorithm and Figure 4.11 the segmentation result after the application of morphological operators. The first stage of filtering regards the rejection of areas that cannot represent a cell as they do not have a cell nuclei, thus blue areas extracted from clustering are not included in the corresponding initially segmented regions. The second stage of filtering, successive and not in parallel to the first one, refers to the rejection of areas that do not possess the shape characteristics to represent a cell, which means that candidate cell segments are too small, too big, too long and non circular or non elliptical.

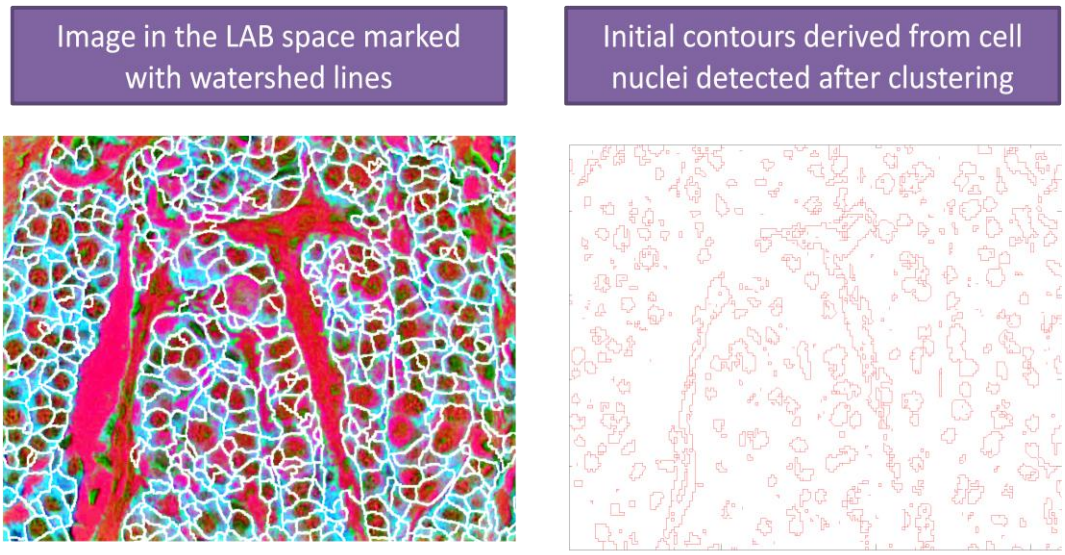

Figure 4.10 Input for the active contours segmentation: IHC image in LAB space marked with watershed lines (left) and initialization of snake with the boundary of the cell nuclei derived from Mean Shift Clustering

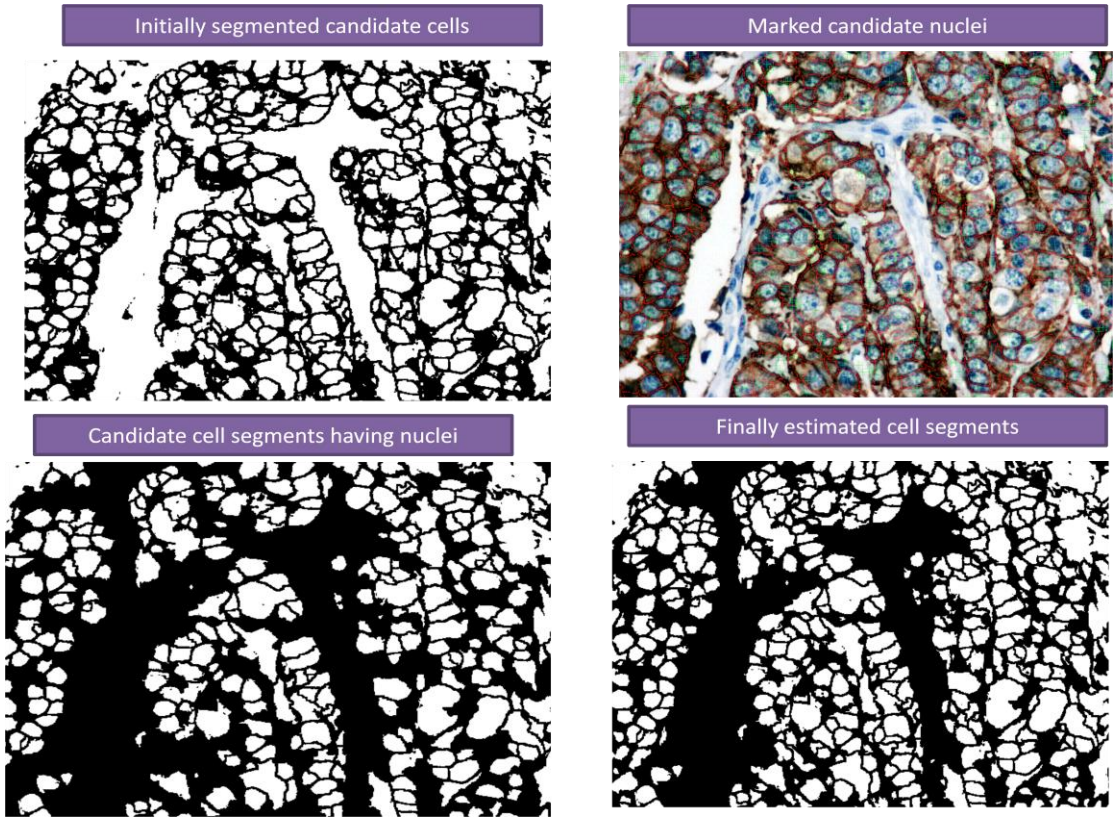

Figure 4.11 Segmentation result after application of active contours and mathematical morphology

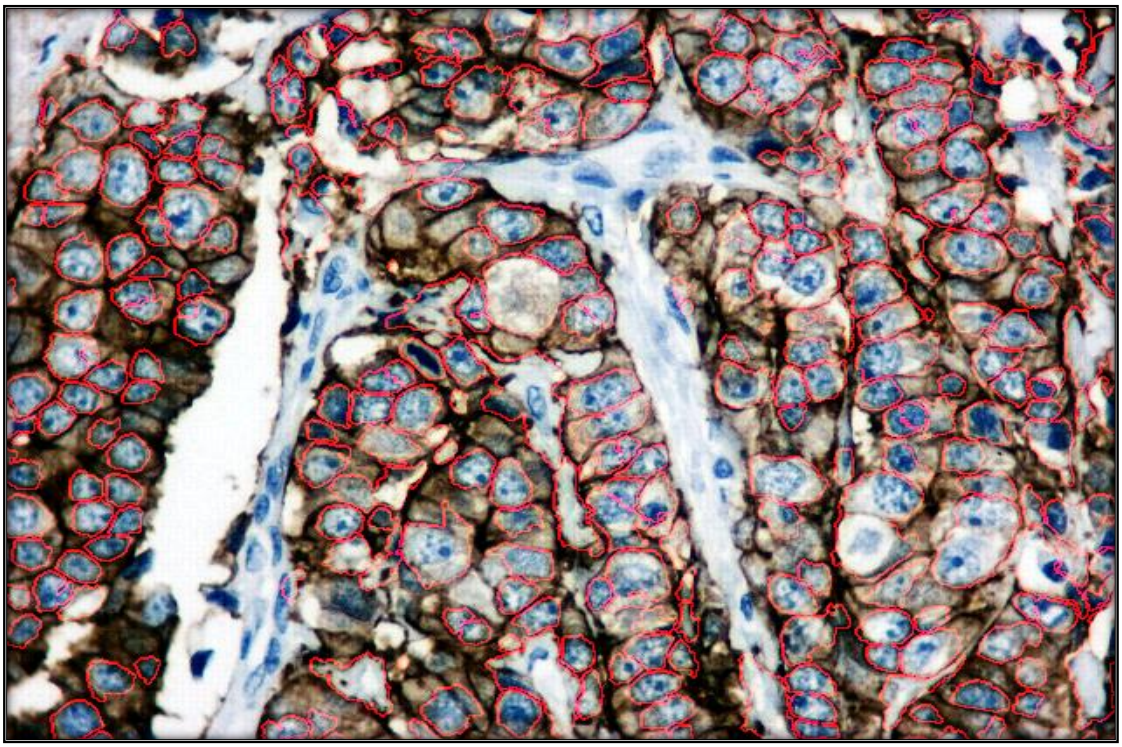

Figure 4.12 Segmentation of the immunohistochemical image sample applying our proposed algorithm with the cell boundaries superimposed on the equalized RGB image

The final result of our proposed segmentation algorithm is depicted in Figure 4.12. Despite of the limitations originated from the image quality and the high degree of complexity, even for a pathology expert, the accuracy of the segmentation is remarkable. The extended percentage of the areas have been accurately segmented while a qualitatively rejection of non cell regions is noticed, which very important as oversegmentation is restricted in cell segmentation applications.

4.6. Experimental results on Segmentation

We followed the same algorithmic procedure for all the 40 IHC image samples of our dataset. Figure 4.13 depicts the processing time needed for the segmentation of each image, revealing that despite of the complexity within the image regions the technique performed very fast. The slower performance in the last samples was due to the different staining protocol utilized in the second laboratory, indicating the well known variability in tissue sample preparation in immunohistochemistry. It is important to mention that the classic active contours technique with random initialization did not manage to converge on time and did not produce meaningful regions. As an attempt to quantitatively measure the quality of the segmentation procedure we calculated the precision, recall and the F-measure of the process [67], based on the ground truth produced by the expert. Yet, precision indicates the percentage of correctly segmented cells among all the final segments the algorithm extracted, while recall represents the percentage of truly recognized cells among the true cells present in the tissue sample, as measured by the expert. The F-measure, defined as 2*precision*recall/(precision and recall), is the only approximation of the statistical term "accuracy" we may have in image segmentation quality evaluation, as the term true negative in region extraction is not easily defined. Precision, recall and the F-measure are depicted in Figures 4.14, 4.15, 4.16 respectively, indicating the efficiency of the algorithm even in the difficult cases.

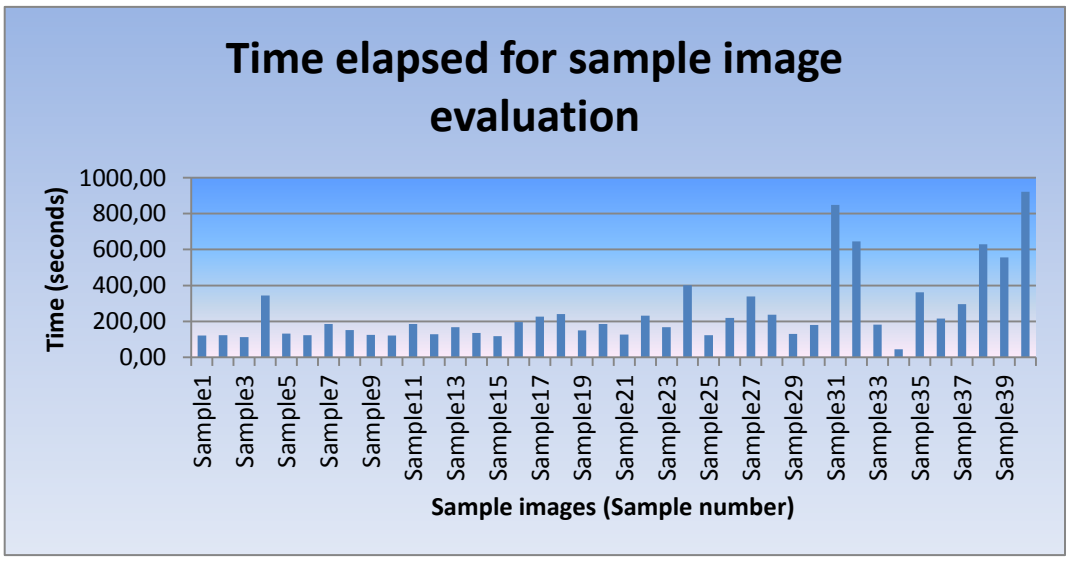

Figure 4.13 Processing time for each of the 40 IHC images of our dataset

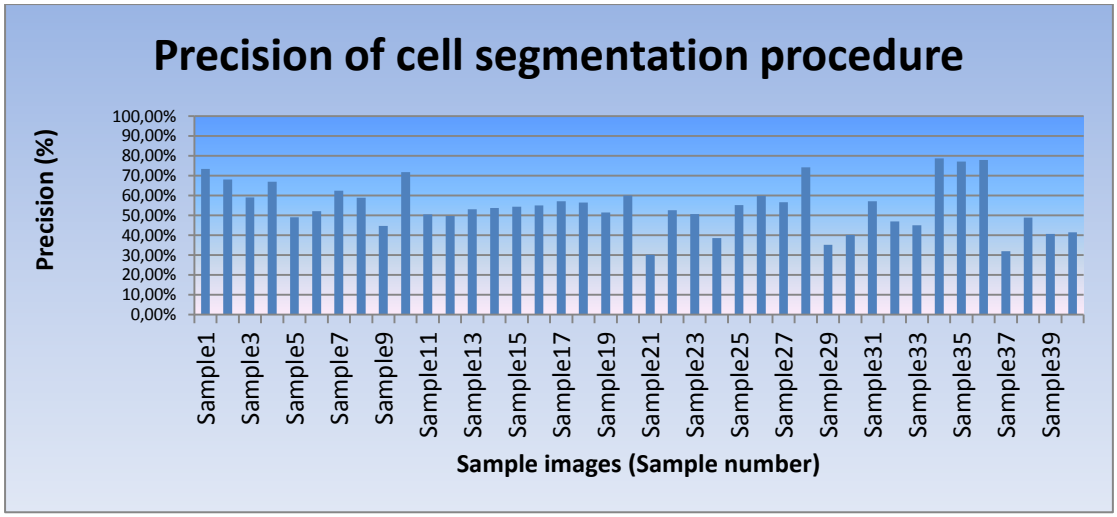

Figure 4.14 Performance the segmentation algorithm based on precision

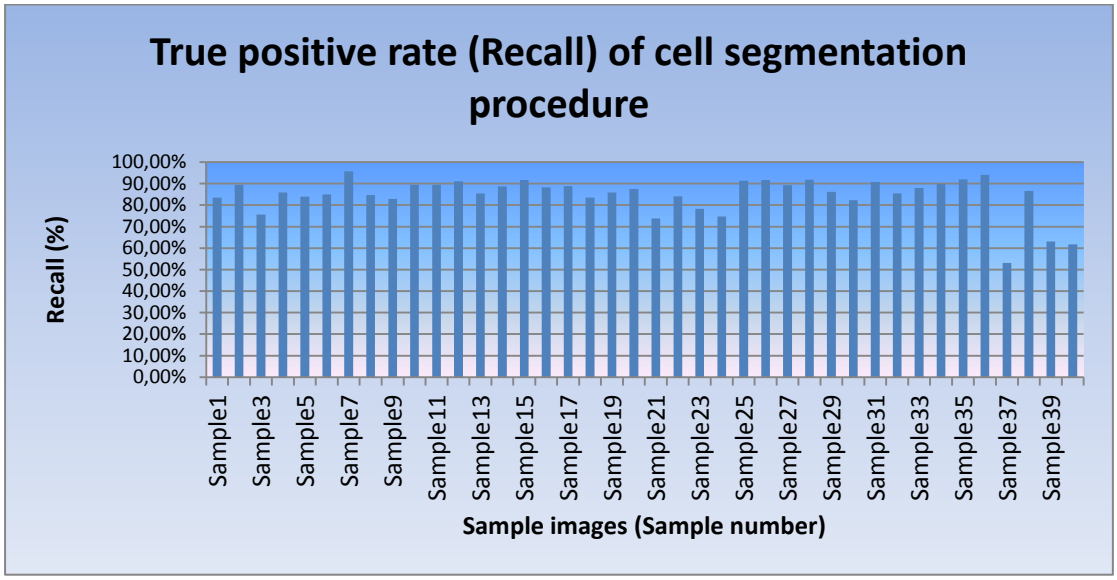

Figure 4.15 Performance the segmentation algorithm based on recall

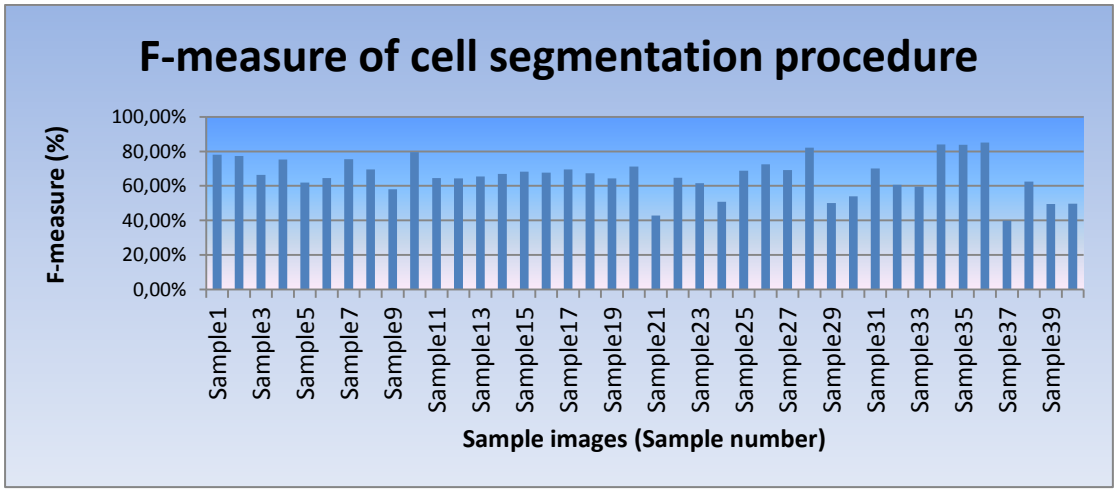

Figure 4.16 Performance the segmentation algorithm based on F-measure

Considering the above, the contribution of the presented methodology regarding the segmentation procedure is twofold: accurate segmentation of existing cells within the image and qualitative discrimination of regions of interest (cells) and good filtering of the irrelevant image areas. The high Recall value significantly reveals the power of the proposed technique to automatically detect the cells within a tissue sample, emulating the evaluation methodology of the expert.

The vast majority of the techniques present in international bibliography regarding cell segmentation terminate the implementation and evaluation procedure when the image is segmented, focused on the visual estimation of the segmentation quality. Continuing the evaluation of our approach and in order to quantitatively estimate the results extracted, we compare our algorithm with two other indicative methods: the marked watershed transform, a representative and classic method in segmentation fields and a very specialized one [68], targeting on membrane staining evaluation through color deconvolution and a customized algorithm for cell segmentation. In order to perform comparative evaluation, two indicative immunohistochemical image samples were selected, including a very difficult case and a common one, having being manually segmented by a pathology expert. The specialist has marked the candidate cell regions among which she finally selected the true cell areas. Apart from the visual segmentation results produced by the three testing techniques, our methodology and the two indicative other ones, the precision, recall, specificity, accuracy, false positive rate and F-measure metrics [67] were measured, as these indicator metrics are commonly used for evaluating classification quality. As a ground truth we accept the manual segmentation originated from the doctor. True positive instances arise when a region has been accurately recognized, true negative instances mean that the algorithm has not detected them, yet successfully not considered them as cells being regions that the doctor also rejected, false positive instances are measured when regions have been wrongly considered as cells and false negatives hits are measured for the number of cell regions (as defined by the specialist) that have not been detected. The marked segmented images from the three techniques along with the manually marked segmentation produced by the expert and considered as ground truth are depicted in Figure 4.17. The produced values for the statistical metrics are summarized in Table 4.1. The results indicate the efficiency and the robustness of our methodology. The marked watershed transform using regional maxima and distance transforms as input images, commonly used in image segmentation fields, does not perform well if the image content is complex, as clearly indicated in the second sample image paradigm. In addition, its main drawback regarding oversegmentation is present in this cell segmentation application. The low scores of precision and recall reveal that too many irrelevant regions are selected. The color deconvolution scheme [68] targeted to IHC image segmentation performs well in both image tested examples but it tends to detect irrelevant and incomplete regions, considering only the color staining of the membrane, yet detecting regions in the intermediate tissue, introducing errors in

the tissue evaluation procedure. Our technique outperforms the other methods in almost all statistical metrics. The main characteristic, which was confirmed in all the sample images as previous statistical analysis revealed, is its robustness in detecting the existing cells with high scores of probability. Eliminating the "missing" cells is of paramount importance for the tissue evaluation procedure following the cell areas extraction stage, yet the prospect of our technique in real medical and laboratory applications as an assisting tool is high.

Table 4.1 Comparison of our methodology to other techniques

Quantitative comparison of our methodology to other representative techniques							
		Precision	**Recall**	**Specificity**	**Accuracy**	**FP rate**	**F measure**
Mean case	Our methodology	74,56%	93,41%	80,54%	85,42%	19,46%	82,93%
	Color deconvolution	63,97%	95,60%	67,11%	77,92%	32,89%	76,65%
	Marked watershed	38,39%	47,25%	53,69%	51,25%	46,31%	42,36%
Difficult case	Our methodology	69,37%	82,80%	53,42%	69,88%	46,58%	75,49%
	Color deconvolution	66,39%	84,95%	45,21%	67,47%	54,79%	74,53%
	Marked watershed	20,31%	14,29%	32,00%	22,29%	69,86%	16,77%

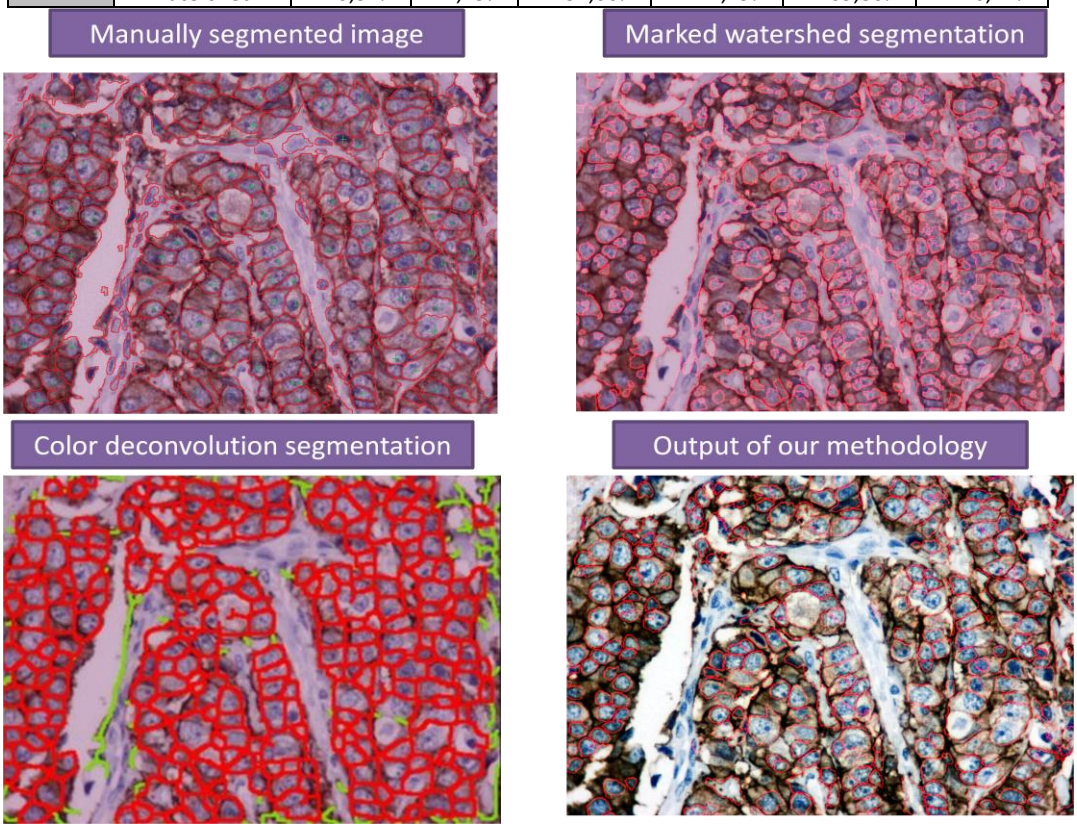

Figure 4.17 Comparison of the segmentation results from three testing techniques along with the ground truth image derived from the pathologist

4.7. Membrane staining evaluation and IHC score classification

As a final stage of our methodology and proceeding towards the step of tissue characterization, we attempted to score the HER2 overexpression having already detected the cells forming the tissue and determined their complete boundaries. For this study, tissue evaluation will rely on the pathogenesis of the tested sample (yes or no), yet we encode the internationally standard IHC scores to YES (complete and strong staining - HER2 score +3) or NO (score 0, +1,+2). As a future work, we intend to further improve the capabilities of our approach for assigning different kinds of scores through a classification formulation. In order to assign a score, it is essential to calculate the percentage of cells overexpressing the protein among all the existing cells, in terms of the completeness and intensity of their membrane staining. The first prerequisite has already been achieved through the segmentation process, having accomplished to calculate complete and linked (not broken) boundaries. The intensity of staining is determined by the value of each membrane pixel within the equalized grayscale image. Having labeled each cell region through the segmentation stage, we can fully specify the location of individual cells and the pixels forming their internal area and boundary (cell membranes). By simply thresholding the intensity to strong (dark region or low intensity value), moderate (intensity of intermediate value) and weak (light or high intensity value) we can determine the staining intensity of a point belonging to the region boundary. In addition, a check if the tested pixel has blue color is performed, rejecting probable segmentation errors having assigned a nuclei pixel as a point belonging to the membrane of the cell; this is a possible case that there is no cytoplasm area within the cell. Having determined the number of points forming the contour (membrane) and the number of stained cells, we can evaluate the completeness of membrane staining of a single cell and all cells located in the image. If the percentage of the stained pixels among their total number within the boundary is over a threshold (90% for the needs of our methodology) then the cell is marked as stained. This is done sequentially for all the cells detected within the image sample. The percentage of stained cells within the entire tissue can now be compared with the corresponding score derived from the standardized scoring system used by the pathologists. Percentage of cell staining over 10% is considered as HER2 positive in our consideration. We recall that the 10% threshold is arbitrary, but clinically approved.

All images in our dataset were processed during the classification stage of our algorithm. The tissue slides have already been evaluated and scored by the pathology specialist, resulting in 35 pathogenic and 5 healthy characterized tissue samples. In order to estimate the classification accuracy of our technique, performance statistics were extracted in terms of precision, recall, false positive rate, accuracy, specificity and F-measure. Measuring the specificity and sensitivity metrics for distinct values of threshold T, which represented the reference percentage of completely stained cells within the image above which the tissue is characterized as pathogenic, we construct the corresponding Receiver Operating Curve (ROC curve) for the implemented classifier, producing an Area Under the Curve value (AUC) of 0.93, implying that the classification accuracy is very high. The ROC Curve is illustrated in Figure 4.18. The operation point was selected at the threshold value of 10% (confirming the gold standard in IHC scoring) as other points operated in regions of possible suspicious or misleading outcomes as any tissue was classified as pathogenic, which seems to be a problematic situation during the processing of random samples and datasets. Of course this constitutes a

preliminary but strong evidence that the proposed approach to tissue characterization has the potential of producing valuable and meaningful results. The same set of images was processed by the tool the authors developed in [67], incorporated in the reference segmentation method we compared our segmentation performance findings with. This is a representative method from the bibliography targeting at the same scientific field as the proposed algorithm. The performance metrics of both techniques are summarized in Table 2.

Table 2. Performance evaluation of the proposed tissue evaluation stage vs the reference method

	Performance metrics of the implemented classification procedure and the reference methodology					
Method	**Precision**	**Recall**	**FP rate**	**Accuracy**	**Specificity**	**F-measure**
Our method	**96,97%**	**91,43%**	**20,00%**	**90%**	**80,00%**	**80,00%**
Reference method	**87,5%**	**100%**	**100%**	**87,5%**	**0,00%**	**93,33%**

The reference method derives zero specificity and its extreme false positive rate reveal a problematic classifier tending to classify test samples as only HER2 positive; all five instances of healthy tissue were assigned as pathogenic. Our classifier appears robust, indicating its potential for applicability to laboratory assessments of tissue evaluation.

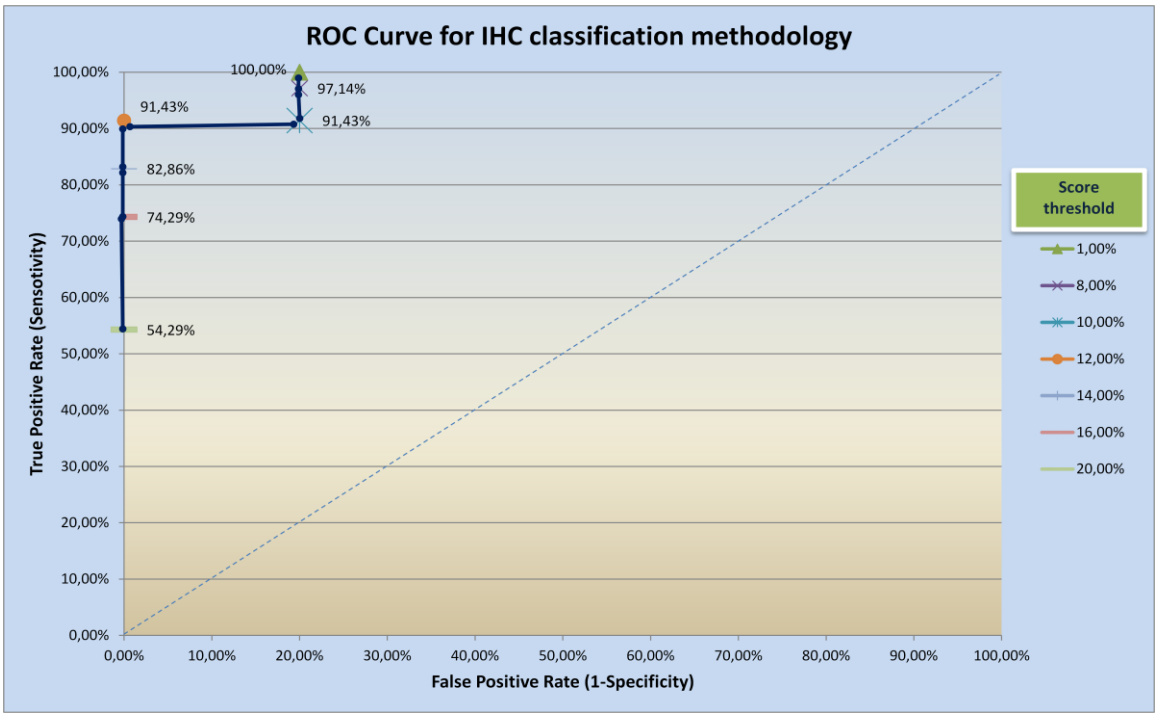

Figure 4.18 ROC analysis our implemented classifier

5. Conclusions

In this master thesis we study feature extraction from two imaging modalities, namely polarimetry and microscopy. Polarimetry is based on the fact that intrinsic qualities of materials have an effect on the way light interacts with them, whether in transmission or reflection. Originating from a biological scenario and utilizing materials that dispose similar optical parameters to biological components, we developed a statistical modeling of the intensity distributions of polarimetric images depicting target components. This modeling contributed in the discrimination of the target from the background, giving rise to object detection and characterization. After the preliminary results of this consideration, testing was performed on real biological data from lung cancer tissue. Statistical metrics confirm that different kinds of tissue pathogenesis can be discriminated using polarimetry, as differentially affected tissue samples absorb, transmit and depolarize light in a different manner.

On the other hand, microscope imaging provides histological information on a microscopic level, regarding the structure, coloring and shape characteristics of cells. We developed an innovative cell segmentation algorithm to accurately determine cell regions and their boundaries within an immunohistochemical image. Proceeding further, we implemented a technique for the assessment of oncoprotein HER2 over expression and the characterization of cancer tissue according to an internationally established scoring system. Breast cancer cell-nuclei segmentation and membrane border extraction was achieved by fusing information derived from image processing approaches aiming at intensity and color characteristics. The results from the analysis of immunohistochemical images confirm the prospects of the proposed methodology for accurate qualitative and quantitative evaluation of oncogene overexpression that compromises with the specialists' diagnosis. Performance metrics reveal the efficiency of both area segmentation and tissue (sample) classification stages, encouraging its use on laboratory assessments as a supporting, easy and promising tool for the clinician. It is worth mentioning that the algorithmic setup remained unchanged for all image samples processed, supporting the robust performance of the method. The innovation of the proposed scheme lies on the appropriate parameterization of sub modules (especially the watershed and active contours) and the fusion of information from intensity and color, which increase the accuracy of final results and the computational efficiency of implementation. Performance metrics reveale that the segmentation algorithm is capable of detecting the existing cell areas within the tissue sample with high probability and provides good filtering of irrelevant segments based on mathematical morphology.

Challenges on the proposed segmentation scheme include the introduction of additional information originating from texture analysis and its fusion with the color information already used. A possible training of the algorithm via neural networks is expected to improve the classification results, as this direction would lead to a more suitable estimation of the parameters used in the internal stages of the segmentation algorithm. A closer cooperation with pathology experts is intended in order to provide more and different datasets of histological images, which will contribute to more detailed validation of the effectiveness and robustness of both the segmentation and classification results. To this direction, one improvement of the proposed approach w would be the incorporation of a user friendly interface to the overall procedure, giving the potential of serving as a supplementary tool in everyday laboratory tissue evaluation procedures. Additional challenges may include:

1) Experiments with a larger number of images and extensive comparisons with existing tools
2) Evaluations of the same images from different doctors as to consider possible improvement of cross-expert evaluation!
3) Studies from many laboratories as to consider the influences of multicenter studies

References

[1] David T. Moran, J. Carter Rowley, "Visual Histology Atlas", e-book, www.VisualHistology.com

[2] www.BeStrong.org.gr, Greek Non Profiteering Organism Friend of Cancer

[3] Lacey JV Jr, Devessa SS, Brinton LA, "Recent Trends in breast cancer incidence and mortality", Environ. Mol. Mutagen, Vol 39, pp 82-88, 2002

[4] http://www.bococ.org.cy/ Oncologigal Centre of Cyprus

[5] Jeffrey S. Ross, Jonathan A. Fletcher, Gerald P. Linette, James Stec et al, "The Oncologist", Vol 8, pp. 307-325, 2003

[6] Elledge RM, Green S, Ciocca D, Pugh R, Allred DC, Clrak GM, et al, "HER-2 expression and response to tamoxifen in estrogen receptor-positive breast cancer: a Southwest Oncology Group Study", Clin Cancer Res, Vol 4, pp 7-12, 1998

[7] Sylvie Menard, Elda Tagliabue, Manuela Campiglio and Serenella M. Pupa, "Role of HER2 Gene Overexpression in Breast Carcinoma", Journal of Cellular Physiology, Vol 182, pp 150–162, 2000

[8] S. Scholl, I. Bieche, C. Pallud, M. H, Champeme, F. Beuvon, K. Hacene, W. Gullick, P. Pouillart and R. Lidereau, "Relevanche of multiple biological parameters in breast cancer prognosis", The Breast, Vol 5, pp 21-30, 1996

[9] Love RR, Duc NB, Havighurst TC, Mohsin SK, Zhang Q, DeMets DL et al, "HER2/neu overexpression and response to oophorectomy plus tamoxifen adjuvant therapy in estrogen receptor-positive premenomausal women with operable breast cancer", J Clin Oncol, Vol 21, pp 453-457, 2003

[10] Allred DC, Clark GM, Tandon AK, Molina R, Tormey DC, Osborne CK, et al, " HER-2/neu in node-negative breast cancer: prognostic significance of overexpression influenced by the presence of in situ carcinoma", J Clin Oncol, Vol 10, pp 599-605, 1992

[11] Muss HB, Thor AD, Berry DA, Kute T, Liu ET, Koemer F, et al, "cerbB-2 expression and response to adjuvant therapy in women with node-positive early breast cancer", N Engl J Mes, Vol 330, pp 1260-1266, 1994

[12] Palk S, Bryant J, Park C, Fisher B, Tan-Chiu E, Hyams D, et al, " erbB-2 and response to doxorubicin in patients with axillary lymph node-positive, hormone receptor-negative breast cancer", J Natl Cancer Inst, Vol 90, pp 1361-7-, 1998

[13] Cobleigh MA, Vogel CL, Tripathy D, Robert NJ, Scholl S, Fehrenbacher L, et al, " Multinational study of the efficacy and safety of humanized anti-HER2 monoclonal antibody in women who have HER2-overexpressing metastatic breast cancer that has

progressed after chemotherapy for metastatic disease", J Clin Oncol, Vol 17, pp 2639-2648, 1999

[14] Chang J, Mohsin SK, Weiss H, Hilsenbeck SG, Lucci AJ, Gutierrez MC, et al, "Induction of apoptosis and decrease in proliferation in primary breast cancers with neoadjuvant Herceptin", Breast Cancer Res Treat, 2003

[15] Zenonas Theodosiou, Ioannis N. Kasampalidis, George Livanos, Michalis Zervakis, Ioannis Pitas and Kleoniki Lyroudia, "Automated Analysis of FISH and Immunohistochemistry Images: A Review", International Society for Analytical Cytology Cytometry Vol 71, pp 439–450, 2007

[16] G.C. Giakos, "Novel Biomolecular NanoPhotonic Devices, Sensors, Photonic Nanocrystals and Biochips: Advances in Medical Diagnostics, Environmental and Defense ", IEEE International Workshop on Imaging Systems and Techniques – IST 2007, Krakow, Poland, May 4-5, 2007

[17] J.S. Baba, J.R. Chung, A.H. DeLaughter, B.D. Cameron, and G.L. Cote, "Development and calibration of an automated Mueller matrix polarization imaging system", Journal of Biomedical Optics, Vol. 7, No. 3, pp. 341-349, 2002.

[18] G. C. Giakos, "Multifusion Multispectral Lightwave Polarimetric Detection Principles and Systems", IEEE Transactions on Instrumentation and Measurement, vol. 55, no. 6, pp. 1904-1912, No 6, 2006.

[19] G.C. Giakos, V. Adya, K. Valluru, P. Farajipour, S. Marotta, J.T. Paxitzis, M. Becker, P. Bathini, K. Ambadipudi, S.M. Mandadi, "Molecular imaging of tissue with high-contrast multispectral photosensitizing polarimetric imaging techniques," 2009 IEEE International Workshop on Imaging Systems and Techniques, (IST '09), Shenzhen, China, pp. 63-66, 2009.

[20] G.C. Giakos, Paturi, S. Atreya, Bathini P., Sukumar S., Ambadipudi K., Valluru K., Wagenar D., Adya V., Reddy M., "New Pathways Towards the Enhancement of the Image Quality", IEEE IMTC Technical Conference, Warsaw, Poland, 2007.

[21] George Giakos, K.Valluru, V.Adya, K.Ambadipudi, S.Paturi, M.Becker, P.Farajipour, S.Marotta, J.Paxitis, B.Mandani, M.Zervakis and G.Livanos, "Stokes parameters imaging of multi-index of refraction biological phantoms utilizing optically active molecular contrast agents", Measurement Science and Technology, Special issue in Imaging Systems and Techniques, Vol 20 pp 12-16, 2009

[22] G.C. Giakos, S. Atreya Paturi, K. Valluru, P. Bathini, V. Adya, S. Sukumar, D. Sheffer, "Optical Active Molecules used as Molecular Contrast Agents for Enhanced Imaging", Proceedings to IMTC 2008 – IEEE International Instrumentation and Measurement Technology Conference Victoria, Vancouver Island, Canada, , pp. 1809-1813, 2008.

[23] E. Collett, Polarized Light, Marcel Dekker, 1993.

[24] G. C. Giakos, "Multifusion Multispectral Lightwave Polarimetric Detection Principles and Systems", IEEE Transactions on Instrumentation and Measurement, vol. 55, no. 6, pp. 1904-1912, 2006

[25] Azzam, R. M. A., " Photopolarimetric Measurement of the Mueller Matrix by Fourier Analysis of a Single Detected Signal," Optical Letters, Vol. 2, pp.148-150, 1978

[26] D.B. Chenault, and J.L. Pezzaniti,"Polarization Imaging through Scattering Media", vol. 4133, SPIE 2000

[27] R. A. Lewis, K. D. Rogers, C. J. Hall, E. Towns-Andrews, S. Slawson, A. Evans, S. E. Pinder, I. O. Ellis, C. R. M. Boggis, A. P. Hufton and D. R. Dance, "Breast cancer diagnosis using scattered X-rays", Journal of Synchrotron Radiation, Vol 7, Part 5, pp. 348-352, 2000

[28] M. Felton, K. P. Gurton, D. Ligon, and A. Raglin, "Discrimination of Objects Within Polarimetric Imagery Using Principal Component and Cluster Analysis," Army Research Laboratory, ARL-TR-4216, 2007

[29] G. Livanos , M. Zervakis , G.C. Giakos , K. Valluru , S. Paturi and S. Marotta, "Modeling the characteristics of material distributions in polarimetric images", Image Processing, IET, Vol 5, Issue 5, pp 429 – 439, 2011

[30] X.Zhuang, T.Wang, P.Zhang, "A highly robust estimator through partially likelihood function modeling and its application in computer vision", IEEE Trans.Pattern Anal. Mach.Intell., Vol 14, pp 19-35, 1992

[31] DA-Chuan Cheng, Xiaoyi Jiang, Arno Schmidt-Truckass, "Image Segmentation Using Histogram Fitting and Spatial Information", P.Perner and O.Salvetti (Eds): Springer-Verlag Berlin Heidelberg , pp 47-57, 2007

[32] Moon, T.K., "The expectation-maximization algorithm", Signal Processing Magazine, IEEE, Vol. 13, Issue 6, pp 47 – 60, 1996

[33] Jianguo Zhang and Tieniu Tan , "Brief review of invariant texture analysis methods", Pattern Recognition, Vol, Issue 3, pp 735-747, 2002

[34] A. Papoulis and S. U. Pillai, "Probability, Random Variables and Stochastic Processes", Mc Graw Hill, 2002

[35] Jarry G, Henry F and Kaiser R, "Anisotropy and multiple scattering in thick mammalian tissues" J. Opt. Soc. Am. A, Vol 17, pp 149–153, 2000

[36] Mourant J R, Canpolat M, Brocker C, Esponda-Ramos O, Johnson T M, Matanock A, Stetter K and Freyer J P, "Light scattering from cells: the contribution of

the nucleus and the effects of proliferative status" *J. Biomed. Opt., Vol* 5, pp 131–137, 2000

[37] G C Giakos, S Marotta, C Narayan, J Petermann, S Shrestha, J Baluch, D Pingili, D B Sheffer, L Zhang, M Zervakis, G Livanos and M Kounelakis, "Polarimetric phenomenology of photons with lung cancer tissue", Meas. Sci. Technol., Vol **22,** 114018 (12pp), 2011

[38] Clive R. Taylor, MD, DPhil , "The Total Test Approach to Sandardization of Immunohistochemistry", Arch Pathol Lab Med, Vol 124, 2000

[39] Peter Onody, Francoise Bertrand, Francoise Muzeau, Ivan Bieche, Rosette Lidereau, "Fluorescence In Situ Hybridization and Immunohistochemical Assays for Her-2/neu Status Determination; Application to Node-Negative Breast Cancer", Arch Pathol Lab Med, Vol 125, 2001

[40] Mark R. Wick, Nancy C. Mills, and William K. Brix, "Tissue Procurement, Processing and Staining Techniques", Cambridge University Press 978-0-521-87410-6 - Diagnostic Histochemistry, Chapter 1

[41] J. A. Ramos-Vara, "Technical Aspects of Immunohistochemistry", Vet Pathol Vol 42, pp 405–426, 2005

[42] David Gancberg, Tero Järvinen, Angelo di Leo, Ghizlane Rouas, Fatima Cardoso, Marianne Paesmans, Alain Verhest, Martine J. Piccart, Jorma Isola and Denis Larsimont, "Evaluation of HER-2/*NEU* protein expression in breast cancer byimmunohistochemistry: an interlaboratory study assessing the reproducibility of HER-2/*NEU* testing", Breast Cancer Research and Treatment, Vol 74, pp 113–120, 2002

[43] Seshi R. Sompuram, Vani Kodela, Keming Zhang, Halasya Ramanathan, Gail Radcliffe, Peter Falb, and Steven A. Bogen, "A Novel Quality Control Slide for Quantitative Immunohistochemistry Testing", The Journal of Histochemistry & Cytochemistry Vol50, pp 1425–1433, 2002

[44] "Comparison of automated and manual determination of Her2 status in breast cancer for diagnostic use: A comparative methodological study using the Ventana BenchMark automated staining systems and manual tests", Agnes Bankfalvi, Werner Boecker and Angelika Reiner, 2004

[45] Tsuda H, Akiyama F, Terasaki H, Hasegawa T, Kurosumi M, Shimadzu M, et al. "Detection of HER-2/neu DNA amplification in primary breast carcinoma: Interobserver reproducibility and correlation with immunohistochemistry HER-2/neu overexpression", Cancer, Vol 92, pp 2965-2974, 2001

[46] R. C. Gonzalez and R.E. Woods, Digital Image Processing 2nd Edition, Prentice Hall, New Jersey, 2002.Florida, Richard (2002), The Rise of the Creative Class and How It's Transforming Work, Leisure and Everyday Life, Basic Books.

[47] J. B. MacQueen, "Some Methods for classification and Analysis of Multivariate Observations, Proceedings of 5-th Berkeley Symposium on Mathematical Statistics and Probability", Berkeley, University of California Press, Vol , pp 281-297

[48] Fukunaga, K. & Hostetler, L., “ The estimation of the gradient of a density function, with applications in pattern recognition” IEEE Transactions on Information Theory, Vol 21, pp 32–40, 1975

[49] Cheng, Y., “Mean shift, mode seeking, and clustering”, IEEE Transactions on Pattern Analysis and Machine Intelligence, Vol 17, pp 790–799

[50] Comaniciu, D. & Meer, P. “Mean shift: A robust approach toward feature space analysis” IEEE Transactions on Pattern Analysis and Machine Intelligence, Vol 24, pp 603–619

[51] Wang, J., Thiesson, B., Xu, Y. & Cohen, M., “Image and video segmentation by anisotropic kernel mean shift”, In European Conference on Computer Vision, Vol 2, pp: 238–249), 2004

[52] Jos B.T.M. Roerdink and Arnold Meijster, “The Watershed Transform: Definitions, Algorithms and Parallelization Strategies”, Fundamenta Informaticae, Vol 41, pp 187-228, 2001

[53] Meyer, F., and Beucher, S. “Morphological segmentation”, J. Visual Commun. and Image Repres. Vol 1, pp 21-45, 1990

[54] Vincent, L., and Soille, P.,“Watersheds in digital spaces: an efficient algorithm based on immersion simulations”, IEEE Trans. Patt. Anal. Mach. Intell., Vol 13,pp 583-598

[55] Meyer, F., “Topographic distance and watershed lines”, Signal Processing, Vol 38, pp 113-125, 1994

[56] Moga, A. N., and Gabbouj, M., “Parallel marker-based image segmentation with watershed transformation”, Journal of Parallel and Distributed Computing Vol 51, pp 27-45,1998

[57] Jitendra Malik,Serge Belongie, Thomas Leung, Jianbo Shi, "Contour and texture analysis for image segmentation", International Journal on Computer Vision, Issue 43, pp 7-27, 2001

[58] Tony F. Chan, Luminita A. Vese, "Active Contours Without Edges", IEEE Transactions on Image Processing, Vol 10, No 2, 2001

[59] Gilles Aubert and Luminita Vese, “A variational method in image recovery”, Society for Industrial and Applied Mathematics, Journal of Numerical analysis, Vol34, No 5, pp 1948-1979, 1997

[60] R.Mofidi,R.Walsh, P.F. Ridgway, T.Crotty, E.W. McDermott, T.V. Keaveny, M.J. Duffy, “Objective measurement of breast cancer oestrogen status through digital image analysis”, A.D.K. Hill and N. O’Higgins, EJSO 2003

[61] Am J Clin, ”Quantitative Evaluation of Her-2/neu Status in Breast Cancer by Fluorescence In Situ Hybridization and by Immunohistochemistry With Image Analysis”, Pathol 115(6), 2001

[62] ”Image Analysis Using the Aperio ScanScope”, Allen H.Olson, 2006

[63]”Application of Automatic Thresholding in Image Analysis Scoring of Cells in Human Solid Tumors Labeled for Proliferation Markers”, Jean R. Weaver and Jessie L-S. Au, 1997

[64] Desok Kim, Christopher W. Gregory, Gary J. Smith, and James L. Mohler, ”Immunohistochemical Quantitation of Androgen Receptor Expression Using Color Video Image Analysis”, 1998

[65] Paul D. Smith, Karen J. McLean, Michael A. Murphy, Yvette Wilson, Mark Murphy, Ann M. Turnley, Mark J.Cook ,“A brightness-area-product-based protocol for the quantitative assessment of antigen abundance in fluorescent immunohistochemistry”, 2005

[66] Vachier, C and Vincent L, “Evaluation of image extrema using alternating filters by reconstruction”, Proc. SPIE Vol. 2568, 1995

[67] Vilppu J. Tuominen, Teemu T. Tohonen and Jorma Isola, “ImmunoMembrane: a publicly available web application for digital image analysis of HER2 immunohistochemistry”, Histopathology, Vol 60, pp 758-767, 2012

Appendix

Conference and journal publications referring to the presented work:

❖ Analysis of Immunohistochemical Images

1. International Society for Analytical Cytology Impact factor 0.939

Cytometry Part A 71A:439–450 (2007)

"Automated Analysis of FISH and Immunohistochemistry Images: A Review"

Zenonas Theodosiou,[1] Ioannis N. Kasampalidis,[1] George Livanos,[2] Michalis Zervakis,[2] Ioannis Pitas,[1]* and Kleoniki Lyroudia[3]
[1]Department of Informatics, Aristotle University of Thessaloniki, 54124 Thessaloniki, Greece
[2]Department of Electronic and Computer Engineering, Technical University of Crete, University Campus, Kounoupidiana, 73100 Chania, Greece
[3]Department of Endodontology, School of Dentistry, Aristotle University of Thessaloniki, 54124 Thessaloniki, Greece

Fluorescent in-situ hybridization (FISH) and immunohistochemistry (IHC) constitute a pair of complimentary techniques for detecting gene amplification and overexpression, respectively. The advantages of IHC include relatively cheap materials and high sample durability, while FISH is the more accurate and reproducible method. Evaluation of FISH and IHC images is still largely performed manually, with automated or semi-automated techniques increasing in popularity.Here, we provide a comprehensive review of a number of (semi-) automated FISH and IHC image processing systems, focusing on the algorithmic aspects of each technique. Our review verifies the increasingly important role of such methods in FISH and IHC; however, manual intervention is still necessary in order to resolve particularly challenging or ambiguous cases. In addition, large-scale validation is required in order for these systems to enter standard clinical practice.

2. IST 2013, IEEE International conference 21-23 October 2013

"Automated analysis of immunohistochemical images based on curve evolution approaches"

G. Livanos, M. Zervakis
Department of Electronics and Computer Engineering
Technical University of Crete
Chania, P.C. 73100, Crete, Greece
G. C. Giakos
Department of Electrical and Computer Engineering
The University of Akron
Akron Ohio, 44325, USA

Abstract— The HER2/neu oncogene is notable both for its role in the pathogenesis of breast cancer and its role as a target of treatment. Qualitative or quantitative protein evaluation has been achieved using immunohistochemistry (IHC) on frozen and archival tissues, a widely adopted technique due to the standardization of the internal procedural steps and its easy and low-cost applicability to any laboratory. The goal of the present study is to introduce an efficient tool for the automated detection of HER2 protein overexpression in tissues, providing accurate, instant, yet objective interpretation outcomes through a formalized procedure. The comparison of results with classifications by specialists who evaluated the same tissue samples dataset confirms the efficiency and prospect of the methodology.

❖ Polarimetric imaging

Journals

3. IEEE TRANSACTIONS ON INSTRUMENTATION AND MEASUREMENT, VOL. 59, NO. 11, NOVEMBER 2010 Impact factor 1.106

"Efficient Molecular Imaging Techniques Using Optically Active Molecules"

G. C. Giakos, Fellow, IEEE, S. Atreya Paturi, K. Valluru, P. Bathini, V. Adya, S. Sukumar, K. Ambadipudi, B. Mandadi, M. Becker, S. Athawale, P. Farajipour, S. Marotta, D. Sheffer, George Livanos, and Michael Zervakis

Abstract—Efficient imaging techniques aimed at the increasing of the image contrast of a structure, surrounded by a scattering medium, using optically active and high index of refraction molecules as molecular contrast agents, are presented. Specifically, an enhanced degree of linear polarization (DOLP) target detection and imaging is obtained by doping the surrounding medium with molecular contrast agents consisting of aqueous glucose, aqueous alcohol, and salt molecules, in conjunction with advanced polarimetric imaging techniques. The outcome of this paper opens new horizons in the areas of imaging, with emphasis on medical arena, industry, and detection technology.

4. IOP PUBLISHING MEASUREMENT SCIENCE AND TECHNOLOGY Meas. Sci. Technol. 20 (2009) 104003 (12pp) Impact factor 1.317

"Stokes parameter imaging of multi-index of refraction biological phantoms utilizing optically active molecular contrast agents"

G C Giakos[1,2], K Valluru[2], V Adya[2], K Ambadipudi[2], S Paturi[2], P Bathini[2], M Becker[2], P Farajipour[2], S Marotta[2], J Paxitzis[2], B Mandadi[2], M Zervakis[3] and G Livanos[3]

[1] Department of Electrical and Computer Engineering, The University of Akron, Akron, OH 44325, USA

[2] Department of Biomedical Engineering, The University of Akron, Akron, OH 44325, USA

[3] Department of Electronic and Computer Engineering, Technical University of Crete, Chania 73100,Greece

Abstract

The purpose of this study is to assess the potential of novel molecular polarimetric imaging techniques utilizing multi-index of refraction targets, i.e. composite targets made from optically different media, immersed into biological fluids doped with optically active molecules and enzymes. The outcome of this study indicates that the application of Stokes parameter detection principles with concominant administration of fluids containing suitable optically active molecular contrast agents and high index of refraction molecules could enhance the detection and imaging process of internal structures by providing enhanced penetration depth, high contrast and high depolarized scatter rejection.

5. MEASUREMENT SCIENCE AND TECHNOLOGY
Meas. Sci. Technol. **22** (2011) 114018 (12pp) Impact factor 1.494

"Polarimetric phenomenology of photons with lung cancer tissue"

G C Giakos[1,2], S Marotta[2], C Narayan[2], J Petermann[1], S Shrestha[1], J Baluch[1], D Pingili[1], D B Sheffer[1], L Zhang[3], M Zervakis[4], G Livanos[4] and M Kounelakis[4]

[1] Department of Electrical and Computer Engineering, The University of Akron, Akron, OH 44325, USA
[2] Department of Biomedical Engineering, The University of Akron, Akron, OH 44325, USA
[3] Department of Chemistry, Cleveland State University, Cleveland, OH 44114, USA
[4] Department of Electronic and Computer Engineering, Technical University of Crete, Chania 3100,Greece

Abstract
The objective of this study is to explore the polarimetric phenomenology of light interaction with healthy and early-stage lung cancer tissue samples by applying efficient polarimetric backscattering detection techniques combined with polarimetric exploratory data analysis. Preliminary results indicate that enhanced discrimination signatures can be obtained for certain types of early-stage lung cancers based on their depolarization, backscattered intensity and retardance characteristics.

6. Image Processing, IET, August 2011, Volume: 5, Issue: 5, page(s): 429 – 439
Impact factor 0.639

"Modeling the characteristics of material distributions in polarimetric images"

G. Livanos [(1)], M. Zervakis [(1)], G.C. Giakos [(2)-(3)], K. Valluru [(3)], S. Paturi[(3)], and S. Marotta [(3)]

[(1)]Department of Electronic and Computer Engineering
Technical University of Crete
Chania 73100, Greece
[(2)] Department of Electrical and Computer Engineering
[(3)] Department of Biomedical Engineering
The University of Akron
Akron, OH, 44325, USA

Abstract – Contrast measurements become of increasing importance in digital imaging, where region of interest (ROI) differences can be effectively identified, processed and segmented. The image contrast among different structures varies with the material properties, material composition, and geometrical parameters, and it is difficult to be determined only from its physical, electrical, or optical parameters. The novelty of this study consists in fusing statistical analysis with polarimetric principles. As a result, quantification of image contrast in terms of Stokes parameters together with the modeling of intensity distribution for the corresponding target areas can be proved a powerful tool for analyzing the different properties of operational modalities and/or materials depicted in digital images. By fusing the above concepts, we explored the intrinsic potential of an efficient molecular imaging technique aimed at increasing the optical contrast of a structure surrounded by a scattering medium.

Conferences

7. IST 2010, IEEE International Conference, Thessaloniki, 1-2 July 2010

" BACKSCATTERED POLARIMETRIC DETECTION FROM BIOLOGICAL TISSUE"

G.C. Giakos [(1)], S. Marotta [(2)], K. Ambadipudi [(2)], K. Valluru [(2)], J. Petermann [(1)], C. Narayan [(2)] , D. Natarajamani [(2)], D. Pingili [(1)]

[(1)] Department of Electrical and Computer Engineering [(2)]Department of Biomedical Engineering

M.G. Kounelakis, G. Livanos, M.E. Zervakis

Dept. of Electronic & Computers Engineering

Technical University of Crete

Chania, Crete, Greece

Abstract—In this study, backscattering optical measurements from high scattering media and biological tissue were performed using different polarimetric detection techniques. The outcome of this study may facilitate the early diagnosis, monitoring, and assessment of disease progress, with high sensitivity and specificity.

8. www.springerlink.com : 5th European IFMBE Conference, IFMBE Proceedings 37, pp. 381–384, 2011.

"Histogram modeling of polarimetric images for analysis of material properties"

G. Livanos [1], M. Zervakis [1] and G.C. Giakos [2-3]

[1] Department of Electronic and Computer Engineering, Technical University of Crete, Chania 73100, Greece

[2] Department of Electrical and Computer Engineering

[3] **Department of Biomedical Engineering, The University of Akron, Akron, OH, 44325, USA**

Abstract— Contrast measurements become of increasing importance in digital imaging, where region of interest (ROI) differences can be effectively identified, processed and segmented. The image contrast among different structures varies with the material properties, material composition, and geometrical parameters, and it is difficult to be determined only from its physical, electrical, or optical parameters. The novelty of this study consists in fusing statistical analysis with polarimetric principles. As a result, quantification of image contrast in terms of Stokes parameters together with the modeling of intensity distribution for the corresponding target areas can be proved a powerful tool for analyzing the different properties of operational modalities and/or materials depicted in digital images. By fusing the above concepts, we explored the intrinsic potential of an efficient molecular imaging technique aimed at increasing the optical contrast of a structure surrounded by a scattering medium.

9. IST 2011, IEEE International Conference, Batu Ferringhi, Penang, Malaysia
17-18 May 2011

"Near Infrared Light Interaction with Lung Cancer Cells"

G.C. Giakos [1]-[2], S. Marotta [2], C. Narayan [2], J.Petermann [1], S. Sestra, D. Pingili [1], S. A.Tsokaktsidis [1], D.B. Sheffer [1], and W. Xu [1]
[1] Department of Electrical and Computer Engineering
[2] Department of Biomedical Engineering, The University of Akron, Akron, Ohio
M. Zervakis [3], G. Livanos [3], M. Kounelakis [3]
Department of Electronic and Computer Engineering, Technical University of Crete, Chania 73100, Greece

Abstract— The objective of this study is to explore the phenomenology of near infrared (NIR) light interaction with healthy and early-lung cancer by combining efficient polarimetric backscattering detection techniques with Polarimetric Exploratory Data Analysis (pEDA). Preliminary results indicate that enhanced discrimination signatures can be obtained for certain types of lung cancers.